Psychological Review
1997, Vol. 104, No. 3, 618–658

0033-295X/97/$3.00

Cortical Dynamics of Three-Dimensional Figure–Ground Perception of Two-Dimensional Pictures

Stephen Grossberg
Boston University

This article develops the FACADE theory of 3-dimensional (3-D) vision and figure–ground separation to explain data concerning how 2-dimensional pictures give rise to 3-D percepts of occluding and occluded objects. The model describes how geometrical and contrastive properties of a picture can either cooperate or compete when forming the boundaries and surface representations that subserve conscious percepts. Spatially long-range cooperation and spatially short-range competition work together to separate the boundaries of occluding figures from their occluded neighbors. This boundary ownership process is sensitive to image T junctions at which occluded figures contact occluding figures. These boundaries control the filling-in of color within multiple depth-sensitive surface representations. Feedback between surface and boundary representations strengthens consistent boundaries while inhibiting inconsistent ones. Both the boundary and the surface representations of occluded objects may be amodally completed, while the surface representations of unoccluded objects become visible through modal completion. Functional roles for conscious modal and amodal representations in object recognition, spatial attention, and reaching behaviors are discussed. Model interactions are interpreted in terms of visual, temporal, and parietal cortices.

The human urge to represent the three-dimensional (3-D) world using two-dimensional (2-D) pictorial representations dates back at least to Paleolithic times. Artists from ancient to modern times have struggled to understand how a few lines or color patches on a flat surface can induce mental representations of occluding objects in front of occluded objects. This article analyzes how a 2-D picture can generate a percept of a 3-D scene in which such figure–ground separation occurs. The article accomplishes this by developing a neural theory of biological vision called *FACADE theory* (Grossberg, 1993, 1994; Grossberg & McLoughlin, 1995), which heretofore has provided a unified analysis of many perceptual data that may, at the outset, appear to be unrelated. It explains these data as manifestations of brain mechanisms that generate preattentive 3-D representations of boundaries and surfaces and that use these representations to engage attentive mechanisms for visual recognition, spatial orientation, and search (Grossberg, Mingolla, & Ross, 1994).

1. Three-Dimensional Pop-Out and Amodal Completion

This article further develops FACADE theory to explain some pictorial visual percepts that have played a major role in classical debates about how biological vision works. These percepts are influenced by the often subtle relationships that exist between the geometrical and contrastive properties of a picture. The percepts generated by changing these relationships challenge one to think more deeply about how 2-D pictures give rise to depthful 3-D percepts. Two notable themes in such an analysis concern how the percepts generated by line drawings differ from those generated by colored surface regions and how a partially occluded object in a picture can get completed, and thereby recognized, behind an occluding object, even if the completed representation is not seen as a visible contrast or color difference. Such a completion event is often called an *amodal* percept (Michotte, Thines, & Crabbe, 1964) to distinguish it from *modal* percepts that do carry a visible perceptual sign.

Amodal percepts may occur even if there is no obvious occluding or occluded object. For example, in Figure 1A, a vivid vertical illusory contour is generated by the offset grating, even though there is little or no brightness or color difference on either side of the contour. Thus, this illusory contour is an amodal percept, one that can be consciously recognized even though it does not generate a visible perceptual sign. In contrast, the percept of an Ehrenstein disk in Figure 1B is a modal percept because it generates a brightness difference between the interior and the exterior of the disk, even though the background luminance is uniform throughout the image.

An analysis of the conditions that lead to modal versus amodal percepts can be used to shed light on the larger question of how an image or a scene is parsed into object representations, how the processes of visual perception and object recognition are related, how an observer can be conscious of both visible and amodal percepts, and how these distinct perceptual representations contribute to adaptive behavior during a typical perception–action cycle. Data of this kind also can be used to clarify how a percept, whether modal or amodal, achieves its perceptual

---

Stephen Grossberg, Department of Cognitive and Neural Systems and Center for Adaptive Systems, Boston University.

The research in this article was supported by Grant ONR N00014-92-J-4015 from the Advanced Research Projects Agency and by Grants ONR N00014-91-J-4100, ONR N00014-95-1-0409, and ONR N00014-95-1-0657 from the Office of Naval Research.

I thank Robin Locke for her valuable assistance in the preparation of this article and Diana Meyers for her assistance with the figures.

Correspondence concerning this article should be addressed to Stephen Grossberg, Department of Cognitive and Neural Systems, Boston University, 677 Beacon Street, Boston, Massachusetts 02215. Electronic mail may be sent via Internet to steve@cns.bu.edu.

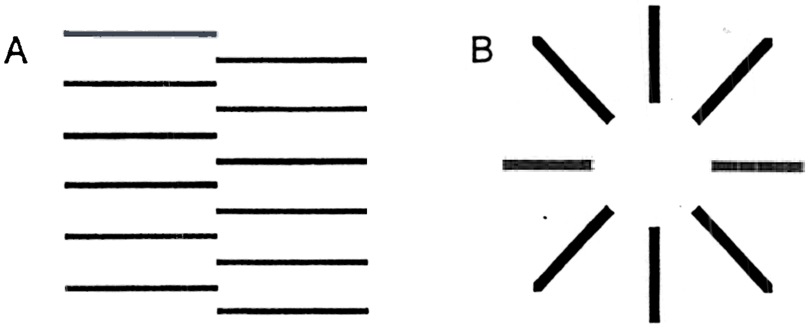

Figure 1. A: The offset black horizontal lines induce a percept of a vertical boundary that can be recognized even though it does not generate a visible brightness or color difference. B: The circular boundary of the Ehrenstein disk becomes visible because it does induce a surface brightness difference between the disk and its surround.

stability. Of particular interest are percepts, both modal and amodal, that are bistable through time and that flip intermittently between alternative percepts of the same image.

2. Perceptual Stratification

Images that undergo perceptual stratification illustrate some of these themes in a vivid way (Kanizsa, 1985; Petter, 1956; Rock, 1993). Figure 2A, for example, is just a combination of interconnected white regions on a black background. Perceptually, however, Figure 2A generates a bistable percept of an occluding object and an occluded object. It can be perceived either as a white cross in front of a white outline square or as a white outline square in front of a white cross. The former percept generally occurs. This is usually attributed to the fact that a thinner structure tends to be perceived behind a thicker one (Petter, 1956).

The stratification percept of Figure 2A raises many issues. How does a cross generate a percept "in front of" a square in a 2-D picture? How does the boundary of the cross get completed across the white regions where it intersects the square? How does the white color within the completed cross boundary get captured into a surface that is surrounded by this boundary and assigned to a depth plane in front of the square? How do the incomplete square boundaries get amodally completed "behind" the cross to facilitate recognition of the square? Why don't the completed square boundaries capture the white color within them where they intersect the cross? When the percept switches, so that the square appears in front of the cross, why do the completed square boundaries succeed in capturing the white color that previously was attributed to the cross, whereas the completed cross boundaries are merely amodally completed behind the square? Why is the percept bistable? Why does the cross win over the square more often than not?

Variants of the image in Figure 2A were used by Kanizsa (1985) to argue against a number of influential positions in the history of perception. One such position was the likelihood principle of Helmholtz (1873), namely, that "we always believe that we see such objects as would, under conditions of normal vision, produce the retinal image of which we are actually conscious." Many other perceptual thinkers have advocated variants of such an inference theory by emphasizing that past experienc can disambiguate an ambiguous stimulus. Notable among then is Gregory (1970).

Kanizsa (1985) introduced Figures 2B–D as counterexamples to this hypothesis. In each figure, the principle of stratification determines the percept in each image region where the intersection of the cross and the square is left ambiguous. The resulting percept is one of the square weaving over and under the cross, even though such a percept is much less likely than one in which the square would appear entirely in front of the cross in each image.

From the present perspective, the images in Figure 2 illustrate subtle relationships between the geometric properties of an image—such as the spatial organization of its edges, textures, and shading—and the contrastive properties of an image—such as the luminance and color differences that help to define the spatial organization. In particular, image geometry does not influence only the boundary representations, and image contrasts do not influence only the surface representations that subserve visual percepts. Instead, I illustrate herein how geometrical and contrastive properties can each influence both boundary representations and surface representations, but in different ways and to different degrees in response to different pictures or scenes.

For example, in Figure 2B, the two pairs of vertical black lines change both the image geometry and the contrast relationships found in Figure 2A. These edges create boundaries that help to capture the intervening white color into a vertical surface of the square that pops out in front of the horizontal bars of the cross. The boundaries of the horizontal bars are then amodally completed behind the square surface, even though the vertical bars of the cross still appear to lie in front of the cross most of the time. This percept raises the question of how the vertical black lines in Figure 2B override the tendency in Figure 2A for the horizontal bars of the cross to complete their boundaries. In particular, what prevents the horizontal boundaries of the cross from penetrating the vertical black lines and creating a bistable percept there, as in Figure 2A? It appears that the horizontal illusory contours that help to complete the cross boundaries in Figure 2A cannot compete effectively with the "real" vertical black lines that induce the complete vertical boundaries in Figure 2B.

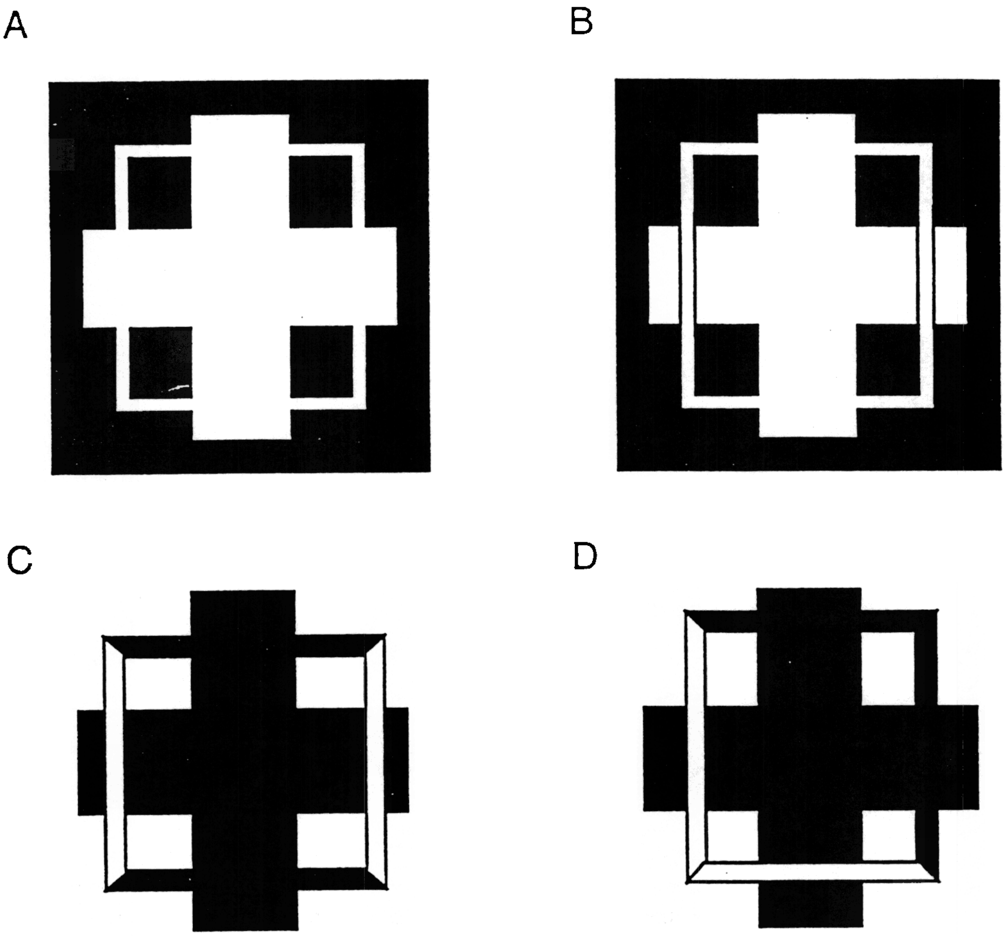

Figure 2. Examples of perceptual stratification. A: The percept of a cross in front of a partially occluded, but amodally completed, outline square is most frequent. B–D: Adding edges and contrast differences to the image in A disambiguates some figure–ground relationships, whereas the others still favor a cross-in-front interpretation. As a result, percepts in which the square is seen to weave over and under the cross are generated, rather than the simpler percepts in which the outline square would appear in front of the cross in each example. *Note.* A is from "Nuove Ricerche Sperimentali Sulla Totalizzazione Percettiva," by G. Petter, 1956, *Rivista di Psicologia, 50.* Copyright 1956 by Giunti: Gruppo Editoriale. Adapted with permission. B–D are from "Seeing and Thinking," by G. Kanizsa, 1985, *Acta Psycologia, 59.* Copyright 1985 by Elsevier Science. Adapted with permission.

In Figure 2C, the vertical black lines in Figure 2B are replaced with the black surface regions of the cross. Here, the vertical black lines on either side of the square are collinearly completed into boundaries that penetrate regions of the cross. These completed vertical boundaries capture the black color that they cover and thereby complete the vertical black edges that bound the square. They also help to capture the intervening vertical white regions so that they form part of the surface representation of the occluding square. As in Figure 2B, the horizontal boundaries of the cross are amodally completed behind the square. Similar processes organize the percept in Figure 2D.

3. Boundary Ownership and T Junctions

The percepts in Figures 2B–D illustrate how a few simple strokes on paper can reorganize the geometry of a figure to support quite different global percepts of occluding and occluded surfaces. Figures 3 and 4 supply additional information about how this happens. The images in Figure 3 are all line drawings. Here, black edges surround uniformly white regions, so changes in image geometry covary with changes in image contrast. In addition, all the edges have the same thickness and contrast with respect to their background. Hence, any perceptual effects of changing edge locations may be attributed primarily to their spatial organization in the image. In contrast, the images in Figure 4 are built up from regions of uniform surface color. Here, there are no changes in image geometry. All perceptual differences are due to changes in image contrast. Thus, the images in Figures 3 and 4 tend to dissociate the effects on perception of changes in image geometry and contrast, respectively.

Due to the fact that the black edges surround uniformly white regions in Figure 3, the boundaries induced by these edges

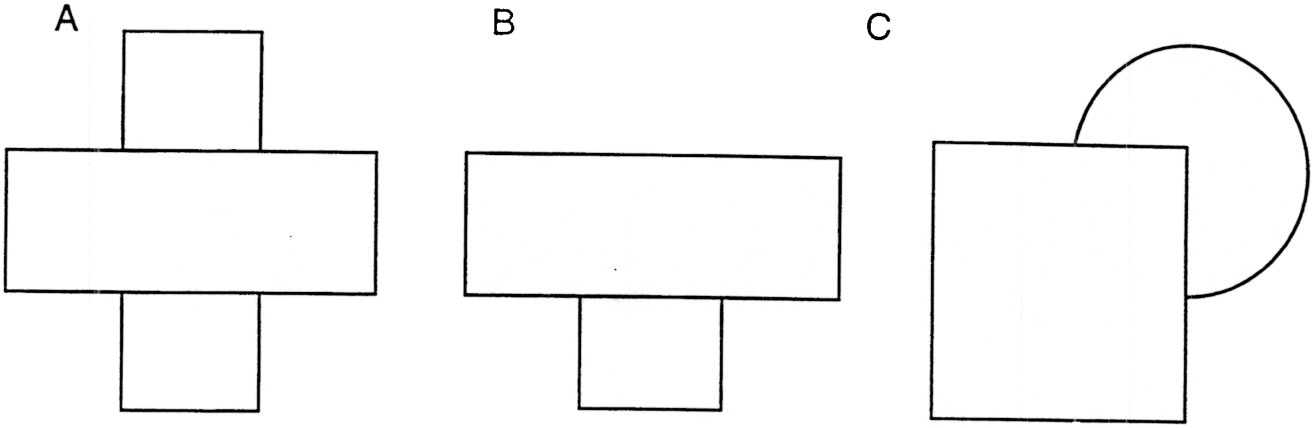

Figure 3. A: The horizontal bar appears to lie in front of a partially occluded vertical bar that is amodally completed behind it. The alternative percept of two vertical bars abutting the horizontal bar is much less frequent. B: Where only one vertical bar exists, its upper horizontal edge still seems to belong to the horizontal bar. C: The square appears to lie in front of a partially occluded circle that is amodally completed behind it. The percept of a Pac-man figure abutting a square is much less frequent. In all these figures, a shared boundary appears to belong to the occluding figure.

determine the final surface organization of each percept. Despite this simplification, the images in Figure 3 raise a number of challenging issues. For example, in Figure 3A, a horizontal bar appears to lie in front of a partially occluded vertical bar that is amodally completed behind it. The alternative percept of two rectangles abutting the horizontal bar is much less frequent, although it provides a more literal description of the image. Why are the horizontal boundaries that are shared by the two abutting rectangles in Figure 3A attributed to only the horizontal bar? This "border ownership" relationship has been noted by a number of scientists (B. L. Anderson & Julesz, 1995; Bregman, 1981; Grossberg, 1994; Kanizsa, 1979; Nakayama, Shimojo, & Silverman, 1989). Once the shared boundaries are attributed to the occluding horizontal bar, the vertical boundaries are somehow freed from interference by these horizontal boundaries and can then amodally complete vertical boundaries behind the horizontal bar.

Figure 3B shows that the process of attributing border ownership does not depend on the existence of collinear boundaries above and below the horizontal bar. When only one rectangle exists below the horizontal bar, the lower horizontal edge still seems to belong to the horizontal bar. In addition, the rectangular vertical bar is perceptually detached from the horizontal bar and appears to be part of a partially occluded object, even though this object does not appear to be amodally completed behind the horizontal bar. This percept hereby suggests that the processes that govern border ownership are initiated locally at the T junctions where the boundaries intersect.

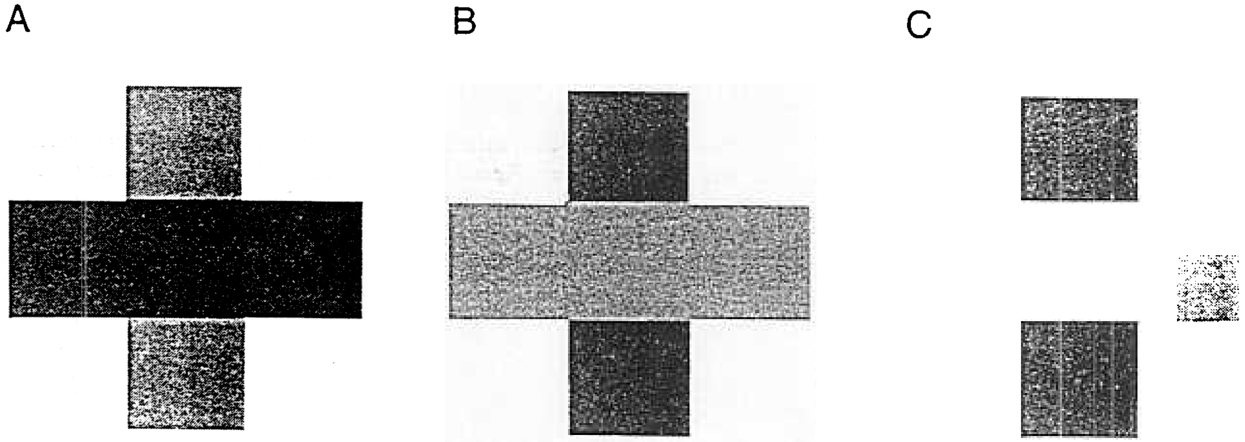

Figure 4. Some images built up from surfaces of uniform color. A: A black horizontal bar is perceived to be in front of a partially occluded, amodally completed vertical bar. B–C: The gray vertical bar usually appears to be in front of the partially occluded black vertical bar, but it is easier in C than in B to perceive the black regions as two separate surfaces.

Figure 3C illustrates a variant of this property. Here, the boundaries shared by the square and Pac-man shapes define two T junctions that are not collinear. These shared boundaries are used to form a percept of an occluding square surface. The remaining Pac-man boundaries at the T junctions are perceptually detached from the square boundaries and are used to amodally complete a curved boundary behind the square. These amodally completed boundaries combine with the modal Pac-man boundaries to initiate recognition of the Pac-man as a (nearly) circular, but partially occluded, object. Amodal boundary completion can hereby occur between boundaries that are not collinear.

In summary, Figure 3 shows that pop-out of an occluding surface can occur if the partially occluded boundaries are collinearly completed behind an occluding surface, as in Figure 3A; if they are completed in a curvilinear fashion, as in Figure 3C; or if they are not completed at all, as in Figure 3B. These cases suggest that local properties at T junctions somehow interact with global properties of each image to trigger the pop-out event.

These percepts raise the question of whether the T junctions in an image are detected by T-junction feature detectors in the brain or whether the brain responds selectively to T junctions even though explicit T-junction cells do not exist. The percept of Figure 2A is suggestive because in the limit of a very thin white square, the regions where the square and the cross intersect define eight T junctions. How, then, can the percept of Figure 2A be bistable if T-junction cells exist in the brain for the purpose of separating the stems of the Ts from their tops? Why wouldn't the cross always win? Yet, how can the cross and the square be separated at all if such cells do not exist? I show how to resolve this paradox below.

4. Cooperation and Competition Between Geometry and Contrast

The images in Figure 4 replicate the same image regions that are in Figure 3A. These regions consist of regions of different luminance rather than changes in bounding edges. The contrasts of the horizontal and vertical bars relative to the background can hereby be reversed. Because these contrast relations change without a change in the bounding forms, any change of percept can be attributed to an interaction between these contrast relationships with respect to the fixed geometry of the forms.

In Figure 4A, as in Figure 3A, the percept is one of a horizontal bar (here, black) in front of a partially occluded, amodally completed vertical bar (here, gray). Figure 4B reverses the contrasts of the horizontal and vertical bars relative to those of Figure 4A and uses the same pair of contrasts in both images. The percept of amodal completion is again the same as in Figure 4A. However, as the contrast of the horizontal bar with the background decreases, as in Figure 4C, there always comes a point when the two black regions do not appear to be amodally completed behind the horizontal bar. Instead, they are perceived as two independent black regions, which even may appear to be closer than the intervening gray bar. The breakdown of amodal completion is most strikingly seen by considering the limiting case in which the contrast of the horizontal bar with the background is zero. Then, the image consists of two black squares on a white background.

A similar point may be made by considering the Bregman–Kanizsa image in Figure 5B (Bregman, 1981; Kanizsa, 1979). As in Figure 4A, the black occluder in Figure 5B appears to pop out in front of the gray fragments. When this happens, the gray fragments can be amodally completed behind the black occluder to make them much more recognizable than are the same set of gray fragments in Figure 5C. Reversing the contrasts between Figures 5B and 5D does not destroy this effect, much as in Figures 4B and 4C. However, a progressive decrease of the occluder's contrast in either Figure 5B or 5D will eventually reach the point that the *B* fragments all appear as independent components, as in Figure 5C, rather than as amodally completed *B* shapes.

Figures 4 and 5 illustrate that image geometry and contrast can cause perceptual boundary and surface processes to either cooperate or compete. In Figure 4A, they cooperate: The black horizontal bar has a larger contrast than the gray bars with respect to the white background. I show below how these contrast relations favor boundary ownership by the black surface of its bounding horizontal edges. The T junctions in the image hereby lose their tops to the occluding object. This attachment process detaches the T tops from their stems. This allows the vertical boundaries that end in the T stems to be amodally completed behind the black occluding surface.

In Figure 4C, geometry and contrast compete. The T-junction geometry still favors pop-out of the horizontal bar, but the reversal of contrast between the vertical and horizontal bars does not. Instead, strong vertical black–white edges and very weak horizontal gray–white edges can prevent the detachment of T tops from their stems. The strong black–white and black–gray edges can then create square boundaries that combine to surround the black surfaces, thereby altering the final percept.

5. Pop-Out and Transparency in Percepts of White Displays

Figures 2–5 illustrate how different combinations of geometric and contrastive image properties can lead to different percepts of occluding objects in front of amodally completed occluded objects. In all these cases, the occluding objects appear to be opaque, and the occluded objects are amodally rather than modally completed behind them. Moreover, the completion of occluding and occluded object forms does not have a major effect on perceived brightness.

To more completely understand how image geometry and contrast work together, consider Figure 6, White's (1979) assimilation display. In this image, the same set of contrasts is arranged differently within the same image geometry to generate different percepts. Below, these percepts also are traced to interactions between geometric and contrastive effects on perceptual boundaries and surfaces. In particular, although the gray vertical bars on both sides of the figure have the same luminance, they generate strikingly different brightness percepts. If this percept were due simply to brightness contrast, the gray bars on the left, being primarily on a background of vertical white bars, would look darker than those on the right, which are primarily on a background of vertical black bars. The opposite percept is obtained, which is why the percept is often cited as an example

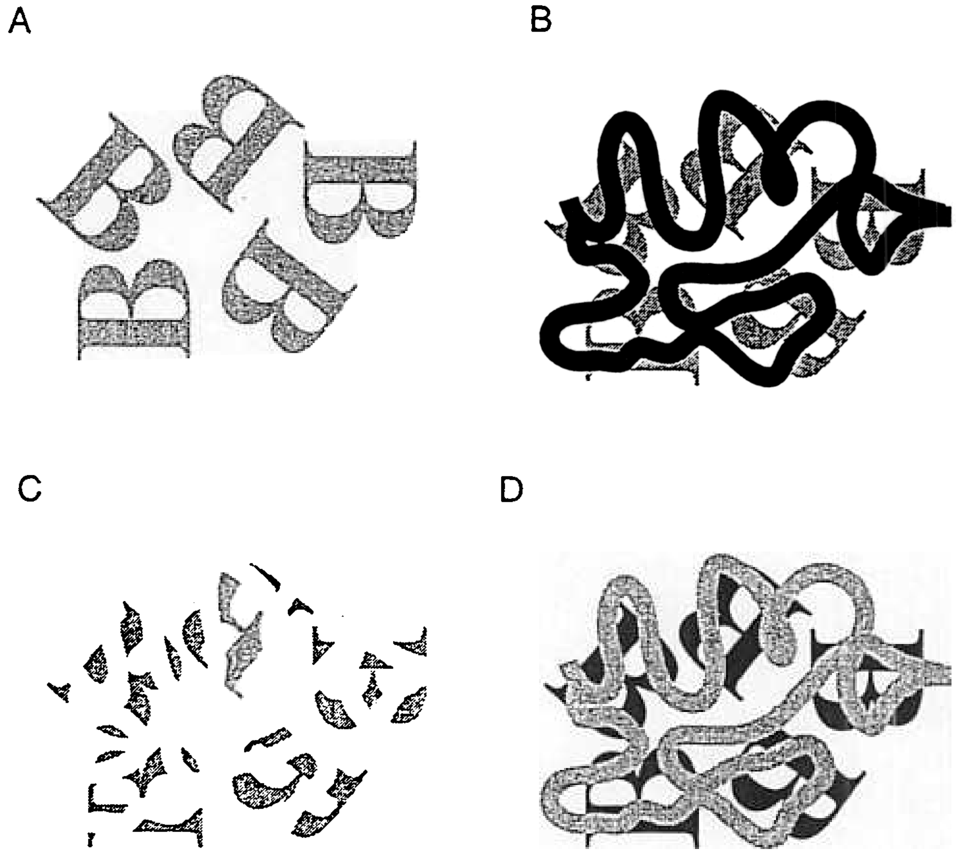

Figure 5. Role of occluding region in recognition of occluded letters. A: Uppercase gray *B* letters. B: *B* letters appear to be partially occluded by a black snakelike occluder. C: Same *B* shapes as in B, except the occluder is white and therefore merges with the remainder of the white background. Although the exposed portions of the letters are identical in B and C, they are much better recognized in B. This difference in recognition correlates with the perception that the black occluder pops out in front of the gray *B* fragments, thereby enabling the gray *B* fragments to be amodally completed behind the black occluder. The black occluder also appears to own the boundaries between it and the *B* fragments. D: Reversal of the figure–ground colors in the Bregman–Kanizsa image (Bregman, 1981; Kanizsa, 1979) in B still supports pop-out of the gray occluder in front of the partially occluded *B* shapes unless the gray gets so close to white that a percept like that in C is obtained. *Note.* C is from "Stereoscopic Depth: Its Relation to Image Segmentation, Grouping, and the Recognition of Occluded Objects," by K. Nakayama, S. Shimojo, and G. H. Silverman, 1989, *Nature, 320,* p. 26x. Copyright 1989 by Macmillan Magazines Ltd. Adapted with permission.

of brightness assimilation by the flanking black or white bars to the gray bars.

The White (1979) effect has generated a considerable amount of experimental activity (e.g., Moulden & Kingdom, 1989; Spehar, Gilchrist, & Arend, 1995; White, 1981; Zaidi, 1990). The discussion below focuses on properties that distinguish the White effect from simple brightness assimilation. For example, even though the White effect is stronger at high spatial frequencies, it does not disappear at low spatial frequencies (White, 1979), unlike the standard assimilation effect described by Helson (1964). Several researchers have proposed that filters with specialized properties may help to generate the effect. White (1981) suggested that three separate processes contribute: (a) lightness contrast, (b) lightness assimilation due to the inability of the visual system to resolve grating contrasts at high spatial frequencies, and (c) lightness assimilation due to pattern-specific lateral inhibition between the test regions and their surrounds. Moulden and Kingdom proposed that two processes are involved: a local one that is sensitive to the corners where the gray bars intersect the black and white grating bars and a longer range process that is proposed to involve orientationally elongated cortical filters. Zaidi (1990) argued that Moulden and Kingdom's analysis was insufficient and that "a number of subsequent stages, including a spatial integration stage, would have to be added to their model for it to be an adequate description of White's effect" (p. 1254). The nature of these subsequent stages has been clarified by experiments by Spehar et al. (1995), who showed that White's effect occurs when the luminance of the target patches falls between that of the inducing stripes of the square wave pattern. They concluded that "this

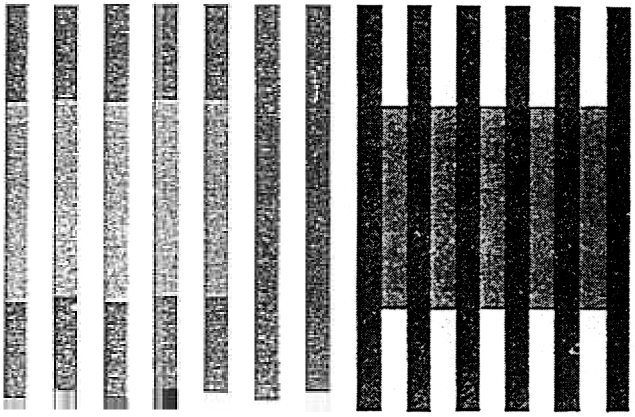

Figure 6. The White (1979) effect: The gray vertical bars have equal luminance in both cases, but the bars on the left look lighter than the bars on the right.

critical role of luminance relationships is not predicted by existing models of these illusions" (p. 2603) and that "other factors related to more global perceptual interpretation of the displays (suggested by existing T-junctions, X-junctions, transparency) might be responsible" (p. 2613). The present analysis is restricted to how these more global factors may contribute.

In particular, the display in the right side of Figure 6 shares some properties of the Bregman–Kanizsa display of Figure 5B (Bregman, 1981; Kanizsa, 1979). In this comparison, the vertical black bars in Figure 6 play the role of the black occluder in Figure 5B, and the shorter gray bars play the role of the *B* fragments. As in the Bregman–Kanizsa percept, when the black bars of the White percept pop out, the boundaries of the gray rectangles can be amodally completed behind them. Then, the white and gray regions lie on a more distant "depth plane" than the black occluding bars. When this happens, the perceived darkening of the gray bars can be explained as a brightness contrast effect due to the white background on this depth plane.

Spehar et al.'s (1995) data can be interpreted in light of this explanation as follows: The conditions under which they observed a strong White effect are the same conditions under which geometry and contrast cooperate to generate a figure–ground percept. In the analysis given in Section 19, pattern-specific inhibition plays a role, as White (1981) proposed, but a role that influences the conditions for figure–ground separation rather than lightness assimilation per se.

A similar percept may be generated by the image in the left side of Figure 6. Here, when the white bars appear to be occluders, then the horizontal black–gray edges can be amodally completed behind them. The gray surface can then appear lighter because of brightness contrast from the black background on this depth plane.

An alternative percept also can be generated by this image because of a shift of attention within an individual observer or because of individual differences in the balance between geometrical and contrastive factors across individuals. In this percept, horizontal illusory contours join the black–gray edges. When this happens, the gray bars may be perceived as part of a transparent white surface that lies in front of the black bars. The lightness of the bars can then be increased by assimilation from the white bars for reasons that I discuss below.

In summary, Figures 4 and 6 show that a change of contrast relations in an image without a change in its geometry can lead to either 3-D pop-out or not, as in Figure 4, or to either opaque or transparent surface percepts, as in Figure 6. These various percepts also call attention to the issue of how brightness contrast can be restricted to a prescribed depth plane even when there are no explicit depth cues in a 2-D image.

6. Interactions Between Brightness and Depth: Boundary–Surface Consistency

Figures 2–6 illustrate how different combinations of geometric and contrastive image properties can lead to different percepts of occluding objects in front of occluded objects. In this section, I summarize data that show that the magnitude of the perceived depth difference between occluding and occluded objects can covary with the amplitude of the perceived brightness difference. Moreover, such a covariation of brightness and depth does not require that a percept of an occluded object occurs. Rather, it is sufficient for regions of differing brightness and depth to be adjacent, as in Figure 3B.

Many researchers have studied the effects of brightness on perceived depth. Egusa (1983) summarized the literature, going back to Ashley (1898), showing that the object having the greater brightness contrast with the background is perceived to be nearer. In his own experiments, Egusa used a stimulus consisting of two adjacent hemifields of different brightness (Figure 7A). The participant was asked to state which appeared nearer and to judge the perceived depth between them. These studies confirmed earlier ones that demonstrated the brightness–depth interaction. Egusa interpreted these results as a reflection of the process whereby figure–ground separation occurs.

In Egusa's (1983) study, there was no percept of a partially occluded object. Such a percept does occur when an observer views a Kanizsa square under appropriate viewing conditions (Figure 7B). Several studies have shown that the square's apparent brightness and depth covary relative to the picture background (Bradley & Dumais, 1984; Kanizsa, 1955, 1974; Purghé & Coren, 1992). In addition, the square appears to partially occlude the four circular disks at its corners, leaving only four Pac-man regions visible.

The Kanizsa square percept is particularly challenging because both the square itself and its brightness difference relative to the background are visual illusions. Why should an illusory brightness difference lead to a percept of perceived depth and occlusion? A recurrent theme in this experimental literature concerns the possible role of cognitive knowledge about figure and ground. A knowledge-based argument is difficult to sustain when such percepts are generated using inducers that generate unfamiliar shapes, rather than familiar shapes such as squares. It is also not clear from this perspective why a depth difference is perceived under the reduced conditions used by Egusa and his predecessors.

The explanation that is suggested below is given in terms of interactions between mechanisms that reconcile geometrical and contrastive constraints on image perception. In particular, the boundary and surface representations that comprise a pictorial

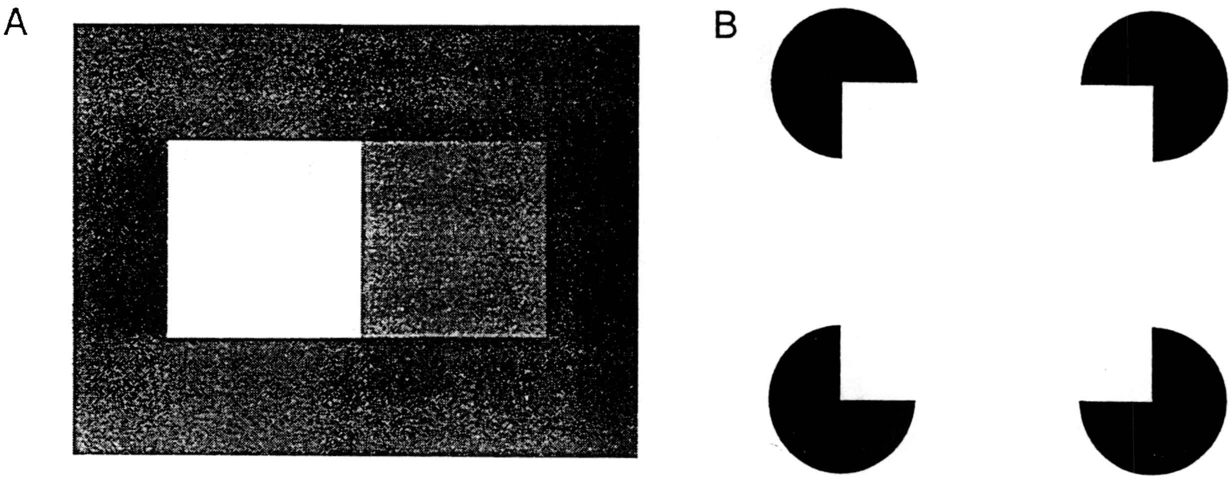

Figure 7. Brightness–depth interactions. A: The hemifield with greater contrast with respect to the background tends to look closer. B: The illusory Kanizsa square tends to look closer as it is made to look brighter by varying the size, shape, or spacing of its inducers.

percept need to be mutually consistent. The explanation in Section 22 suggests how feedback interactions between these representations achieve boundary–surface consistency. Real or illusory brightness differences that emerge in the surface representations use this feedback process to reorganize the boundaries to support a perceived depth difference, as well as whatever amodal completions of partially occluded objects are consistent with the image.

7. Are Both Boundaries and Surfaces Amodally Completed?

When amodal completion occurs, as in the stratification images in Figure 2, the rectangular images in Figure 3, or the Bregman–Kanizsa images (Bregman, 1981; Kanizsa, 1979) in Figure 5, an observer can recognize that completion has occurred despite the absence of visible perceptual signs. One way to think about this is in terms of boundary completion. That argument goes as follows: At pairs of T junctions where occluding and occluded object boundaries intersect (say, in Figure 5), the occluded object boundaries use the stems of the Ts to complete themselves behind the surface of the occluding object. It is then argued that boundaries are perceptually invisible within the brain system wherein they are formed. Boundary visibility is, instead, attributed to the brain system wherein surfaces are formed. Thus, if one can explain how occluded boundaries are completed and why their occluded surfaces are not also completed, then a basis for recognizing but not seeing amodal percepts would be achieved. An explanation of this type was developed by Grossberg (1994).

Although such an argument contains a strong kernel of truth, it may not be sufficient to explain all amodal percepts, as one realizes by inspecting several types of images. For example, in Figures 2A and 2B, one has the strong impression that the amodal completions of the square are white, yet in Figures 2C and 2D, they seem to be black. One could argue in these cases that these impressions are based on the likelihood principle (Helmholtz, 1873) or other hypothesis-testing theories of vision and might have little to do with a perceptual process per se. By such an argument, the amodal percepts could be attributed to amodal boundary completion (which is needed to recognize the completed form in the first place, as in the Bregman–Kanizsa *B* images in Figure 5), and this amodal boundary percept combines with a cognitive hypothesis about the occluded surface that is based on prior experience.

The percepts generated by Figure 8 and many related images make such a cognitive argument difficult to support. Kanizsa (1979) noted that likelihood or other hypothesis-testing arguments would argue for amodal continuation of the checkerboard pattern behind the occluding circular disks. Instead, one has the strong impression that a white cross lies behind the upper left disk and that a black cross lies behind the lower right disk. This percept also was used by Kanizsa to argue against the Gestaltist principle of Prägnanz. Prägnanz proposes that perception works to achieve the most structurally coherent and maximally regular configuration that is possible from an image—in this case, a checkerboard pattern. See Rock (1993) for a discussion of Prägnanz from this perspective.

Figure 8 provides other lessons about perception as well, such as why boundaries are invisible within the brain's boundary formation system and why boundary completion, by itself, cannot explain the amodal percept of a white cross beneath the upper left disk and a black cross beneath the lower right disk. To understand why boundary completion is invisible, note that each gray disk in Figure 8 intersects alternating black and white squares along its perimeter. Each successive square defines a contrast of opposite polarity (black–gray, white–gray) with respect to the disk. These alternating dark–light and light–dark edges combine to form the circular boundary that surrounds the gray disk. Thus, boundaries of opposite contrast polarity, or direction of contrast, are pooled to form the output of the boundary completion system. This conclusion, which was first incorporated into perceptual models in the 1980s (Cohen &

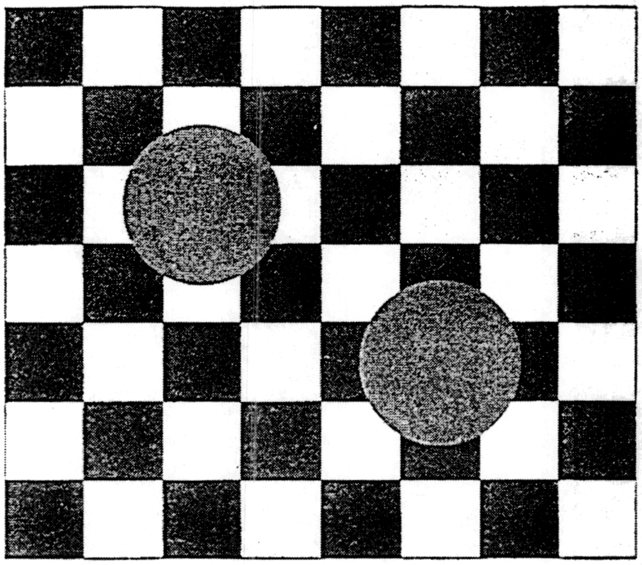

Figure 8. The black and white squares of the background group into long vertical and horizontal boundaries that cross the figure, even though the black–white and white–black edges have opposite contrast polarity, or direction of contrast. The intermediate gray of the disks creates alternating black–gray and white–gray edges that have opposite direction of contrast yet group into unitary disk boundaries. Thus, the boundary system pools signals from opposite directions of contrast to bridge textured and shaded contrast-polarity reversals. In addition, as Kanizsa (1979) noted, amodal completion behind the disks does not lead to the more "likely" perception of squares that the checkerboard would suggest. Instead, one is aware of a white cross and a black cross that are partially occluded by the gray disks. *Note.* From *Organization in Vision: Essays in Gestalt Perception* (p. 97), by G. Kanizsa, 1979, New York: Praeger. Copyright 1979 by Praeger. Adapted with permission of Greenwood Publishing Group, Inc., Westport, CT.

Grossberg, 1984; Grossberg, 1984; Grossberg & Mingolla, 1985a, 1985b), clarifies how the brain can separate object boundaries from their backgrounds in the many situations where texture and shading break the total object boundary into fragments with opposite contrast polarity. By pooling together light–dark and dark–light contrast signals in their outputs, boundaries lose their ability to carry a visible perceptual sign that can distinguish light from dark. In this sense, all boundaries are invisible.

To see why amodal boundary completion may not be sufficient to explain all amodal percepts, suppose that the occluding gray disks pop out and free the contiguous checkerboard boundaries to be amodally completed behind them. The completed amodal percepts of both occluded objects approximate the shape of a cross. This cross boundary is amodally completed, much as the circular boundaries in Figure 3C are completed behind the occluding square. Given that both cross boundaries are the same, another source of information must exist to determine that the upper left occluded region seems to be white whereas the lower right occluded region seems to be black. A likelihood principle (Helmholtz, 1873) explanation would imply that both regions should appear to contain black and white squares, which is false. If hypothesis-testing mechanisms cannot explain the percept, then one must turn to perceptual mechanisms to explain it. In particular, how can an occluded surface not be visible yet nonetheless signify an amodal surface color? How can one be amodally aware of a surface color that one cannot consciously see?

FACADE theory offers neural explanations of all the percepts derived from Figures 1–8. For example, explaining the percept in Figure 8 uses the fact that boundary and surface formation occur progressively over a series of processing stages. The final stage of 3-D surface formation within the model is interpreted to support conscious awareness of visible brightnesses and colors and is the processing stage at which 3-D figure–ground perception of occluding and occluded surfaces occurs. This processing stage was identified with extrastriate cortical visual area V4 by Grossberg (1993, 1994). Data consistent with this hypothesis have been reported by Schiller (1995). An earlier stage of model boundary formation was interpreted to occur in extrastriate cortical area V2 and to project directly to inferotemporal (IT) cortical areas that subserve visual object recognition. As noted above, this boundary signal does not support a visible perceptual sign and thus is predicted to be amodally recognized via the V2 → IT pathway.

This article exploits the fact that, at the same processing level where boundaries are completed, there is a surface formation stage. The boundary representation was interpreted by Grossberg (1993, 1994) to occur in the interstripes (or pale stripes) of area V2, whereas the surface representation was interpreted to occur in the thin stripes of V2 (see Livingstone & Hubel, 1988, for relevant data). In this article, I develop the hypothesis that both the boundary and the surface representations within area V2 project directly to IT object recognition processes. This direct surface projection is predicted to subserve amodal surface recognition, whether or not it is supplemented by a modal surface representation in area V4. FACADE theory posits that the final, modal stage of surface formation in area V4 also projects to object recognition centers. In all, the theory predicts that at least two stages of surface formation are involved in 3-D perception and object recognition: an amodal and a modal, or visible, projection.

Why are two such representations needed, and why does only the latter representation achieve conscious visible perception? It was shown by Grossberg (1994), and is reviewed below, that the early surface representation (V2) selects brightness and color information from each of the two eyes separately before this information is binocularly fused into a final binocular surface representation (V4). These monocular surface representations utilize binocular boundaries (V2) to selectively capture those brightness and color signals that are consistent with the boundaries. Once captured, these signals are selectively bound to a surface representation with the same depth as the boundaries. Such a surface representation, however, uses brightness and color signals from only one eye. I propose that the binocular boundaries and the pairs of binocularly consistent, but monocularly derived, surface representations are all used to form the final binocular surface representation at a subsequent processing level (V4). It is here that occluding and occluded surfaces are fully separated and completed.

Why is only the final binocular surface representation visible? Why are the occluded parts of object surfaces completed amodally in only the earlier surface representation? In addition to carrying out 3-D figure–ground separation, I suggest that the consciously visible sign of the modal surface representation correlates with its role in guiding sensory–motor skills, such as reaching the exposed surface of a visible target. The amodal surface representation may be used by more indirect cognitive processes to organize more complex sensory–motor behaviors, such as reaching behind visible obstacles toward partially occluded objects. This hypothesis suggests one reason why areas like V2 and V4 may have different combinations of projections to recognition, movement, and planning areas such as the temporal cortex, the motor cortex, and the frontal cortex, respectively (Felleman & van Essen, 1991).

8. Review of FACADE Theory

FACADE theory derives its name from its goal of explaining how the brain forms perceptual representations of Form-And-Color-And-DEpth. The theory proposes how human visual systems are designed to complete representations of object boundaries that overcome noise caused by the eyes' optics or barriers caused by occluding objects; to complete surface representations of brightness, color, depth, and form that are invariant under variable illumination conditions; and to learn to recognize salient objects and events in the environment. These three functions are performed by the three main subsystems of the theory: the boundary contour system (BCS), the feature contour system (FCS), and the object recognition system (ORS), respectively, as indicated in the macrocircuit of Figure 9. Grossberg (1994) and Grossberg and Merrill (1996) reviewed experimental evidence that the BCS models aspects of the interblob cortical stream; the FCS models aspects of the blob cortical stream from the lateral geniculate nucleus (LGN) to extrastriate visual area V4 (see Figure 10); and the ORS models aspects of the IT cortex, the frontal cortex, and the hippocampal system, among other structures.

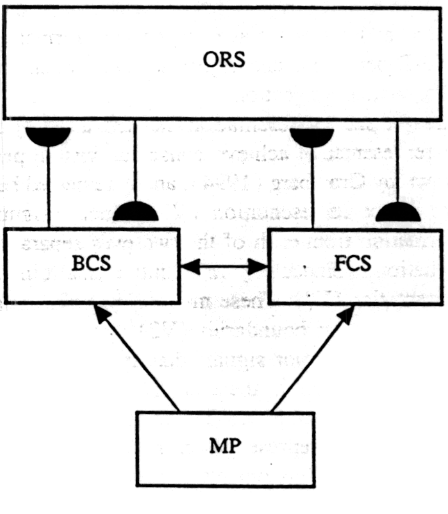

Figure 9. Completed boundaries within the boundary contour system (BCS) can be recognized within the visual object recognition system (ORS) through direct BCS → ORS interactions whether or not they are seen in the feature contour system (FCS) by separating two regions with different filled-in brightnesses, colors, or depths. The monocular preprocessing (MP) stage is defined in Section 8.

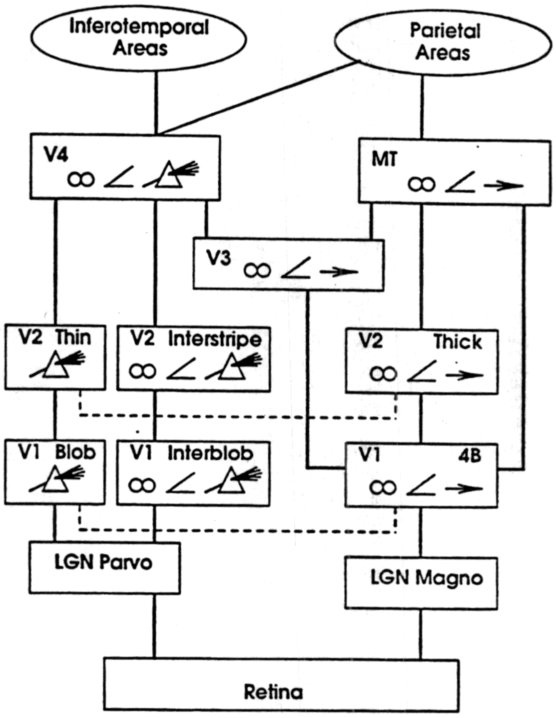

Figure 10. Schematic diagram of anatomical connections and neuronal selectivities of early visual areas in the macaque monkey. LGN = lateral geniculate nucleus (parvocellular [parvo] and magnocellular [magno] divisions). Divisions of visual areas V1 and V2: blob = cytochrome oxidase blob regions, interblob = cytochrome oxidase-poor regions surrounding the blobs, 4B = lamina 4B, thin = thin (narrow) cytochrome oxidase strips, interstripe = cytochrome oxidase-poor regions between the thin and thick stripes, thick = thick (wide) cytochrome oxidase strips, V3 = Visual Area 3, V4 = Visual Area(s) 4, and MT = middle temporal area. Areas V2, V3, V4, and MT have connections to other areas not explicitly represented here. Area V3 may also receive projections from V2 interstripes or thin stripes. Heavy lines indicate robust primary connections, and thin lines indicate weaker, more variable connections. Dotted lines represent observed connections that require additional verification. Icons: rainbow = tuned and/or opponent wavelength selectivity (incidence at least 40%), angle symbol = orientation selectivity (incidence at least 20%), spectacles = binocular disparity selectivity and/or strong binocular interactions (V2; incidence at least 20%), and right-pointing arrow = direction of motion selectivity (incidence at least 20%). *Note.* From "Concurrent Processing Streams in Monkey Visual Cortex," by E. A. DeYoe and D. C. van Essen, 1988, *Trends in Neurosciences, 11,* p. 223. Copyright 1988 by Elsevier Science. Adapted with permission.

A unifying theme that constrains the design of the theory's mechanisms is that there exist fundamental limitations of the visual measurement process. In particular, the computational demands on a system that is designed to detect invariant surface colors are, in many respects, complementary to the demands placed on a system that is designed to detect invariant boundary structures. As summarized in Figure 11, the BCS forms boundaries *inwardly* and in an *oriented* fashion between cooperating

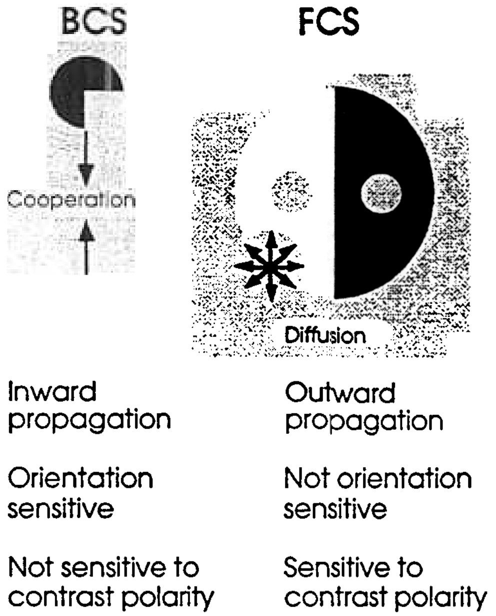

Figure 11. Some complementary computational properties of the boundary contour system (BCS) and the feature contour system (FCS).

pairs or larger numbers of inducers, such as the Pac-men of a Kanizsa square. Moreover, as discussed in Section 7, BCS outputs pool opposite contrast polarities, and in this sense are *insensitive* to contrast polarity, to form object boundaries over regions where contrast reversals exist. The FCS fills in surface properties *outwardly* and in an *unoriented* fashion using a diffusion of activity that is contained by BCS boundaries. The FCS generates visible representations that are *sensitive* to contrast polarity.

To compute their complementary properties, the BCS and the FCS process the signals from each monocular preprocessing (MP) stage in parallel (see Figure 9). Interactions between the BCS and the FCS overcome their complementary deficiencies. The macrocircuit in Figure 12 summarizes how levels of the BCS and the FCS interact through multiple feedforward and feedback pathways to generate a visible 3-D surface representation of occluding and occluded objects at the final level of the FCS, which is called the *binocular Filling-In Domain* (FIDO), that is proposed to occur in area V4. How this is accomplished in the theory is reviewed below to set the stage for explaining the percepts generated by Figures 1–8.

In addition to the complementary relationship between the BCS and the FCS, there also exist informational uncertainties at individual processing levels within each of these systems. For example, the computations within the FCS that reduce uncertainty due to variable illumination conditions create new uncertainties about surface brightnesses and colors that are resolved at a higher FCS level by the diffusive process that fills in surface properties such as brightness, color, and depth. The computations within the BCS that reduce uncertainty about boundary orientation create new uncertainties about boundary position that are resolved at a higher BCS level by a process of boundary completion. FACADE theory describes how the visual system as a whole can compensate for such uncertainties using both parallel and hierarchical stages of neural processing. The theory hereby articulates the hypothesis that the visual system is designed to achieve heterarchical compensation for uncertainties of measurement (Grossberg, Mingolla, & Todorović, 1989).

The review of FACADE theory is given in two stages. First, the monocular mechanisms of the BCS and the FCS are described to clarify the basic boundary and surface operations. Then, the binocular extension of FACADE theory is reviewed to introduce the processing stages that are needed to explain the types of percepts surveyed above. These summaries are given in heuristic terms to bring out the main ideas. Readers who desire mathematical descriptions with supportive computer simulations of other data can find them in a number of recent articles (Francis & Grossberg, 1996a, 1996b; Francis, Grossberg, & Mingolla, 1994; Gove, Grossberg, & Mingolla, 1995; Grossberg & McLoughlin, in press; Grossberg, Mingolla, & Williamson, 1995). These simulations collectively demonstrate that the FACADE theory mechanisms discussed herein actually work as described below.

9. A Monocular Boundary Contour System Model of Cortical Boundary Segmentation

The BCS consists of multiple copies, each with cells whose receptive fields are sensitive to a different range of image sizes. Each BCS copy consists of a filter followed by a grouping, or boundary completion, network. There are two parallel BCS architectures. The static BCS models the formation of static boundary segmentations by a cortical processing stream that begins in the LGN and ends in extrastriate cortical area V4 (DeYoe & van Essen, 1988). This processing stream passes through the interblobs of cortical area V1 and the interstripes of cortical area V2. This LGN parvo → interblob → interstripe → V4 processing stream is depicted in Figure 10. The motion BCS models boundary segmentations that are derived from moving forms by the LGN magno → 4B → thick stripe → MT processing stream depicted in Figure 10. The summary in this section considers only the static BCS, and only a single scale of its monocular processing properties, before generalizing to the multiscale binocular case. For summaries of the motion BCS, see Chey, Grossberg, & Mingolla, (1995, in press); Francis and Grossberg (1996b); Grossberg and Mingolla (1993, 1994); and Grossberg and Rudd (1989, 1992).

The static BCS summary omits details that are not needed for this exposition. In particular, details of cell receptive field structure and feedback from V1 to the LGN are omitted. For these additional features, which are not needed to explain the targeted data, see Gove et al. (1995) and Grossberg et al. (1995). Habituative processes within the BCS are summarized, when they are needed, in Section 20. The remaining monocular BCS operations are now described.

The model LGN ON and OFF cells receive input from retinal ON and OFF cells. ON cells are turned on by increments in image contrasts, whereas OFF cells are turned off (see Schiller, 1995, for a review). Because these ON and OFF cells have antagonistic surrounds and obey membrane, or shunting, equations, they help to discount the illuminant, normalize image activities, and extract ratio contrasts from an image (Grossberg, 1983). These image preprocessing properties are needed to simulate even the most basic brightness percepts (Grossberg & Todorović, 1988).

The LGN cell outputs activate the first stage of cortical BCS processing, the simple cells (see Figure 13A). Simple cells are oriented local contrast detectors that respond to a prescribed contrast polarity, or direction of contrast. Spatially displaced LGN ON and OFF cells input to pairs of like-oriented simple cells that are sensitive to opposite directions of contrast. These simple-cell pairs compete before their net activities are half-wave rectified to generate output signals; Ferster (1988) and Liu, Gaska, Jacobson, and Pollen (1992) reported relevant data. The outputs from these oppositely polarized simple cells of like orientation are added at like-oriented complex cells. By pooling outputs from oppositely polarized simple cells, complex cells respond to both polarities, as do all subsequent BCS cell types in the model. In this sense, complex cells are rendered insensitive to direction of contrast. That is how "all boundaries are invisible" arises in the model.

Complex cells activate hypercomplex cells (also called end-stopped complex cells) through an on-center, off-surround network, or spatial competition, whose off-surround carries out an end-stopping operation (see Figure 13A). Through this interaction, complex cells excite hypercomplex cells of the same orientation and position while inhibiting hypercomplex cells of similar orientation at nearby positions. One role of this spatial competition is to spatially sharpen the neural responses to oriented luminance edges. Another role is to initiate the process, called *end-cutting,* whereby boundaries are formed at line ends with boundary orientations that are perpendicular or oblique to the orientation of the line itself, as in Figure 1.

The pooling of oppositely polarized, half-wave rectified signals at complex cells has the same net effect as an oriented, full-wave rectified filter. The sequence of filtering (by simple cells) followed by full-wave rectification (by complex cells) and subsequent lower frequency-oriented filtering (by hypercomplex cells) has become standard in models of texture segregation (Bergen & Landy, 1991; Malik & Perona, 1990; Sutter, Beck, & Graham, 1989) since its introduction in the BCS by Grossberg & Mingolla (1985b).

These processing stages do more than separate texture regions. In particular, the hypercomplex cells input to higher order hypercomplex cells that compete across orientations at each position. This competition acts to sharpen orientational responses at each position. It also completes the end-cutting operation that was initiated at the hypercomplex cells. In the model, end-cuts are fuzzy groupings of higher-order hypercomplex activations in orientations that are almost perpendicular to an inducing line end (see Figure 14). How and why end-cuts are formed is described below.

These two stages of spatial and orientational interaction enable higher order hypercomplex cells to generate a collinear response due to the line itself, as well as a band of almost perpendicular end-cuts (Figure 14B). The collinear responses to lines can support collinear illusory contour formation between an array of spatially disjointed collinear lines (Figure 15A). The end-cut responses enable illusory contours to form perpendicular to, or at oblique angles with, a set of inducing lines (Figure 15B), as in the computer simulation of the Ehrenstein illusion summarized in Figure 16. End-cuts also are seen in Section 14 to play a key role in detaching the boundaries of occluded objects from those of occluding objects. Taken together, the simple, complex, and hypercomplex cells of the model are called the *static-oriented contrast* (SOC) *filter*.

Outputs from the higher-order hypercomplex cells feed into bipole cells that initiate long-range boundary grouping and completion (Figure 13A). Bipole cells have two oriented receptive fields. Their cell bodies fire if both of their receptive fields are sufficiently activated by hypercomplex-cell inputs whose orientation is similar to that of the bipole cell receptive fields. Bipole cells hereby act like a type of statistical and-gate that controls long-range cooperation across the outputs of hypercomplex cells. For example, a horizontal bipole cell is excited by activation of horizontal hypercomplex cells that input to its horizontally oriented receptive fields. A horizontal bipole cell is also inhibited by activation of vertical hypercomplex cells (Figure 13A). This *spatial impenetrability* operation (Grossberg, 1987a; Grossberg & Mingolla, 1987) prevents collinear grouping from occurring across regions wherein noncollinear orientations are present.

Output signals from bipole cells feed back to the hypercomplex cells after undergoing two types of competitive processing. Bipole cell outputs compete across orientation to determine which orientation is receiving the largest amount of cooperative support (see Figure 13B) and across nearby positions to select the best spatial location of the emerging boundary. These competitive interactions are needed because the bipole cell receptive fields are themselves rather broad. Broad bipole cell receptive fields enable the grouping to get started in response to imprecisely aligned image contrasts before the competitive interactions sharpen and spatially deform it. Hypercomplex cells that receive the most cooperative support from bipole grouping further excite the corresponding bipole cells. This cycle of bottom-up and top-down interaction between hypercomplex cells and bipole cells rapidly converges to a final boundary segmentation (see Figure 16C) that completes the statistically most favored boundaries, suppresses less favored boundaries, and coherently binds together appropriate feature combinations in the image. This static-oriented cooperative–competitive feedback circuit may be called the *SOCC loop.* Thus, the SOC filter inputs to the grouping mechanisms of the SOCC loop.

Consider how the SOCC loop completes an illusory contour in response to a Kanizsa figure. Suppose for definiteness that the largest horizontally oriented bipole cell in the network can just span a pair of horizontal Pac-men edges in the Kanizsa figure (Figure 17A). Then, this bipole cell can activate hypercomplex cells near the middle of the Kanizsa figure (Pathway 2 in Figure 17A). After this occurs, many bipole cells in the network can be simultaneously activated by two of the three active hypercomplex locations (as at Pathways 1 and 3 in Figure 17A). The remainder of the illusory contour can then rapidly form in parallel (see Grossberg and Mingolla, 1985a, for illustrative simulations). Because complex cells pool inputs from oppositely polarized simple cells, bipole cells also can form real or illusory contours from oppositely polarized inducers, as when forming the disk boundaries shown in Figure 8.

The main point of the hypercomplex–bipole feedback interaction in Figure 13 is that long-range oriented cooperation interacts with shorter range spatial and orientational competition to

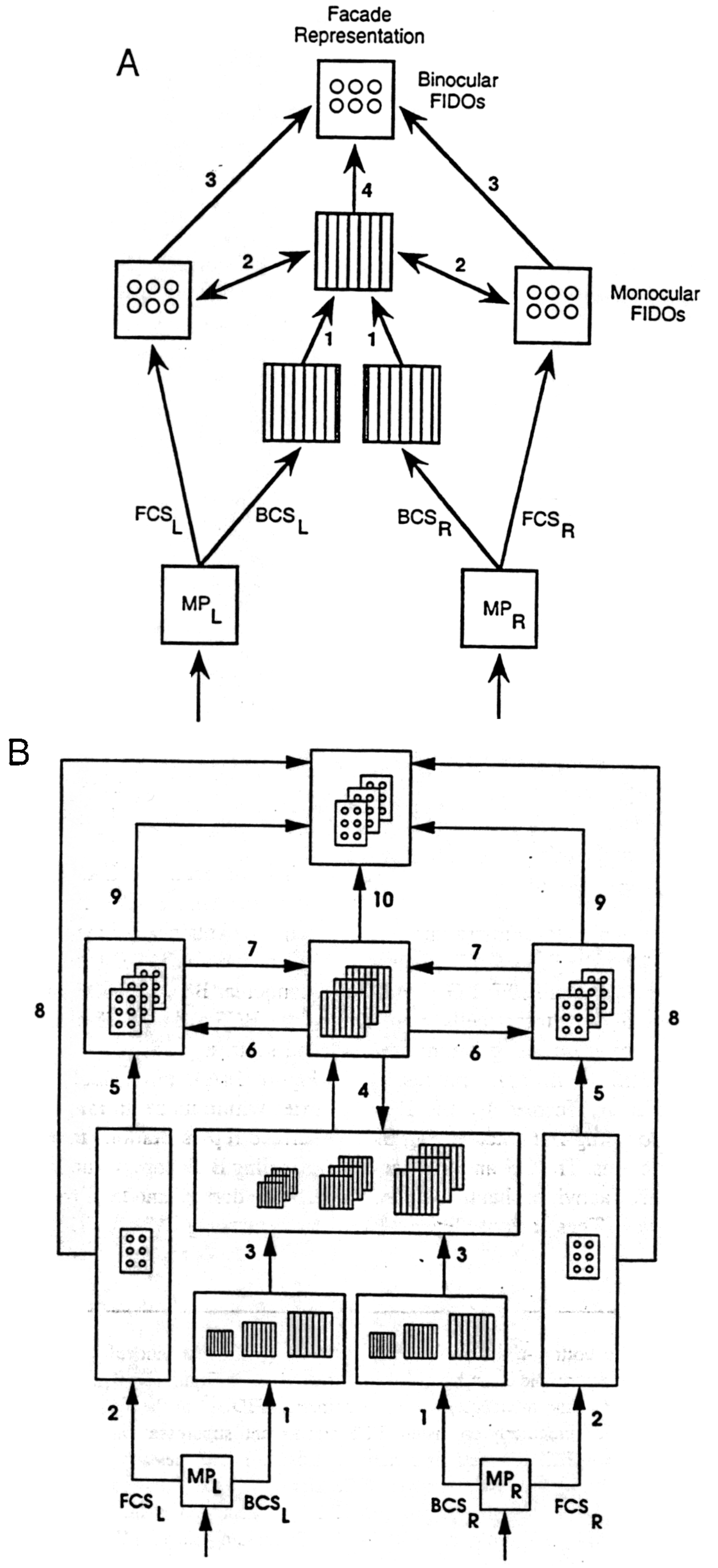

Figure 12. A: Macrocircuit of monocular and binocular interactions of the boundary contour system (BCS) and the feature contour system (FCS) drawn to facilitate comparison with Figure 1 in Grossberg (1987b): Left-eye and right-eye monocular preprocessing stages (MP_L and MP_R) send parallel pathways to the BCS (boxes with vertical lines, designating oriented responses) and the FCS (boxes with three pairs of circles, designating opponent colors). The monocular signals BCS_L and BCS_R activate simple cells,

help select and complete both real and illusory contours. In Figure 13, this is accomplished by a series of processing stages. Grossberg, Mingolla, and Ross (1997) proposed a modified version of this circuit that embodies three refinements of the circuit design. First, the cooperative and competitive network interactions are embedded into a cortical map structure that includes ocular dominance and orientation columns (Blasdel, 1989; Hubel & Wiesel, 1977, 1979). Second, this embedding allows a single type of recurrent spatial competition across the map to realize both spatial competition (across ocular dominance columns) and orientational competition (across orientation columns). Finally, the same cooperative–competitive circuit module that occurs in model area V2 among bipole cells is proposed to also occur, at a smaller spatial scale, in model area V1 among complex cells. In other words, both area V1 and area V2 of the interblob cortical stream are proposed to embody a similar circuit design, albeit at different spatial scales. This refined architecture clarifies why long illusory contours can form in V2 but not in V1 (von der Heydt, Peterhans, & Baumgartner, 1984); why short illusory contours can form in both V1 and V2 (Grosof, Shapley, & Hawken, 1993); why long-range excitatory lateral connections and shorter range inhibitory connections exist in both V1 and V2, albeit with different length scales (Gilbert & Wiesel, 1990; Kisvárday, Toth, Rausch, & Eysel, 1995); and why a spatial impenetrability property exists even in V1 (Kapadia, Ito, Gilbert, & Westheimer, 1995). These circuit refinements are not needed to make the present explanations, although they are consistent with them.

10. Filling-In of Monocular Surface Representations Within the Feature Contour System

Each BCS boundary segmentation generates topographic output signals to the ON and OFF FIDOs (see Figure 13B). These FIDOs also receive inputs from the ON and OFF LGN cells, respectively. The LGN inputs activate their target cells, which allow activation to diffuse rapidly across model gap junctions to neighboring FIDO cells. The diffusive filling-in process is restricted to the compartments that are formed by the BCS boundaries, which create barriers to filling-in by decreasing the permeability of their target gap junctions. The ON and OFF cell inputs, taken together with the diffused activities that they cause, lead to the final filled-in activity levels. These activity levels are not due just to the diffused activities alone. The filled-in OFF activities are subtracted from the ON activities at double-opponent cells. In computer simulations of monocular single-scale versions of the BCS/FCS model, these double-opponent activities represent the surface brightness of each percept (see Figure 13B). Such a double-opponent surface representation is shown in the Ehrenstein brightness simulation in Figure 16D.

The FCS filling-in model provides a computationally precise analysis of the type of filling-in that was classically observed by Krauskopf (1963) and Yarbus (1967) using stabilized images and by Gerrits and his colleagues in patients with retinal scotomata (Gerrits & Timmermann, 1969; Gerrits & Vendrick, 1970). Such an analysis became possible only after it was recognized that there is a parallel BCS system whose boundaries, which are perceptually invisible within the BCS itself, define filling-in compartments within the FCS. These surface filling-in processes have been used to explain classical data about brightness perception (Cohen & Grossberg, 1984; Gove et al., 1995; Grossberg & Todorović, 1988; Grossberg & Wyse, 1991; Pessoa, Mingolla, & Neumann, 1995; Todorović, 1987) and more recent data about brightness and color spreading (Arrington, 1994; Francis & Grossberg, 1996a; Paradiso & Nakayama, 1991; Watanabe & Sato, 1989; Watanabe & Takeichi, 1990). Various other types of data supportive of the BCS/FCS framework are reviewed in subsequent sections of this article.

11. Binocular Boundary Segmentation by the Boundary Contour System

The binocular FACADE theory incorporates the monocular BCS mechanisms into a more comprehensive architecture that helps to explain phenomena about 3-D vision and figure–ground separation. FACADE theory incorporates the operations of the monocular BCS and FCS into a setting wherein multiple copies of the BCS and the FCS exist. These copies represent boundaries and surfaces at different relative depths from an observer (see Figure 18A). In particular, each BCS copy completes boundaries within its depth range. The multiple FCS copies represent surface representations that can fill in at the depths of a corresponding BCS copy. Neural principles from which these systems may be derived and their mechanistic realizations were provided by Grossberg (1994). They were mathematically defined and

which, in turn, activate bottom-up pathways, labeled *1*, to generate a binocular boundary segmentation using the complex-, hypercomplex-, and bipole-cell interactions in Figure 13. The binocular segmentation generates output signals to the monocular filling-in domains (FIDOs) of the FCS via pathways labeled *2*. This interaction captures binocularly consistent FCS signals and suppresses binocularly inconsistent FCS signals. Reciprocal FCS → BCS interactions enhance consistent boundaries and suppress boundaries corresponding to more distant surfaces. The surviving FCS signals activate the binocular FIDOs via Pathways 3, where they interact with an augmented binocular BCS segmentation to fill in a multiple-scale surface representation of form-and-color-and-depth (FACADE). Processing stages MP_L and MP_R are compared with lateral geniculate nucleus data; the simple–complex-cell interaction with cortical area V1 data; the hypercomplex–bipole-cell interaction with cortical area V2 and (possibly) cortical area V4 data, notably about interstripes; the monocular FCS interaction with blob and thin stripe data; and the FACADE representation with V4 data (see Figure 10). Additional interactions from FCS to BCS along pathways labeled *2*, *3*, and *4*, and among FCS and BCS copies, are described in Sections 9–13. B: A finer representation of FACADE interactions.

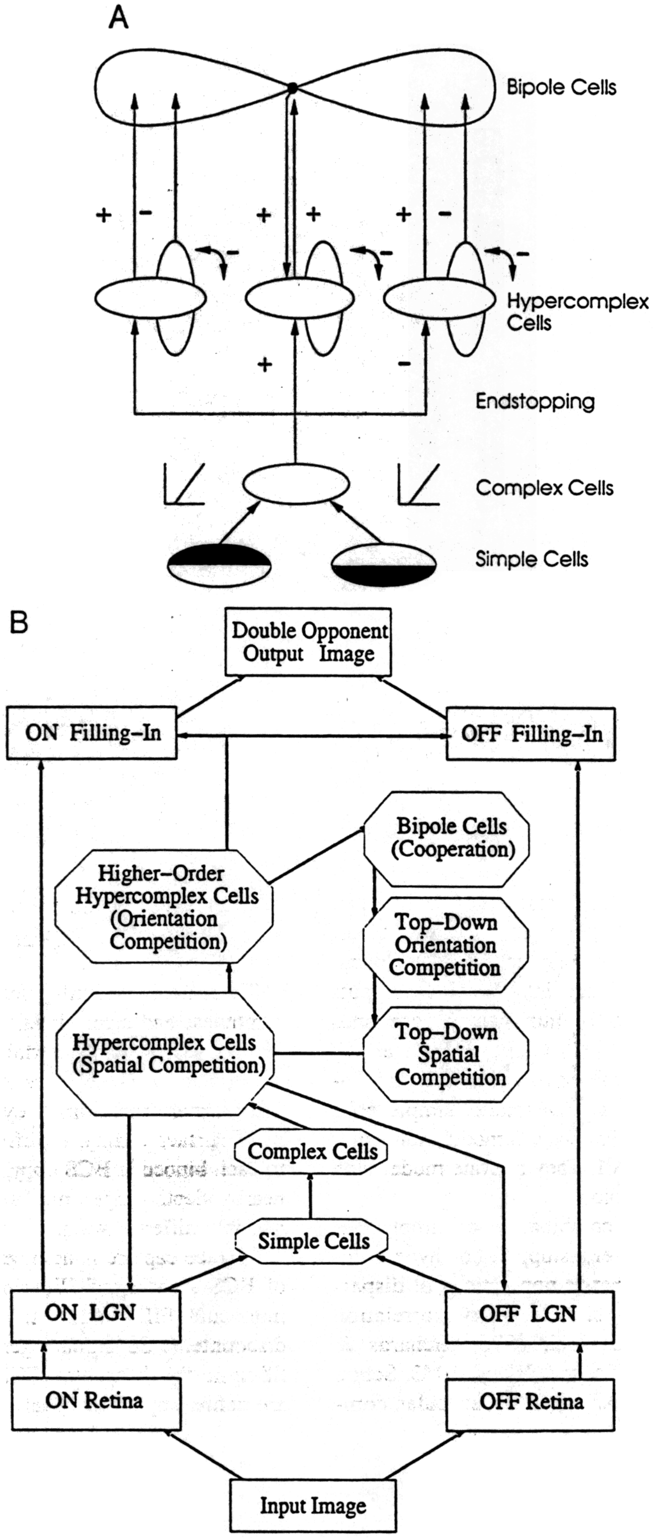

Figure 13. A: Simple cells compute local-oriented contrast. They are sensitive to contrast polarity. Their activities are half-wave rectified to generate output signals. Outputs from oppositely polarized, like-oriented cells are added at complex cells, which thereby compute an oriented full-wave rectification of the image. Complex cells output to an on-center, off-surround filter that activates like-oriented hypercomplex cells at the same position and inhibits similarly oriented hypercomplex cells at nearby positions. The net effect is to end-stop the responses of hypercomplex cells. Hypercomplex cells also carry out inhibition across

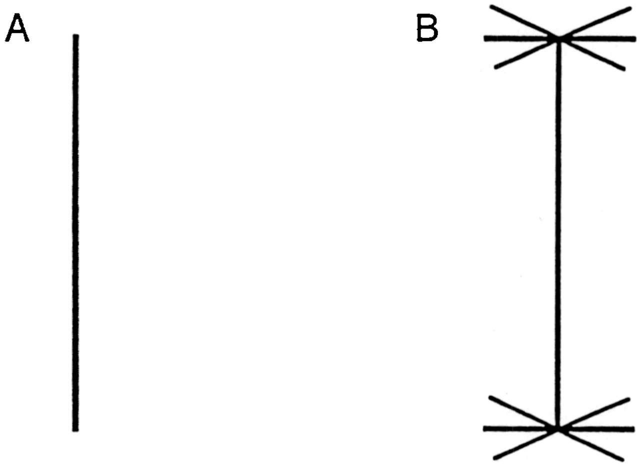

Figure 14. In response to a line (A), hypercomplex cells can generate (B) a collinear response along the line as well as end-cuts at the line end that consist of a fuzzy band of almost perpendicular inducers that can be used to generate noncollinear groupings between sets of line endings.

computationally simulated by Grossberg and McLoughlin (in press). Herein, I give a functional description of the role that each processing stage plays in generating a final percept. Then, I use these processing stages to provide a unified explanation of the targeted data.

The processing stages of FACADE theory are summarized in Figure 12B. Their functional role is briefly outlined below. BCS processing stages are displayed as boxes with vertical lines that designate oriented responses. FCS stages are shown as boxes with three pairs of circles that denote opponent colors. Monocular preprocessing of left-eye ($\mathrm{MP_L}$) and right-eye ($\mathrm{MP_R}$) inputs by the retina and the LGN discounts the illuminant and generates parallel signals to the BCS and the FCS via Pathways 1 and 2, respectively. Pathways 1 model monocular inputs to the interblobs in striate area V1. They activate model simple cells with multiple receptive field sizes. Pathways 2 model monocular inputs to the blobs in striate area V1. They activate model blob cells that are tuned to opponent colors.

Pathways 3 support binocular combination of simple cell outputs at complex and complex end-stopped (or hypercomplex) cells. These interactions generate populations of disparity-sensitive cells that realize a size–disparity correlation (Julesz & Schumer, 1981; Kulikowski, 1978; Richards & Kaye, 1974; Schor & Tyler, 1981; Schor & Wood, 1983; Schor, Wood, & Ogawa, 1984; Tyler, 1975, 1983). In particular, complex cells with larger receptive fields can binocularly fuse a broader range of disparities than can cells with smaller receptive fields (Figure 19). Competition across disparity at each position and among cells of a given size scale sharpens complex cell disparity tuning. Spatial competition (end-stopping) and orientational competition convert complex cell responses into spatially and orientationally sharper responses at hypercomplex cells.

Pathways 4 initiate long-range grouping and boundary completion of the hypercomplex cell outputs by bipole cells. This grouping process collects together the outputs from all hypercomplex cells that are sensitive to a given depth range and inputs them to a shared set of bipole cells. The bipole cells, in turn, send cooperative feedback signals back to these hypercomplex cells (Figure 17B). This feedback process binds together cells of multiple *sizes* into a BCS copy that is sensitive to a prescribed range of *depths*. In this way, each BCS copy completes boundaries within a given depth range. Multiple BCS copies with their own SOCC loops are formed, each corresponding to different (but possibly overlapping) depth ranges. This feedback process also uses the responses from all scales to discover the positionally most accurate alignment of boundaries that can be created within each depth range. For example, at a high curvature boundary, smaller scales can better track the boundary and cooperate with each other, whereas larger scales generate a spatially scattered response and suppress each other through spatial competition. See Griffiths and Chubb (1993), Klein and Stromeyer (1980), Quinn (1985), Sagi and Hochstein (1984), and Wilson and Richards (1989) for relevant data.

12. Three-Dimensional Surface Formation Within the Feature Contour System

These multiple depth-selective BCS copies are used to capture brightness and color signals within depth-selective FCS surface representations. These surface representations occur on monocular FIDOs, so called because they receive their brightness and color signals from a single eye and support depth-selective filling-in of surface quality. A different monocular FIDO corresponds to each binocular BCS copy, although BCS copies that represent nearby depth ranges may send convergent signals, albeit with possibly different weights, to a single monocular FIDO.

Surface capture is achieved by a suitably defined interaction of BCS signals and illuminant-discounted FCS signals at the monocular FIDOs. As in the monocular FCS model, illuminant-discounted FCS signals generate a surface representation by filling-in the discounted FCS signals within compartments that are defined by BCS signals. In the monocular model, BCS sig-

---

orientations. The net effect of spatial and orientational competition is to generate end-cuts at line ends and other sudden changes in oriented contrast (see Figure 14). Hypercomplex cells excite like-oriented bipole cells and inhibit perpendicularly oriented bipole cells. The latter inhibition realizes a property of spatial impenetrability that prevents collinear inducers from grouping across noncollinear forms within the same depth plane. Bipole cells fire if they receive enough net excitation from both of their receptive fields. Boundary completion, including illusory contour formation, is thereby initiated. B: Monocular boundary contour system (BCS)–feature contour system (FCS) macrocircuit. BCS stages are designated by octagonal boxes, and FCS stages are designated by rectangular boxes. LGN = lateral geniculate nucleus.

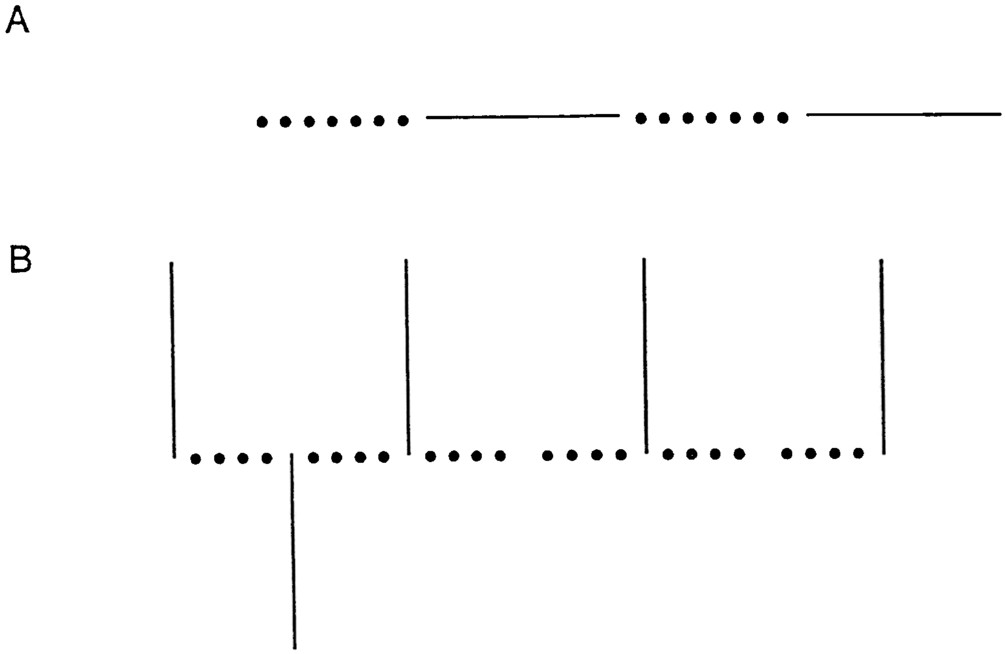

Figure 15. Illusory contours (dotted lines) can be generated both collinear (A) and perpendicular (B) to inducing (solid) lines.

nals function only as barriers, or obstructions, to the diffusion process that carries out the filling-in. In the full FACADE model, BCS signals to the FCS also carry out a selective function. They are filling-in *generators* as well as filling-in *barriers*. Monocular FCS signals that start out with no depth selectivity are captured by these BCS generators on surface representations that code a prescribed range of relative depths from the observer. The same filling-in process that recovers surface brightness and color hereby generates a representation of surface depth and form that is imbued with these perceptual qualities.

The FCS signals reach the monocular FIDOs via Pathways 5. These pathways carry out a one-to-many topographic registration of the monocular FCS signals at all the monocular FIDOs. Pathways 6 carry topographic BCS boundary signals from each BCS copy to its FIDO. These boundary signals selectively capture those FCS inputs from Pathways 5 that are spatially coincident and orientationally aligned with the BCS boundaries. Other FCS inputs are suppressed by the BCS–FCS interaction.

The captured FCS inputs, and only these, can trigger diffusive filling-in of a surface representation on the corresponding FIDO. Because this filled-in surface is activated by depth-selective BCS boundaries, it inherits the same depth as these boundaries. Not every triggered filling-in event can generate a surface representation. Only surface regions that are surrounded by a connected BCS boundary, or fine web of such boundaries, are effectively filled-in. Otherwise, the diffusion of activity dissipates across the FIDO.

Further details of how surface capture occurs are summarized in Grossberg (1994). The remarkable fact is that double-opponent cells, which are familiar as color-processing units in psychophysics (Jameson & Hurvich, 1955; Zrenner et al., 1990) and cortical neurophysiology (Lennie, 1984; Livingstone & Hubel, 1984, 1987), are proposed to carry out the capture property. These double-opponent cells occur, moreover, at the monocular FIDOs, whose surface representations are amodal (viz., not visible). Thus, the model predicts that a cell that has the double-opponent property is not necessarily carrying out a visible color-processing function.

As another example of paradoxical data that the monocular FIDOs clarify, consider the model property that boundaries become binocular at an earlier stage than do surfaces. The model suggests that boundaries are computed within the interblob cortical stream and that surfaces are computed within the blob stream. This linkage is consistent with the fact that interblob complex cells in V1 are already fully binocular whereas blob cells in V1 are monocular (Hubel & Wiesel, 1977; Livingstone & Hubel, 1984).

13. Boundary–Surface Consistency, Interstream Feedback, and the Asymmetry Between Near and Far

These BCS boundaries and FCS surfaces are formed by different, indeed complementary, processes. An analysis in Grossberg (1994) showed that too many boundary and surface fragments are formed as a result of the size–disparity correlation and the way in which monocular and zero-disparity boundaries combine with nonzero-disparity boundaries. Somehow these extra boundaries and surfaces need to be pruned. Pruning is realized by the process whereby the complementary boundary and surface properties interact to achieve boundary–surface consistency. Remarkably, many data about the perception of occluding and occluded objects may be explained as consequences of this pruning operation.

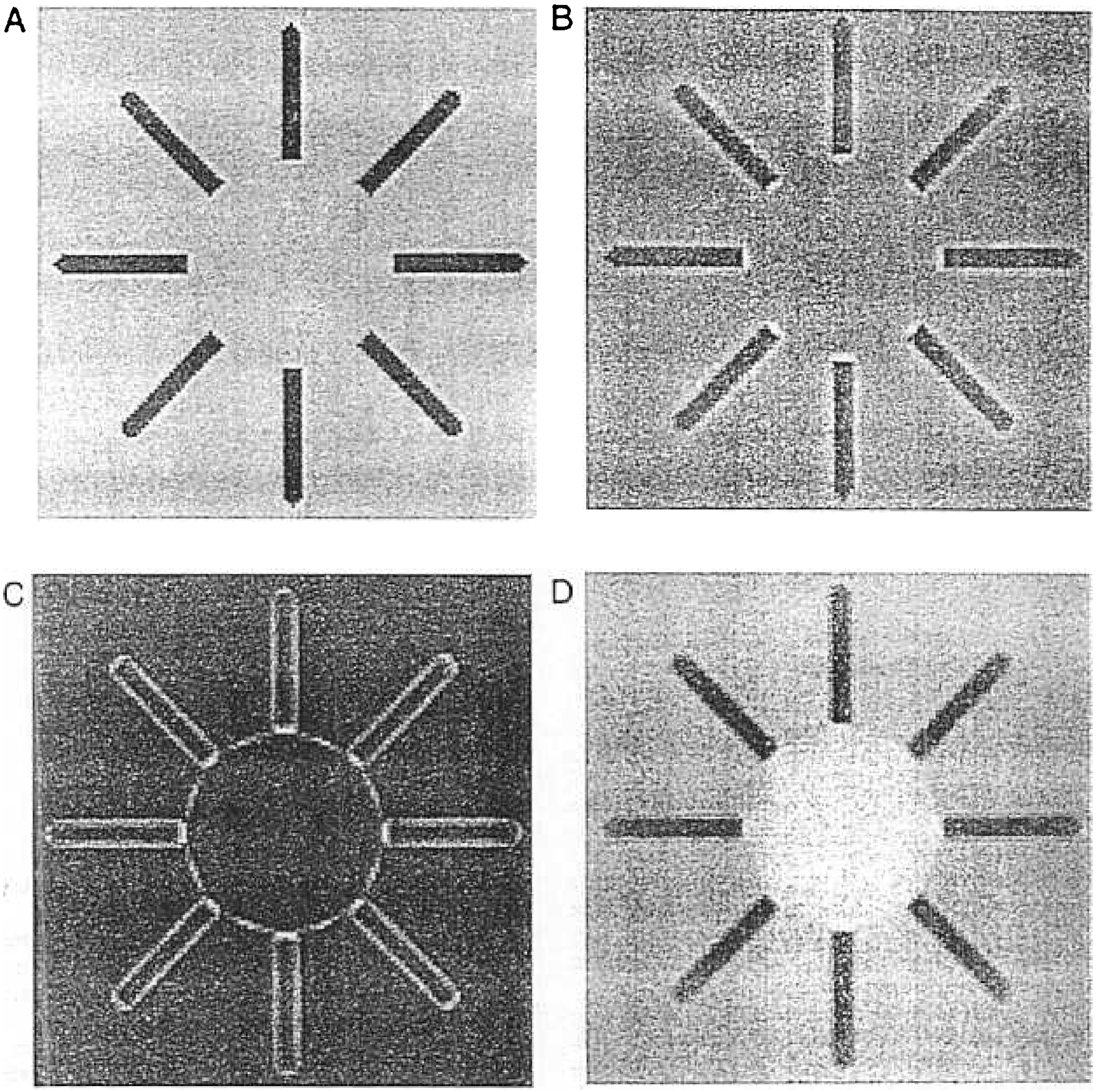

Figure 16. A: The Ehrenstein figure. B: The lateral geniculate nucleus stage response. Both ON and OFF activities are coded as rectified deflections from a neutral gray. Note the brightness buttons at the line ends. C: The equilibrium boundary contour system boundaries. D: Filled-in surface representation. The disk contains stronger featured contour system signals than the background, corresponding to the perception of increased brightness. *Note.* A–D are from "Brightness Perception, Illusory Contours, and Corticogeniculate Feedback," by A. Gove, S. Grossberg, and E. Mingolla, 1995, *Visual Neuroscience, 12,* p. 1034. Copyright 1995 by Cambridge University Press. Reprinted with permission.

Boundary–surface consistency is achieved via Pathways 7 in Figure 12B. Pathways 7 are activated by the contours of successfully filled-in surface regions at the monocular FIDOs. These FCS-to-BCS feedback signals excite the BCS boundaries corresponding to their own positions and depths (Figure 20B). The boundaries that activated the successfully filled-in surfaces are hereby strengthened. The feedback signals also inhibit redundant boundaries at their own positions and larger depths (Figure 20C). This inhibition from near to far is the first example within the theory of the asymmetry between near and far. It is called *boundary pruning.* Boundary pruning spares the closest surface representation that successfully fills in at a given set of positions.

Boundary pruning also removes redundant copies of the boundaries of occluding objects. When the competition from these redundant occluding boundaries is removed, the bound-

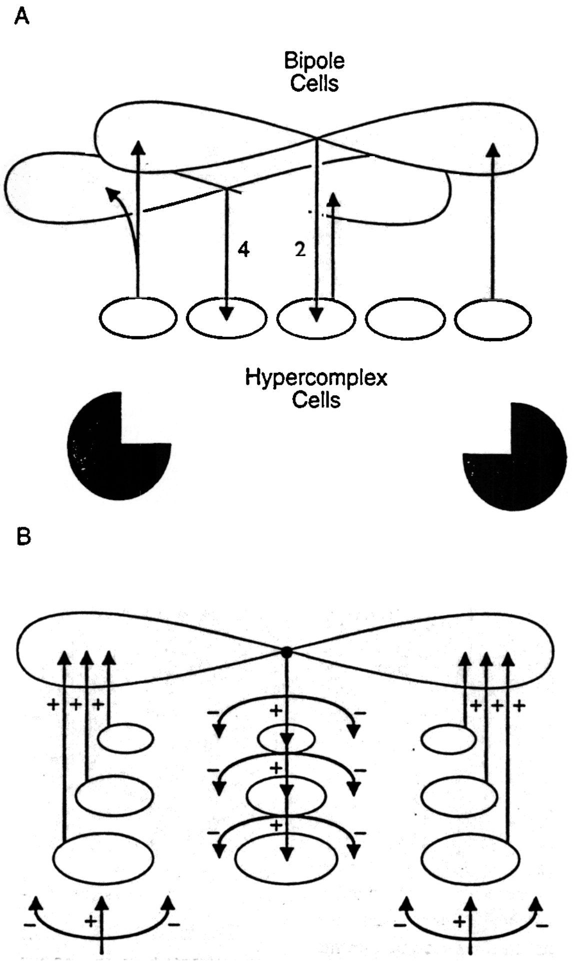

Figure 17. A cooperative–competitive feedback exchange leading to boundary completion. A: Cells in the bottom row represent like-oriented hypercomplex cells whose orientational preferences are approximately aligned across perceptual space. The cells in the top two rows are bipole cells whose receptive-field pairs are oriented along the axis of the competitive cells. Simultaneous activation of the pair of Pathways 1 activates positive boundary completion feedback along Pathway 2. Then, pairs of pathways, such as 1 and 3, activate positive feedback along pathways such as 4. Parallel completion of a sharp boundary between the locations of Pathways 1 then occurs. B: Multiple receptive-field sizes cooperate and compete with a shared pool of bipole cells to form a three-dimensional boundary segmentation corresponding to a prescribed range of relative depths from the observer. This segmentation provides the best consensus of positional and orientational information from all of the interacting signals.

aries of partially occluded objects can be amodally completed behind them. Moreover, when the redundant occluding boundaries collapse, the redundant surfaces that they momentarily supported at the monocular FIDOs collapse. Occluding surfaces are hereby seen to lie in front of occluded surfaces.

The surface representations that are generated at the monocular FIDOs are depth-selective, but they do not combine brightness and color signals from both eyes. Binocular combination of brightness and color signals takes place at the binocular FIDOs. Pathways 8 in Figure 12B control the one-to-many topographic registration of the monocular FCS signals at all the binocular FIDOs, much as Pathways 5 did for the monocular FIDOs. These FCS signals are binocularly matched at the binocular FIDOs. The membrane equations that are obeyed by the target cells at the binocular FIDO combine the monocular FIDO signals in a way that helps to explain Fechner's paradox, or why the world does not look twice as bright when viewed through two eyes rather than one eye (Cohen & Grossberg, 1984). Only the surviving matched signals can be used for filling-in. These surviving matched signals are pruned by inhibitory signals from Pathways 9 (Figure 21). These inhibitory signals eliminate redundant FCS signals using the contour-sensitive signals from the monocular FIDO surfaces that survive the boundary–surface consistency interactions of Pathways 6 and 7. In particular, Pathways 9 inhibit the FCS signals at their own positions and larger depths. As a result, occluding objects cannot redundantly fill in

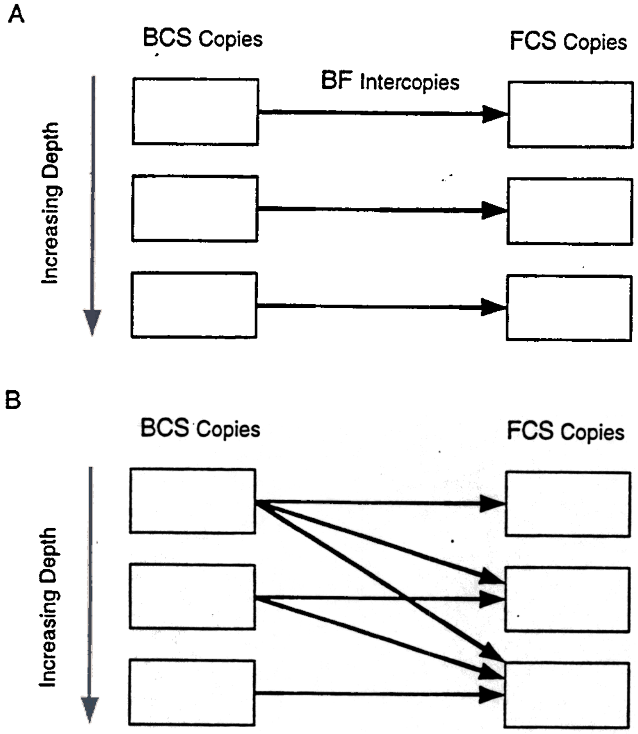

Figure 18. A: Each boundary contour system (BCS) copy generates boundaries within a narrow range of relative depths from the observer. These boundaries act to capture and contain the filling-in of surface brightness and color signals at the corresponding feature contour system (FCS) copy. Each FCS copy contains three pairs of opponent filling-in domains. B: Boundaries corresponding to nearer objects are added to boundaries corresponding to farther objects to prevent more distant surfaces from filling-in behind occluding objects. In more technical terms, each FCS copy receives inhibitory boundary-gating signals from one or more BCS copies. These signals, called *BF intercopies*, are partially ordered from nearer to farther BCS copies.

surface representations at multiple depths. This is the second instance in the theory of the asymmetry between near and far. It is called *surface pruning*.

As in the case of the monocular FIDOs, the FCS signals to the binocular FIDOs can initiate filling-in only where they are spatially coincident and orientationally aligned with BCS boundaries. These boundaries are carried by Pathways 10 in Figure 12B. These BCS-to-FCS pathways carry out depth-selective surface capture of the binocularly matched FCS signals from Pathways 8 after they are pruned by inhibition from Pathways 9.

The boundary signals along Pathways 10 selectively capture those FCS signals that (a) survive within-depth binocular FCS matching (Pathways 8) and across-depth FCS inhibition (Pathways 9), (b) are spatially coincident and orientationally aligned with the BCS boundaries, and (c) are surrounded by a connected boundary or fine web of such boundaries. Pathways 10 also realize the asymmetry between near and far through an operation that is called *boundary enrichment*. It adds the boundaries of near depths at the binocular surface representations of larger depths (Figure 18B). These additional boundaries prevent occluding objects from looking transparent by blocking filling-in of their occluded objects behind them. It can now be better seen how surface pruning and boundary enrichment work together: If boundary enrichment occurred without surface pruning, then the surfaces of occluding objects would be represented at all depths. If surface pruning occurred without boundary enrichment, then occluded objects could fill in behind their occluders.

The total filled-in surface representation across all binocular FIDOs represents the visible percept. It is called a *FACADE representation* because it combines together, or multiplexes, properties of form-and-color-and-depth. The FACADE representation can be activated by one eye or both eyes. Thus, the term *binocular* FIDO does not imply that monocular information cannot be seen. When both eyes are active, the binocular FIDOs work to select the binocularly consistent part and to suppress the rest, as during binocular rivalry.

The model processing stages are neurophysiologically interpreted as follows. The MP_L and MP_R model those properties of the retina and the LGN that are needed for the present purposes. The BCS models the interblob cortical stream between cortical area V1 and V4, whereas the FCS models the blob stream. BCS simple, complex, hypercomplex, and bipole processing is proposed to occur in the interblobs of V1 and the interstripes of V2. The monocular FIDOs are proposed to occur in V2 thin stripes, or possibly V1 blobs. The binocular FIDOs are proposed to occur in area V4. Keeping in mind that the BCS models the interblob cortical stream and the FCS models the blob stream, the feedback signals between them clarify why the cells of these parallel cortical streams can be sensitive to shared combinations of features despite their complementary functional roles.

14. Boundary Detachment Using End-Cuts

The model mechanisms summarized above can now be used to suggest how the boundaries of occluding figures get detached

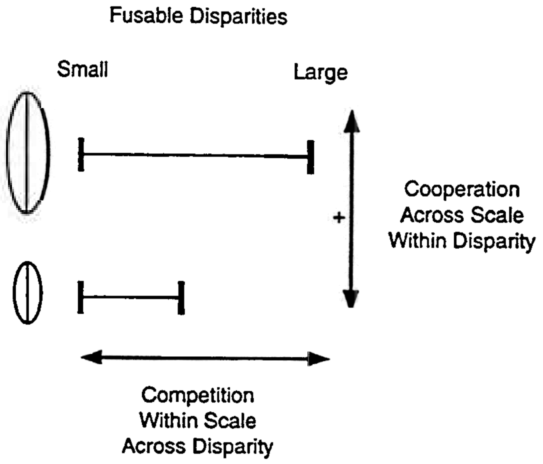

Figure 19. Size–disparity correlation: Larger complex cell scales can fuse a broader range of disparities than can smaller scales. Competition selects the complex cells within each scale and position whose disparity best matches that of the inputs. The cooperation is as described in Figure 17B. *Note.* From "3-D Vision and Figure–Ground Separation by Visual Cortex," by S. Grossberg, 1994, *Perception & Psychophysics, 55,* p. 103. Copyright 1994 by the Psychonomic Society. Reprinted with permission.

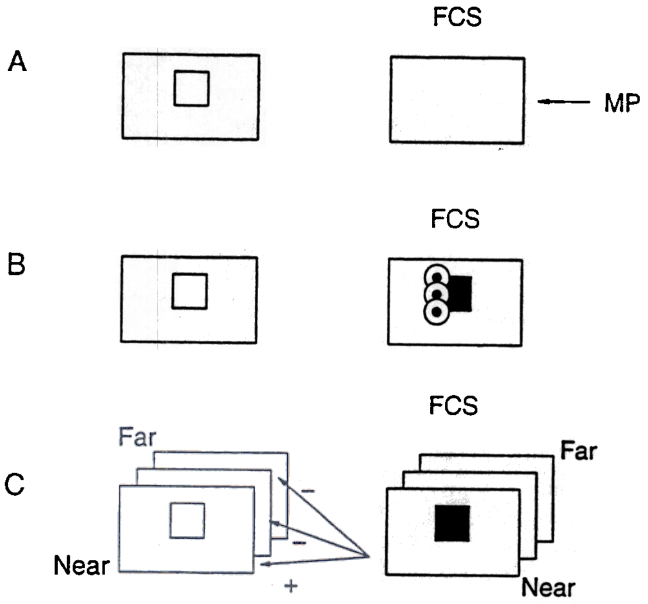

Figure 20. FCS → BCS feedback interactions. A: BCS boundaries are used to regulate filling-in of surface color in the FCS. B: A spatial contrast mechanism determines the outputs from FCS to BCS. Outputs arise at the contours of filled-in FCS regions that are surrounded by connected BCS boundaries. C: The contrast-based FCS outputs excite BCS cells at the same depth and position and inhibit BCS cells at larger depths and the same position. MP = monocular preprocessing.

from those of occluded figures. A key step is the end-cut operation that was discussed in Section 9. End-cuts restore boundaries at positions in an image where oriented receptive fields are insensitive to image contrasts, such as line ends and sharp object corners. The mechanisms that generate end-cuts have played a role in explaining many perceptual properties, ranging from neon color spreading (Grossberg & Mingolla, 1985a), texture segregation (Grossberg & Mingolla, 1985b), and hyperacuity (Grossberg, 1987a) to visual persistence (Francis & Grossberg, 1996b; Francis et al., 1994) and afterimages (Francis & Grossberg, 1996a). These multiple perceptual functions of the end-cut operation provide accumulating evidence for its existence. In other words, end-cuts were not introduced in the model to explain boundary detachment. They were introduced to explain how the visual system compensates for measurement uncertainties that are caused by using oriented receptive fields, a much more basic requirement (Grossberg, 1987a; Grossberg & Mingolla, 1985b).

Figures 22 and 23 review how the SOC filter that was described in Section 9 generates end-cuts at a line end whose thinness prevents it from being detected by oriented simple cells and complex cells of a prescribed size. The end-cut uses interactions between complex and hypercomplex cells to complete the boundary representation at the line end. In particular, complex cells at the vertical line end in Figure 23C excite hypercomplex cells at the line end while inhibiting vertical hypercomplex cells that lie just beyond the line end via the end-stopping operation. These latter hypercomplex cells receive no input from the line. They are hereby totally inhibited. This inhibition changes the competitive balance between hypercomplex cells that compete across orientation. This orientational competition maximizes inhibition between perpendicular orientations. It is a push–pull competition whereby inhibition of a given orientation disinhibits the perpendicular orientation. The inhibited vertical hypercomplex cells disinhibit horizontal hypercomplex cells, as in Figure 23D. These horizontal boundary activations are the end-cuts.

Once formed, end-cuts prevent the line's interior color from spreading beyond the line's boundary during the filling-in process. Figure 22B illustrates how color could spread outside a line were there no end-cut to contain it. Figure 22C shows how color spreading is contained after the end-cut completes the line end. Under certain circumstances, end-cuts do not prevent color from spreading across a boundary, notably during neon color spreading (Bressan, 1995; Ejima, Redies, Takahashi, & Akita, 1984; Redies & Spillman, 1981; van Tuijl, 1975; van Tuijl & de Weert, 1979; Watanabe & Sato, 1989; Watanabe & Takeichi, 1990). The end-cut rules of FACADE theory have been used to provide an explanation of many neon color spreading data (Bressan, 1995; Grossberg, 1987a, 1994; Grossberg & Mingolla, 1985a).

The model mechanisms that explain neon color spreading combine boundary processes such as end-cuts with surface processes such as filling-in. These color spreading mechanisms also play a role in the model's explanations of figure–ground perception and thus are reviewed below. As in the case of end-cuts, they were not derived to explain figure–ground data. Rather, they were derived to explain how the brain compensates for the suppression of surface brightness and color that occurs when it discounts the illuminant, again a basic perceptual requirement (Grossberg & Todorović, 1988).

15. Neon Color Spreading

Figure 24 summarizes how end-cuts help to explain neon color spreading in response to the Redies–Spillmann display in

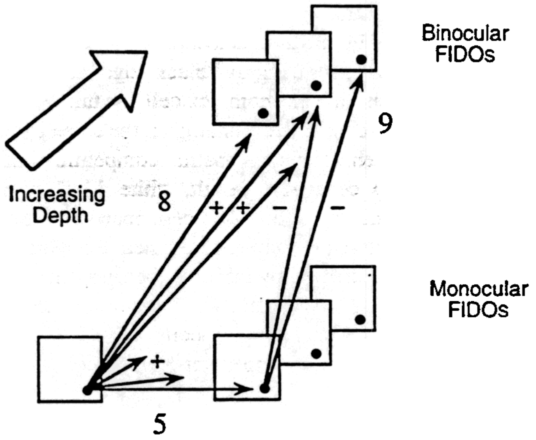

Figure 21. Surface pruning: Successfully filled-in surfaces at the monocular filling-in domains (FIDOs) use Pathways 9 to inhibit feature contour system signals to more distant binocular FIDOs. This inhibition helps to prevent redundant filling-in of the same brightnesses and colors at multiple depths.

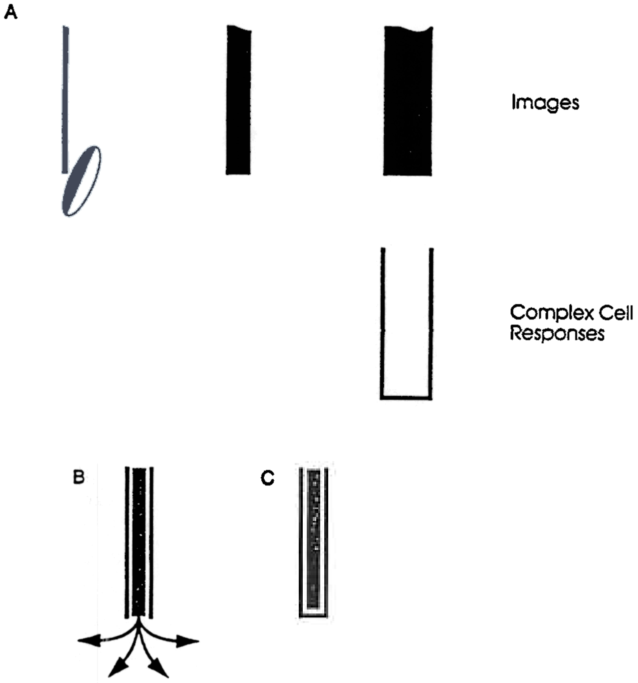

Figure 22. Responses of oriented receptive fields to lines of variable width. A: Narrow lines and thick edges activate a connected band of oriented responses. Intermediate line widths are not detected at the line end. B: For such incomplete boundaries, filling-in could cause diffusion of visible signals out of the line end. C: An end-cut closes the boundary at a line end. *Note.* A–C are from "3-D Vision and Figure–Ground Separation by Visual Cortex," by S. Grossberg, 1994, *Perception & Psychophysics, 55,* p. 74. Copyright 1994 by the Psychonomic Society. Reprinted with permission.

Figure 24A. Inspection of this display leads to a percept of a circular illusory contour that surrounds a transparent gray disk lying in front of a partially occluded white cross on a black background. The present summary describes how end-cuts control color spreading to motivate how the same mechanisms help to explain figure–ground pop-out. The large contrast at the white–black edges in Figure 24A activates model complex cells at these positions more than the gray–black edges activate complex cells at their positions. The complex cells, in turn, excite the model hypercomplex cells corresponding to the same positions (Figure 13A). The end-stopping spatial competition inhibits nearby hypercomplex cells. As a result, white–black complex cells inhibit gray–black hypercomplex cells more than the converse. The gray–black hypercomplex cells near the white–gray ends of the gray cross are hereby inhibited because they receive more lateral inhibition from white–black complex cells than excitation from gray–black complex cells. Figure 24B represents this interaction for the upper vertical bar of the cross: The vertical white–black edges generate large hypercomplex responses (thick solid lines), the vertical gray–black edges generate smaller hypercomplex responses (thin solid lines), and the end-cutting competition suppresses some responses where the gray–black edges join the white–black edges (dotted lines). The net inhibition of the gray–black hypercomplex cells hereby disinhibits higher order hypercomplex cells that are sensitive to the perpendicular orientation, thereby generating end-cuts at the white–gray edges (Figure 24C). These end-cuts supplement the direct inputs from complex cells that occur at these edges if the white bars are sufficiently wide. In summary, different contrasts along an edge can weaken the lesser contrast boundary near the contrast change and create an end-cut at the contrast change.

Cooperative–competitive feedback within the SOCC loop that was described in Section 9 then acts between the four end-cuts of the entire Ehrenstein figure to complete a circular illusory contour boundary (the dotted circle in Figure 24D), as in Figure 16C. As the end-cuts cooperate to form the illusory contour, the cooperative feedback also activates the short-range spatial competition (see Figure 13B) that further weakens the gray–black boundaries near the gray–white image contrasts. The white–black boundaries can survive this top-down inhibition because they are supported by larger bottom-up and top-down excitatory signals than are the gray–black boundaries. When the gray–black boundaries break, gaps appear in the boundary that surrounds the gray cross (see Figure 24D). These

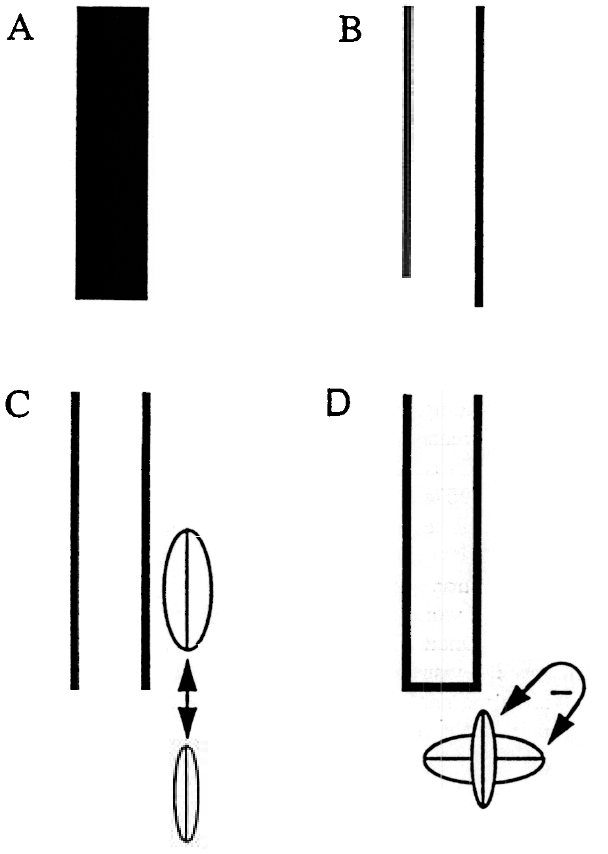

Figure 23. Creation of end-cuts. A: A line of intermediate width. B: Complex cell activations leave a gap at the line end. C: Spatial competition inhibits vertical hypercomplex cells at the line end. D: Orientational competition generates an end-cut by disinhibiting horizontal higher order hypercomplex cells at the line end. *Note.* A–D are from "3-D Vision and Figure–Ground Separation by Visual Cortex," by S. Grossberg, 1994, *Perception & Psychophysics, 55,* p. 75. Copyright 1994 by the Psychonomic Society. Reprinted with permission.

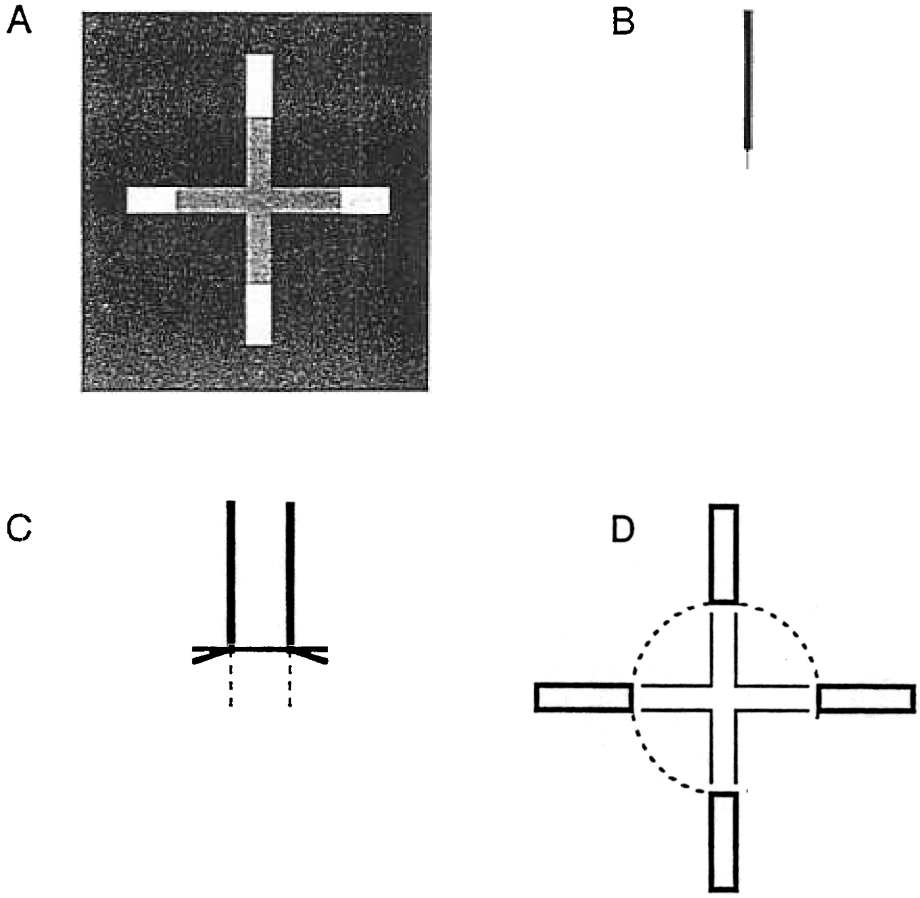

Figure 24. A: A two-dimensional Redies–Spillmann display. B: Spatial competition causes end-gaps to start to form where the boundaries of the gray cross abut the boundaries of the white bars. C: Orientational competition causes end-cuts to start to form at the ends of the white bar boundaries. D: Cooperative–competitive feedback generates an illusory contour through the end-cuts and completes the end-gaps. *Note.* A–D are from "3-D Vision and Figure–Ground Separation by Visual Cortex," by S. Grossberg, 1994, *Perception & Psychophysics, 55,* p. 75. Copyright 1994 by the Psychonomic Society. Reprinted with permission.

end-gaps allow gray color signals to diffuse out of the gray cross and fill in the circular illusory contour within the FCS.

Neon color spreading is thus a percept involving T junctions (at the white–gray–black interfaces) wherein the stems of the Ts are not separated from their tops. Rather, part of the top joins the stem, as also may occur in response to Figure 4C. This is because of the contrast relations that exist at the T junctions in Figure 24A. When viewed in this way, neon color spreading can be understood as a percept wherein geometry and contrast compete.

Watanabe and Cavanagh (1993) provided psychophysical evidence consistent with this analysis. They showed that the direction and the strength of contrast at T junctions need to be taken into account in explaining percepts of transparency. Their data suggest that a T junction may perform as an "implicit X-junction" when it supports an illusory contour, as in Figure 24D. Thus, computational models that define occlusion with T junctions and transparency with X junctions are too simple to explain many percepts of occlusion and transparency.

16. T Junction Sensitivity Without T Junction Operators

To better understand how T tops can get separated from their stems, consider how an SOCC loop responds to a T junction. At a T junction, as in Figure 25A, horizontal bipole cells get cooperative support from both sides of their receptive field, but vertical bipole cells do not. As a result, horizontal bipole cells are more strongly activated than are vertical ones. Therefore, they inhibit vertical ones more than conversely. As in neon color spreading, orientational and positional competition detach the vertical edge from the horizontal edge by inhibiting it where it joins the horizontal edge. Figure 25C illustrates the resulting end-gap. Thus, a network with bipole–hypercomplex cell feedback is sensitive to T junctions even though there are no explicit T junction cells or operators within the network.

This observation raises the following question: Why doesn't one see a gap in the vertical edge? I suggest an answer after I give a review of how the model mechanisms that create end-

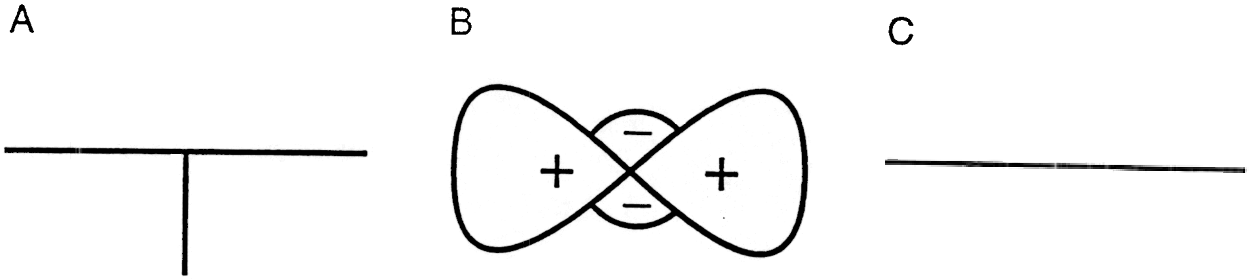

Figure 25. A: At a T junction, the horizontal edge gets cooperative support from both receptive field branches of the horizontal bipole cells. The vertical edge does not. B: The favored horizontal bipole cells can successfully inhibit the vertical bipole cells. C: An end-gap in the vertical boundary arises as a result.

gaps contribute to figure–ground percepts. First, I illustrate this for the Bregman–Kanizsa image (Bregman, 1981; Kanizsa, 1979). Here, too, one needs to understand why boundary gaps are not seen after the boundary of an occluded object is detached from the boundary of its occluder.

17. Bregman–Kanizsa Figure–Ground Pop-Out

The Bregman–Kanizsa percept (Bregman, 1981; Kanizsa, 1979) derived from Figure 5B can be explained by using a key property of the neon color spreading explanation in Section 15; namely, the larger image contrasts at the white–black edges than at the gray–black edges of Figure 24A initiate the detachment of the gray cross from its flanking white rectangles, as in Figure 24B. This detachment process can be explained using feedforward contrast-sensitive mechanisms of the simple, complex, and hypercomplex cells of the SOC filter (see Figure 13A). In particular, the end-stopping spatial competition from complex cells to hypercomplex cells is contrast-sensitive and inhibits like orientations at nearby positions. In the Bregman–Kanizsa percept in Figure 5B, a similar contrast advantage of the black–white edges (of the occluder against the background) exists relative to the gray–white edges (of the *B* fragments against the background). In the feedforward SOC filter, this advantage enables the orientational competition among hypercomplex cells to inhibit the *B* edge at the location where it joins the occluder. The end-stopping spatial competition among hypercomplex cells also can inhibit *B* boundaries at positions near the occluder where orientations are not too different from those of the occluder. Unfortunately, many of the *B* boundaries have orientations that are (almost) perpendicular to occluder boundaries. This also occurs in Figures 2–4 and 6.

The feedback spatial competition from bipole cells to hypercomplex cells does include all orientations. This feedback inhibition supplements the feedforward spatial competition to generate end-gaps. The large bipole signals at the black–white occluder boundary can use this feedback competition to inhibit the smaller signals at the gray–white *B* boundary, thereby initiating detachment of the *B* boundary from the occluder boundary. As noted in Section 16, boundary detachment also may be initiated, as in Figure 25, without this contrast advantage. The edge at the top of a T junction has a geometrical advantage because it can activate both receptive-field branches of a bipole cell. The occluder–*B* boundary interface defines such a T junction. The Bregman–Kanizsa percept (Bregman, 1981; Kanizsa, 1979) in Figure 5B thus benefits from T junction geometry as well as from a favorable combination of relative contrasts in the image. Here, geometry and contrast cooperate.

This observation clarifies how boundary detachment can still occur by using only the T junction geometry if the relative contrasts in the image do not conflict too much with it, as in Figures 4B and 5D. This observation is used below to explain pop-out in response to all the images in Figures 2–6. Grossberg's (1994) explanation of the Bregman–Kanizsa percept (Bregman, 1981; Kanizsa, 1979) in Figure 5B can then be generalized to percepts where geometry and contrast compete and to percepts of line drawings where contrast differences play a minimal role.

First, I explain the percept in Figure 5B, in which geometry and contrast cooperate, before the percept in Figure 5D is treated, in which geometry and contrast compete. The explanations use the properties of the simplified FACADE circuit in Figure 12A that are described in Sections 11–13. These explanations illustrate more concretely how each FACADE mechanism works toward generating figure–ground percepts.

Consider the image in Figure 26A. The image is registered at monocular LGN cells that activate oriented contrast-sensitive simple cells of various spatial scales, as in Figure 26B. The white–black contrast that the occluding black band makes with the white background is greater than the white–gray and gray–black contrasts caused by the occluded *B* shapes. As a result, the activation of BCS simple cells is greater at the white–black contrasts than at the white–gray and gray–black contrasts. This property is designated by boundary thickness in Figure 26B. These monocular simple cells activate binocular complex cells. Consider the case where the image is viewed by both eyes at a distance. It then generates a binocular disparity at each image point. This disparity increases with retinal distance from the foveation point. Larger disparities farther from the foveation point and smaller disparities closer to the foveation point may all correspond to the same planar image. Grossberg (1994) showed how all these disparities may be combined to generate a planar surface percept that corresponds to the same relative depth from the observer by using properties of the cortical magnification factor. For present purposes, let D_1 represent all the

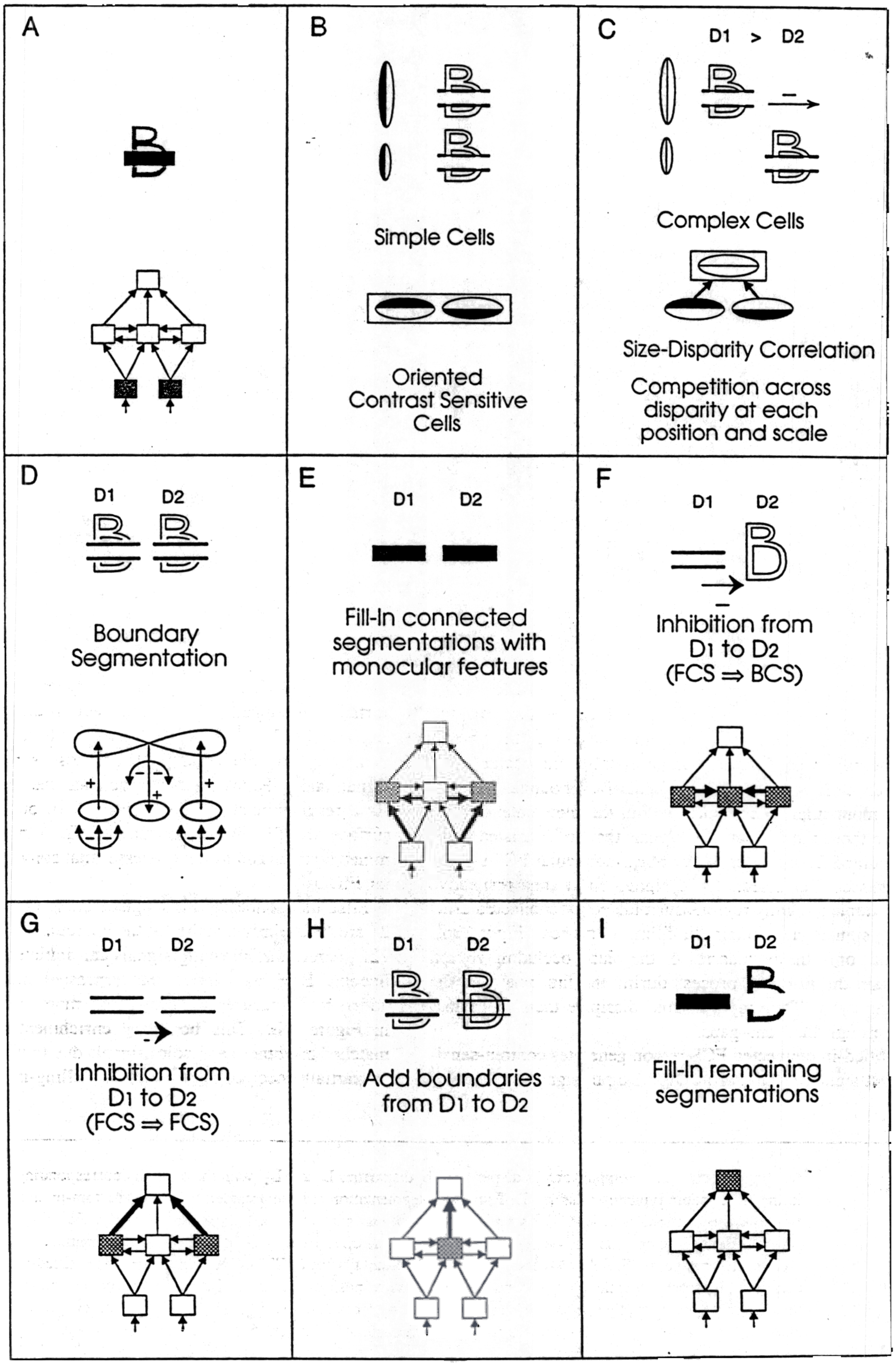

Figure 26. Bregman–Kanizsa (Bregman, 1981; Kanizsa, 1979) figure–ground separation. A: Image. B: Monocular simple cell activations in the boundary contour system (BCS). C: Complex cells at a given

disparities that correspond to the depth of this planar image surface.

In Figure 26C, the larger receptive field size represents the largest scale that can binocularly fuse D_1. Complex cells compete across disparities at each position and scale. The active cells corresponding to larger scales typically win the competition. (Such a multiscale disparity-sensitive competition was computationally simulated by Grossberg and Marshall, 1989.) As a result of this competition, no complex cells fire at the smaller disparity, D_2, of the larger scale. In contrast, smaller scales cannot binocularly fuse as wide a range of disparities as can larger scales. This property is due to the size–disparity correlation (see Figure 19). The smaller scale in Figure 26C was chosen so that it cannot fuse D_1 but it can fuse the slightly smaller disparity, D_2. Because disparity cells are coarsely coded before competition takes place across disparity at each position, the smaller scale complex cells that are tuned to D_2 can respond, albeit crudely, to the image contours. This can happen because there are no complex cells at this smaller scale that can fuse D_1, and thus no competition from D_1 to D_2. To summarize, Figure 26C results from three properties: (a) a size–disparity correlation for binocular fusion; (b) coarse-coded, nonzero-disparity computations at binocular complex cells; and (c) competitive sharpening of disparity-sensitive complex cell responses within each scale, with larger fusable disparities winning over smaller ones.

Figure 26D shows the result of SOCC loop boundary completion across multiple spatial scales, as in Figure 17B. This is the interaction that converts multiple-scale BCS signals into multiple BCS copies that are sensitive to different depths from the observer. As explained above, end-gaps, or holes in the boundary, are formed where the *B* boundaries touch the occluder.

In Figure 26E, the surviving binocular BCS boundaries interact with monocular FCS signals within the monocular FIDOs to capture those monocular FCS signals that are consistent with the binocular BCS boundaries. All other monocular FCS signals are suppressed. The selected FCS signals fill in their respective filling-in domains. Only regions surrounded by connected BCS boundary signals can contain the filling-in process. Figure 26E shows that only the boundaries of the black occluding region can contain the filling-in process during the first phase of the processing cycle. The gray *B* shapes dissipate their brightness signals through their end-gaps.

Each filled-in connected FCS region generates contour-sensitive output signals, as in Figure 26F. Output signals are hereby generated only at the boundaries of the black occluder. These FCS output signals activate parallel pathways. One pathway influences the BCS and the other the FCS, as in Figures 20 and 21. The FCS → BCS signals are excitatory to the corresponding BCS copy. They confirm and strengthen the BCS boundaries that generated their filled-in region within the FCS. These are the boundaries of the black occluder at the depth that best matches inputs to the two eyes. Boundary-pruning FCS → BCS signals inhibit any BCS boundaries that may exist at the same positions but more distant depths. In particular, the boundaries of the black occluder are inhibited at the further depth of D_2. After this happens, the incomplete *B* boundaries at depth D_2 are no longer obstructed by the occluder boundaries. Therefore, they are freed to be collinearly completed by the SOCC loop of the BCS copy at depth D_2, as in Figure 26F. In this way, the boundary of the occluded part of the *B* gets amodally completed behind the occluder (viz., within a BCS copy that represents a larger depth than that of the occluder). Figure 26F also clarifies why no boundary gaps are perceived in the final percept. When the occluder boundary is inhibited within the BCS copy at depth D_2, then the end-gaps on the *B* boundaries are also eliminated there, and their original boundaries are restored. These restored *B* boundaries can be completed behind the occluder if they can link together through bipole cooperation.

These completed *B* boundaries generate direct BCS → ORS signals, as in Figure 9. Thus, a completed letter *B* can be recognized at the ORS, even if only its unoccluded surfaces are seen at the FCS.

Why is the letter *B* not completely seen at the FCS? Visible surface representations arise only within the binocular FIDOs. Excitatory FCS signals along Pathways 8 in Figure 21 attempt to activate the binocular FIDOs. These signals replicate the signals along Pathways 5 that activate the monocular FIDOs. As a result, binocular FIDOs can fill in only a subset of the surfaces that fill in the monocular FIDOs. Which subset is determined by three additional processes that converge on the binocular FIDOs.

First, the monocular FCS signals along Pathways 8 in Figure 21 are binocularly matched at the binocular FIDOs, as in Figure 12B, before the surviving signals can initiate surface filling-in. Second, BCS boundaries that represent nearer surfaces are added to boundaries that represent more distant surfaces, as in Figure 18B. This boundary enrichment process prevents matched brightness and color signals due to unoccluded regions of partially occluded objects from filling-in behind their oc-

---

position and size scale compete across disparity, here disparities D_1 and D_2, with the disparity corresponding to the closer depth typically winning. D: Boundary segmentation at hypercomplex cells after bottom-up and top-down orientational and spatial competition generate end-gaps at weaker edge terminators. E: Filling-in of surfaces at the monocular filling-in domains (FIDOs) is effective only if each surface is surrounded by a connected boundary. F: Contour-sensitive feature contour system (FCS) output signals from the filled-in connected surfaces strengthen BCS boundaries at the same position and depth D_1 but inhibit boundaries at the same position and larger depths, such as D_2, thereby freeing the boundaries of the *B* fragments to be amodally completed. G: Contour-sensitive FCS output signals from the filled-in connected surfaces of a monocular FIDO inhibit the filling-in generators of binocular FIDOs that correspond to larger depths. H: BCS boundaries of nearer depths are added at the FCS binocular FIDOs that correspond to larger depths. I: Filling-in of binocular FIDOs that are surrounded by connected boundaries using monocular FCS signals that are not suppressed by the cross-disparity inhibition of H.

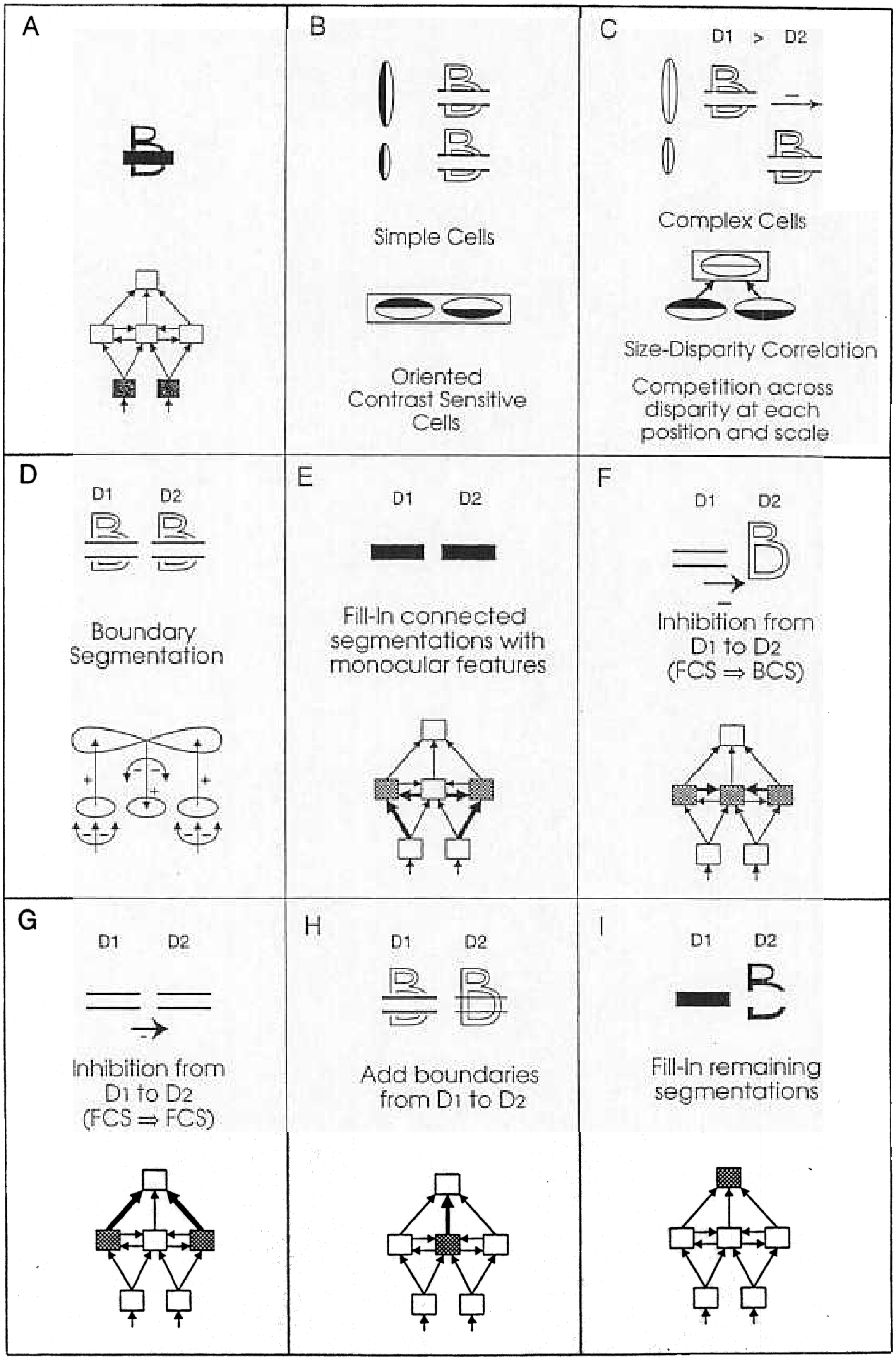

Figure 26. Bregman–Kanizsa (Bregman, 1981; Kanizsa, 1979) figure–ground separation. A: Image. B: Monocular simple cell activations in the boundary contour system (BCS). C: Complex cells at a given

disparities that correspond to the depth of this planar image surface.

In Figure 26C, the larger receptive field size represents the largest scale that can binocularly fuse D_1. Complex cells compete across disparities at each position and scale. The active cells corresponding to larger scales typically win the competition. (Such a multiscale disparity-sensitive competition was computationally simulated by Grossberg and Marshall, 1989.) As a result of this competition, no complex cells fire at the smaller disparity, D_2, of the larger scale. In contrast, smaller scales cannot binocularly fuse as wide a range of disparities as can larger scales. This property is due to the size–disparity correlation (see Figure 19). The smaller scale in Figure 26C was chosen so that it cannot fuse D_1 but it can fuse the slightly smaller disparity, D_2. Because disparity cells are coarsely coded before competition takes place across disparity at each position, the smaller scale complex cells that are tuned to D_2 can respond, albeit crudely, to the image contours. This can happen because there are no complex cells at this smaller scale that can fuse D_1, and thus no competition from D_1 to D_2. To summarize, Figure 26C results from three properties: (a) a size–disparity correlation for binocular fusion; (b) coarse-coded, nonzero-disparity computations at binocular complex cells; and (c) competitive sharpening of disparity-sensitive complex cell responses within each scale, with larger fusable disparities winning over smaller ones.

Figure 26D shows the result of SOCC loop boundary completion across multiple spatial scales, as in Figure 17B. This is the interaction that converts multiple-scale BCS signals into multiple BCS copies that are sensitive to different depths from the observer. As explained above, end-gaps, or holes in the boundary, are formed where the *B* boundaries touch the occluder.

In Figure 26E, the surviving binocular BCS boundaries interact with monocular FCS signals within the monocular FIDOs to capture those monocular FCS signals that are consistent with the binocular BCS boundaries. All other monocular FCS signals are suppressed. The selected FCS signals fill in their respective filling-in domains. Only regions surrounded by connected BCS boundary signals can contain the filling-in process. Figure 26E shows that only the boundaries of the black occluding region can contain the filling-in process during the first phase of the processing cycle. The gray *B* shapes dissipate their brightness signals through their end-gaps.

Each filled-in connected FCS region generates contour-sensitive output signals, as in Figure 26F. Output signals are hereby generated only at the boundaries of the black occluder. These FCS output signals activate parallel pathways. One pathway influences the BCS and the other the FCS, as in Figures 20 and 21. The FCS → BCS signals are excitatory to the corresponding BCS copy. They confirm and strengthen the BCS boundaries that generated their filled-in region within the FCS. These are the boundaries of the black occluder at the depth that best matches inputs to the two eyes. Boundary-pruning FCS → BCS signals inhibit any BCS boundaries that may exist at the same positions but more distant depths. In particular, the boundaries of the black occluder are inhibited at the further depth of D_2. After this happens, the incomplete *B* boundaries at depth D_2 are no longer obstructed by the occluder boundaries. Therefore, they are freed to be collinearly completed by the SOCC loop of the BCS copy at depth D_2, as in Figure 26F. In this way, the boundary of the occluded part of the *B* gets amodally completed behind the occluder (viz., within a BCS copy that represents a larger depth than that of the occluder). Figure 26F also clarifies why no boundary gaps are perceived in the final percept. When the occluder boundary is inhibited within the BCS copy at depth D_2, then the end-gaps on the *B* boundaries are also eliminated there, and their original boundaries are restored. These restored *B* boundaries can be completed behind the occluder if they can link together through bipole cooperation.

These completed *B* boundaries generate direct BCS → ORS signals, as in Figure 9. Thus, a completed letter *B* can be recognized at the ORS, even if only its unoccluded surfaces are seen at the FCS.

Why is the letter *B* not completely seen at the FCS? Visible surface representations arise only within the binocular FIDOs. Excitatory FCS signals along Pathways 8 in Figure 21 attempt to activate the binocular FIDOs. These signals replicate the signals along Pathways 5 that activate the monocular FIDOs. As a result, binocular FIDOs can fill in only a subset of the surfaces that fill in the monocular FIDOs. Which subset is determined by three additional processes that converge on the binocular FIDOs.

First, the monocular FCS signals along Pathways 8 in Figure 21 are binocularly matched at the binocular FIDOs, as in Figure 12B, before the surviving signals can initiate surface filling-in. Second, BCS boundaries that represent nearer surfaces are added to boundaries that represent more distant surfaces, as in Figure 18B. This boundary enrichment process prevents matched brightness and color signals due to unoccluded regions of partially occluded objects from filling-in behind their oc-

position and size scale compete across disparity, here disparities D_1 and D_2, with the disparity corresponding to the closer depth typically winning. D: Boundary segmentation at hypercomplex cells after bottom-up and top-down orientational and spatial competition generate end-gaps at weaker edge terminators. E: Filling-in of surfaces at the monocular filling-in domains (FIDOs) is effective only if each surface is surrounded by a connected boundary. F: Contour-sensitive feature contour system (FCS) output signals from the filled-in connected surfaces strengthen BCS boundaries at the same position and depth D_1 but inhibit boundaries at the same position and larger depths, such as D_2, thereby freeing the boundaries of the *B* fragments to be amodally completed. G: Contour-sensitive FCS output signals from the filled-in connected surfaces of a monocular FIDO inhibit the filling-in generators of binocular FIDOs that correspond to larger depths. H: BCS boundaries of nearer depths are added at the FCS binocular FIDOs that correspond to larger depths. I: Filling-in of binocular FIDOs that are surrounded by connected boundaries using monocular FCS signals that are not suppressed by the cross-disparity inhibition of H.

cluders and thereby making all occluders look transparent. The resulting boundaries are shown in Figure 26H. Boundaries of both the occluding band and the complete occluded *B* coexist at the larger depth of D_2.

These properties, taken together, could redundantly fill in all occluders at multiple depths because their FCS brightness and color signals are projected in a one-to-many fashion to all FIDOs and their BCS boundaries are projected from nearer to more distant FIDOs. The property of surface pruning prevents this from happening. Inhibitory signals are received from the monocular FIDOs along Pathways 9 in Figure 21. They inhibit all FCS signals except those at the nearest surface that can successfully fill in at the monocular FIDOs, as in Figure 26G. This prevents redundant filling-in of the occluder.

The results of these three properties, taken together, are shown in Figure 26H. Occluders cannot fill in indiscriminately at all depths. Nor can the unoccluded parts of partially occluded objects fill in their colors behind occluders. Only the unoccluded parts of objects can fill in on the nearest surface representations that support the filling-in process. The result is shown in Figure 26I. The *B* surface is filled in at depth D_2 only where it is not occluded because of the BCS boundary enrichment signals from the occluder. The occluding surface is not filled in at all at depth D_2 because of the inhibitory surface pruning signals. The occluding surface is filled in at depth D_1 because its FCS signals match BCS boundary signals that completely enclose them in connected regions. Because D_1 is greater than D_2, the black occluding surface appears to be closer than the gray occluded *B* surface.

18. What Happens When Grouping and Contrast Compete?

In Figures 4B and 5D, the occluder does not have a contrast advantage over the *B* fragments. Yet, figure–ground pop-out can still occur. In particular, the feedforward contrast-sensitive responses of the SOC filter do not favor the occluder over the occluded *B*s (see Figure 27B). Alternatively, these are not the interactions that create end-gaps at T junctions. The feedback interactions within the SOCC loop do this. The *B* boundaries are detached from the occluder boundaries in response to Figure 5D by the geometrical advantage of bipole cells collinear with the occluder over bipole cells along the *B* contours near a T junction, as in Figure 25. Spatial competition due to feedback from the favored bipole cells can then create an end-gap at the T junction boundary. In summary, end-gaps can be created if the geometrical advantage of occluder bipole cells via SOCC feedback pathways is stronger than the contrastive advantage of *B* hypercomplex cells via SOC feedforward pathways. Once detachment of the boundary occurs, the rest of the argument goes through as in Section 17, because the boundaries of Figure 26D will again be generated.

If the relative contrast of an occluded shape becomes too much greater than that of the occluder, as in Figure 4C, then

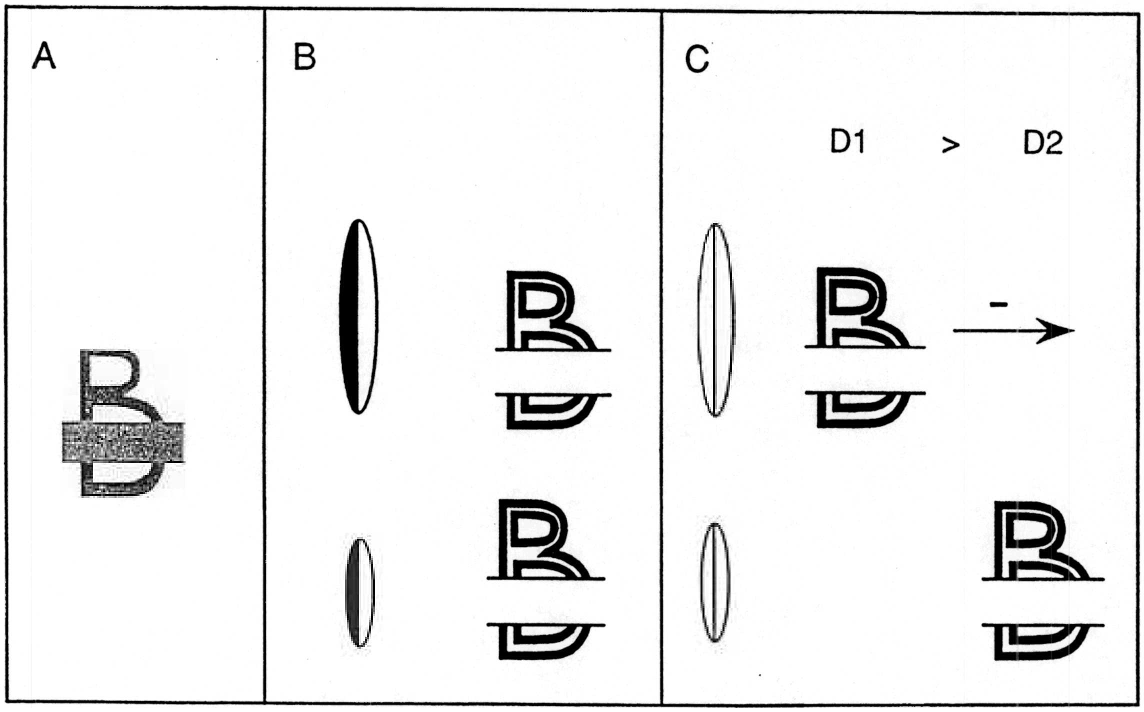

Figure 27. Initial processing of a reverse-contrast Bregman–Kanizsa (Bregman, 1981; Kanizsa, 1979) image (A) by simple cells (B) and complex cells (C). Line thickness represents relative contrast. If bipole–hypercomplex feedback is sufficient to strengthen the occluder boundary so that it can reverse the effects in B and C of greater contrast at the *B* boundaries, then the explanation of occluder pop-out may be completed as in Figures 26D–I.

the occluded shapes might not be completed behind the occluder. This can be explained by the fact that bipole cells are hypothesized to fire under either of two possible sets of conditions: Either the cell body is directly activated by an image contrast or both of its receptive fields are activated, or, alternatively, at least two out of three of the cell body and the two receptive fields are activated. Either rule allows bipole cells to fire up to the very end of a line (Gove et al., 1995; Grossberg et al., 1995). The advantage to bipole cells along an occluder boundary of activating all three (the cell body and both receptive fields) could, in principle, be overwhelmed if the occluder-to-background contrast is sufficiently small. For example, a high-contrast occluded shape could strongly activate bipole cells whose cell bodies lie at, or near, the T junctions. Whenever such a reversal of relative activation occurs, the separate occluded fragments could look closer than the occluder, and amodal completion behind the occluder would not occur.

This experimental probe may be useful for characterizing the structure of bipole cell receptive fields and other network parameters. For example, feedback gains from bipole cells to hypercomplex cells are chosen larger than feedforward gains from complex cells to hypercomplex cells, so that the best combination of cooperating signals can determine the final percept. Thus, during the neon color spreading percept of Figure 24A, the feedback that forms the circular illusory contour breaks the boundaries of the cross to create end-gaps, as in Figure 24D. Models of visual cortical processing have therefore incorporated higher feedback gains than feedforward gains for some time (e.g., Grossberg & Mingolla, 1985b, 1987). Recent data from the visual cortex support this assumption (Douglas, Koch, Mahowald, Martin, & Suarez, 1995). A parametric study of how the relative contrast and length of the T junction tops and stems influence pop-out of the occluder may shed valuable new light on this interaction.

19. Assimilation, Transparency, and Three-Dimensional Pop-Out in White's Effect

The White (1979) display in Figure 6 provides another excellent example of cooperation between geometry and contrast. The gray bars on both sides of the figure have the same luminance. Brightness contrast would suggest that the gray bars on the left, being on a primarily white background of vertical bars, should look darker than those on the right, which are on a primarily dark background of black bars. The opposite percept is obtained.

The percept on the right shares many geometrical and contrastive properties with the Bregman–Kanizsa effect (Bregman, 1981; Kanizsa, 1979) shown in Figure 5B. The vertical black bars play the role of the occluder, and the shorter gray bars play the role of the *B* shapes. Pop-out of the black bars as occluders is facilitated by the fact that their contrast with the white bars exceeds that with the gray bars. This is the relative contrast relationship that Spehar et al. (1995) identified as important for the White (1979) effect to occur. As a result, the T junctions are broken at their stems to create end-gaps where the gray and white bars join the black bars, as in Figure 25C. This fact supports the claim of Spehar et al. that T junctions may play a role in the White effect. The T junction breakage is accomplished by end-cutting mechanisms, which use a form of pattern-specific inhibition, as White (1981) proposed, but for a functional role that he did not envisage.

As in the Bregman–Kanizsa percept (Bregman, 1981; Kanizsa, 1979), the boundaries of the black bars can capture the intervening black surface color while they are detached from the gray and white surface colors. As a result, when the black bars pop out on their own surface representation, the horizontal gray–white boundaries can be amodally completed behind the black bars within a BCS copy that represents a more distant plane. These BCS boundaries can then control filling-in within a binocular FIDO that captures the white and gray contrasts without interference from the black contrasts. The perceived darkening of the gray bars can then be explained as being partly due to brightness contrast between the gray region and its white surround on this FIDO.

In particular, as described in Sections 10 and 12, the FCS gray and white inputs are processed on a different monocular and binocular FIDO than are the black inputs. Here, shunting on-center, off-surround networks contrast-enhance the inputs near luminance discontinuities before filling-in the contrast-enhanced inputs at the next processing stage. Grossberg and Todorović (1988) and Pessoa et al. (1995) described computer simulations that demonstrate how brightness contrast can be achieved using this combination of contrastive and filling-in mechanisms. Earlier FCS monocular processing stages, before those that initiate depth-selective capture of brightness and color signals, can be influenced by the types of filtering effects that Moulden and Kingdom (1989) and White (1981) proposed; see, for example, the monocular stages MP_L and MP_R in Figure 12.

The percept on the left side of Figure 6 has a similar explanation. Here, the gray bars lie on black bars rather than on gray bars. However, the relative contrasts of the occluding white bars to the partially occluded gray and black background are similar to those on the right side. These relative contrasts initiate the same sort of boundary detachment process in both cases, so a similar figure–ground percept is obtained. In contrast, in this case, the occluders are white. The gray regions on the left side now look brighter because they coexist with black on the FIDO that they share, without interference from the white occluders.

Another figure–ground percept also may be obtained in response to the White (1979) display—one in which the gray bars appear to be part of a transparent surface in front of the grating. This alternative percept is facilitated by vertically lengthening the gray bars and altering their relative contrast with respect to black and white. If this is done, then there is a greater potential for competition between geometric and contrast-based effects on bipole grouping, much as in the reverse-contrast Bregman–Kanizsa display (Bregman, 1981; Kanizsa, 1979) in Figure 5D. In particular, if the gray bars are lengthened, then the vertical bipole cells near the horizontal gray–white border get their inputs from a combination of black–white and gray–white edges; they can no longer be fed primarily by black–white edges, as is possible when small gray bars are used. Other things being equal, the geometric advantage still tends to go to the vertical bipole cells that respond to black–white and gray–white vertical edges because these edges are longer than the horizontal black–gray edges of the figure. These vertical bipole-cell receptive fields hereby pool more signals along their full length than can the corresponding horizontal bipole cells (Fig-

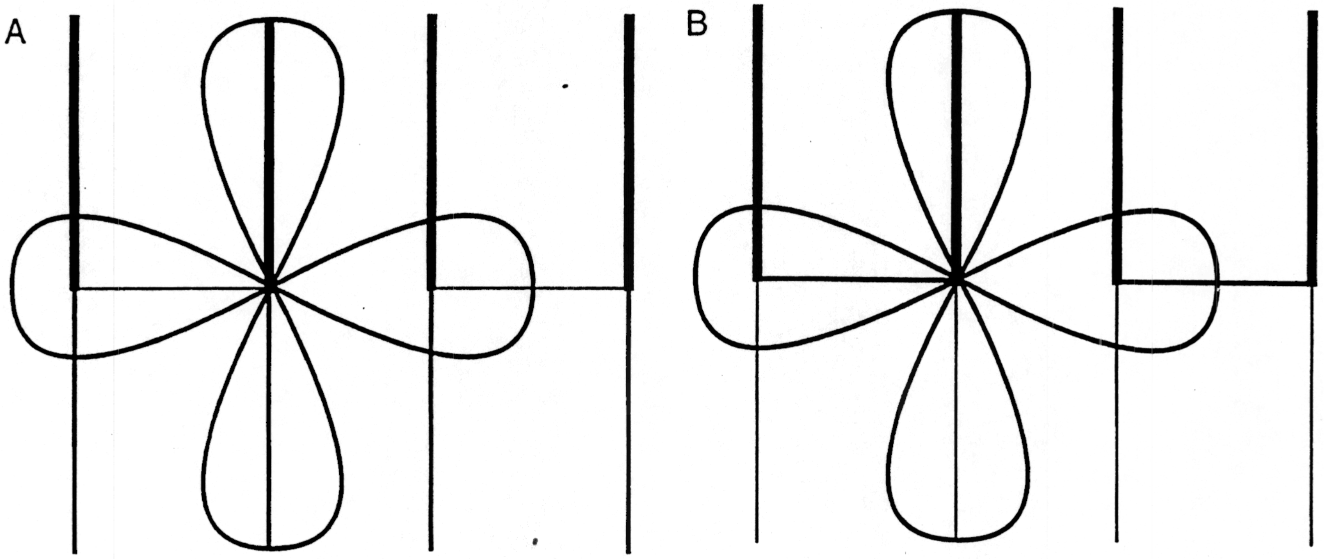

Figure 28. A: Typically, the vertical black–white and gray–white boundaries activate their bipole cells more than the horizontal black–gray edges can excite theirs. B: If the vertical gray–white boundaries (thin vertical lines) are weak enough and the horizontal black–gray boundaries (horizontal lines) are close enough, then horizontal boundary completion can win over vertical completion because the horizontal bipole cells pool a larger total input than the vertical ones.

ure 28A) if the gray–white contrasts are sufficiently large. Then, the white vertical bars pop out, just as in Figure 5D, and the lightening of the gray bars can be explained as a result of brightness contrast between black and gray on the FIDO corresponding to the more distant surface.

Alternatively, suppose that the vertical gray–white edges have low contrast. Then, the amount of signal that is pooled by the vertical bipole cells is reduced. In addition, the horizontal black–gray edges will then have high contrast. Because these horizontal black–gray edges are collinear and close to one another, their horizontal bipole cells may win the competition with the vertical bipole cells and thereby complete horizontal boundaries that span the black–gray edges and the vertical white bars (see Figure 28B). When this happens, a connected rectangular boundary is formed that surrounds the gray bars and their adjacent white-bar fragments. Vertical end-gaps can then be formed in the weak vertical gray–white boundaries where they abut the black–gray boundaries, just as in the explanation of neon color spreading (see Figure 24D). White color from the white bars can then leak into the gray bars, thereby lightening them. This assimilation percept is thus a variant of neon color spreading.

In summary, the above analysis suggests how figure–ground percepts may contribute to the White (1979) effect. In particular, changing the balance of geometrical and contrastive factors may bias the percept from one of opaque occluders to one of transparent occluders. The White effect occurs in both cases but for different reasons that share properties with the Bregman–Kanizsa (Bregman, 1981; Kanizsa, 1979) and 3-D neon color-spreading percepts, respectively. This figure–ground analysis does not deny the possible contributions of early filtering operations. It does, however, help to explain why such filtering operations, taken alone, have proved insufficient to explain the percept.

How can an observer switch between percepts of white vertical occluding bars in front and a transparent rectangular surface in front? As illustrated in Figure 9, top-down attention can amplify the strength of boundaries and surfaces in a given region at the expense of boundaries nearby. Bottom-up effects of differential acuity due to where the eyes fixate the image may have a similar effect. Finally, habituation of signals in active pathways that support one interpretation may shift the competitive balance to favor other pathways that favor an alternative interpretation. This habituative process is explored more fully in the next section.

20. Depth Stratification, Geometrical Grouping, and Rivalry

The above explanation suggests how geometric and contrast-based grouping factors may compete with each other to generate a bistable percept. Geometrical grouping factors may also compete among themselves to generate multiple percepts. Figure 2A displays an ambiguous pattern that illustrates Kanizsa's (1979, 1985) concept of perceptual *stratification*. This figure can be perceived either as a white cross in front of a partially occluded white outline square or as a white outline square in front of a partially occluded white cross. The former percept usually occurs. In general, a thinner structure tends to be perceived behind a thicker one (Petter, 1956).

The stratification percept can be explained using properties of bipole cell cooperation, end-cuts, and amodal completion behind an occluder. These properties provide a mechanistic way to understand the classical Gestalt principle of good continua-

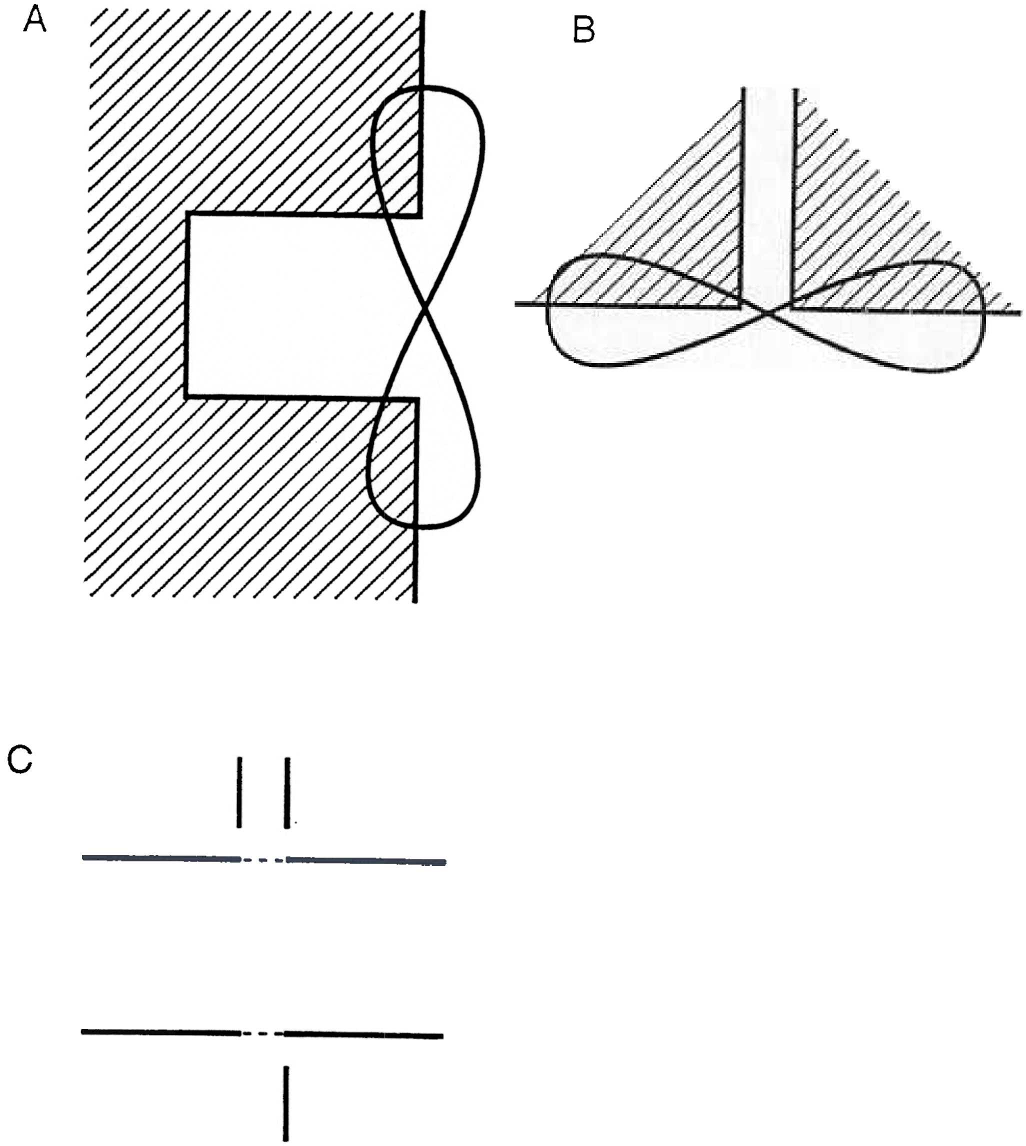

Figure 29. The bipole cells that try to complete the outline square boundary in A get less total input than the bipoles that try to complete the cross boundaries in B. As a result, the cross boundaries win, and pop-out is obtained by the usual mechanisms, including bipole competition of the cross boundaries and end-gaps at the square boundaries, as in C.

tion, which is often used to explain stratification (Rock, 1993). Two key issues are why do thinner structures usually get occluded and why do they not always get occluded?

Once one knows the receptive field structure of a bipole cell, an intuitively appealing answer may be given. This explanation adapts bipole properties that were used to analyze the White (1979) effect in Figure 29 to the case of Kanizsa (1979, 1985) stratification. Consider the thin vertical edges of the outline square and the abutting thick horizontal edges of the cross, for definiteness. Because the vertical outline square is thin and the square is thick, the vertical bipole cells need to cooperate over a much longer distance than do the horizontal bipole cells. As a result, the vertical bipole cells (Figure 29A) may receive a much smaller total input from the outline square than the horizontal bipole cells receive from the cross (Figure 29B). The horizontal bipole cells are therefore favored to win the orientational competition with the vertical bipole cells via the feedback pathways of the SOCC loop (see Figure 13B). When they do, they control the feedback pathways within the SOCC loop. This enables the horizontal bipole cells to complete the horizontal cross boundaries, as in Figure 29C. While this is happening, the horizontal bipole cells activate the feedback spatial competition within the SOCC feedback loop (see Figure 13B). As a result, end-gaps are created at the ends of the square boundaries where they abut the cross boundaries, as in Figure 29C.

The completed cross boundaries and broken square boundaries are now computationally analogous to the completed occluder boundaries and broken *B* boundaries of the Bregman–Kanizsa display (Bregman, 1981; Kanizsa, 1979) in Figure 26D. As in the case of the Bregman–Kanizsa black occluder, the cross boundaries capture and fill in the intervening white color at their binocular FIDO. The square boundaries are amodally completed behind the cross at a more distant BCS copy, much as the *B* boundaries are completed behind the occluder in Figure 26F. As in the explanation of the White (1979) effect, the competitive balance between vertical and horizontal boundaries can be altered by changing the position at which the eyes foveate, by a top-down shift of spatial attention, or by the type of habituative process that is described below. When the balance shifts, the outline square can pop in front.

This explanation can also be used to explain the variants of stratification that are shown in Figures 2B–D. In particular, the "real" contrastive boundaries of the outline square in these figures enable their bipole cells to win the competition by providing continuous contrasts across the width of the cross and thereby overcoming the disadvantage that is depicted in Figure 29A. The bipole cells of the square are thus favored in several ways: They have continuous bottom-up inputs along an entire edge of the square, whereas the bipole cells of the cross do not, as in Figure 29B. Locations at which bottom-up inputs are received can generate stronger boundaries than locations that do not because, in the former case, bottom-up inputs and SOCC feedback cooperate to form the boundary, whereas in the latter case, SOCC feedback alone supports boundary formation. Finally, at locations where, say, a vertical line or edge of a square exists, as in Figure 2B–D, horizontal bipole cells of the cross are inhibited by spatial impenetrability (see Section 9). These factors conspire to enable bipole cells of the square to always win the competition with bipole cells of the cross wherever a continuous line or edge of the square exists.

In response to many images where vertical and horizontal boundaries are more equally balanced, monocular rivalry can occur (Kaufman, 1974). Grossberg (1980, Section 12) provided an explanation of why achromatic gratings are perceived to alternate more slowly than chromatic gratings (Rauschecker, Campbell, & Atkinson, 1973). Grossberg (1987b, Sections 27–28) extended this explanation to include parametric properties of binocular rivalry, as in the experiments of Blake (1977), Blake and Camisa (1979), Blake and Fox (1974), Blake and Lema (1978), Fox and Check (1972), Hollins and Bailey (1981), and Wales and Fox (1970). Arrington (1993) used the Grossberg model to quantitatively simulate parametric properties of the binocular rivalry data of Mueller and Blake (1989). Grossberg (1991), Francis and Grossberg (1996a, 1996b), and Francis et al. (1994) explained visual persistence data using the same mechanisms.

Why should persistence and rivalry data be explicable by the same mechanisms? The mechanisms that trigger the rivalry percept are hypothesized to be habituative transmitters that multiply, or gate, bottom-up signals in the pathways from complex cells to hypercomplex cells and top-down signals from bipole cells to hypercomplex cells (Figure 13B). The functional role of these gates is predicted to be the rapid reset of a BCS boundary segmentation when its scenic input shuts off or moves. The rapid reset is traced to an antagonistic rebound that occurs from ON cells to OFF cells when changing inputs alter the habituative balance between the ON and OFF cells. The rebounding OFF cells inhibit the corresponding bipole cells and thereby prevent them from resonating for too long by means of bipole–hypercomplex positive feedback after the image shuts off. Were it not for this active inhibitory process, massive image smearing could occur every time a perceived object moves.

In the stratification percept of Figure 2A, this model suggests that the cross percept usually wins because it generates a stronger total input to its bipole cells than does the square. The cross-compatible habituative transmitters take longer to habituate to the point where the square-compatible inputs can win the orientational competition and switch to the alternative percept.

21. Figure–Ground Pop-Out of Line Drawings

Using the above concepts, the pop-out percepts that are derived from the line drawings in Figure 3 can also be explained. Consider Figure 3A for definiteness. Figure 30 summarizes an explanation using the same format as in Figure 26. The key observations are as follows: In Figure 30D, the vertical rectangle's boundaries get detached from the horizontal rectangle's boundaries because of the geometrical advantage of the horizontal bipole cells over the vertical bipole cells. The deleted vertical boundary gets completed in Figure 26F at depth D_2 after the horizontal rectangle boundary is inhibited there. Everything else then goes through as in the explanation of the Bregman–Kanizsa percept (Bregman, 1981; Kanizsa, 1979) in Figure 26.

A similar argument can be used to explain the percept of Figure 3C, wherein the amodal completion approximates a circle. Once the boundaries of the square are detached from those of the incomplete circle, the latter can generate a curved boundary completion at depth D_2, albeit not necessarily a perfect circle. Figure 16C illustrates curved boundary completion by the BCS. The percept of Figure 3C is often attributed to concepts like Prägnanz and likelihood or to the brain's preference for generic or nonaccidental solutions (e.g., Rock, 1993). The main idea is that the percept of a Pac-man figure abutting a square would be a purely coincidental interpretation of the image, rather than a generic one. There are many related percepts, however, where such an argument would be harder to make (e.g., the percept of Figure 2B). The present explanation holds whether the percept is generic or nonaccidental.

What about the percept in Figure 3B? Here, the horizontal rectangle can get detached from the vertical rectangle as before, as in Figure 31D. But now, there is only one incomplete rectangular fragment, not two. How do the inhibited ends of the vertical boundaries get restored? This is not due to amodal boundary completion behind the occluder, as in Figure 31F. However, as in that explanation, when the boundaries of the horizontal rectangle are inhibited at depth D_2, their bipole inhibition of the vertical boundaries at depth D_2 is also eliminated, as in Figure 31F. This disinhibition of the vertical hypercomplex cells at D_2 enables the ends of the vertical boundaries to be restored by their bottom-up inputs. One point worth emphasizing is why the depth D_2 representation of Figure 31I does not contain the horizontal rectangle but that of Figure 31H does. This is so

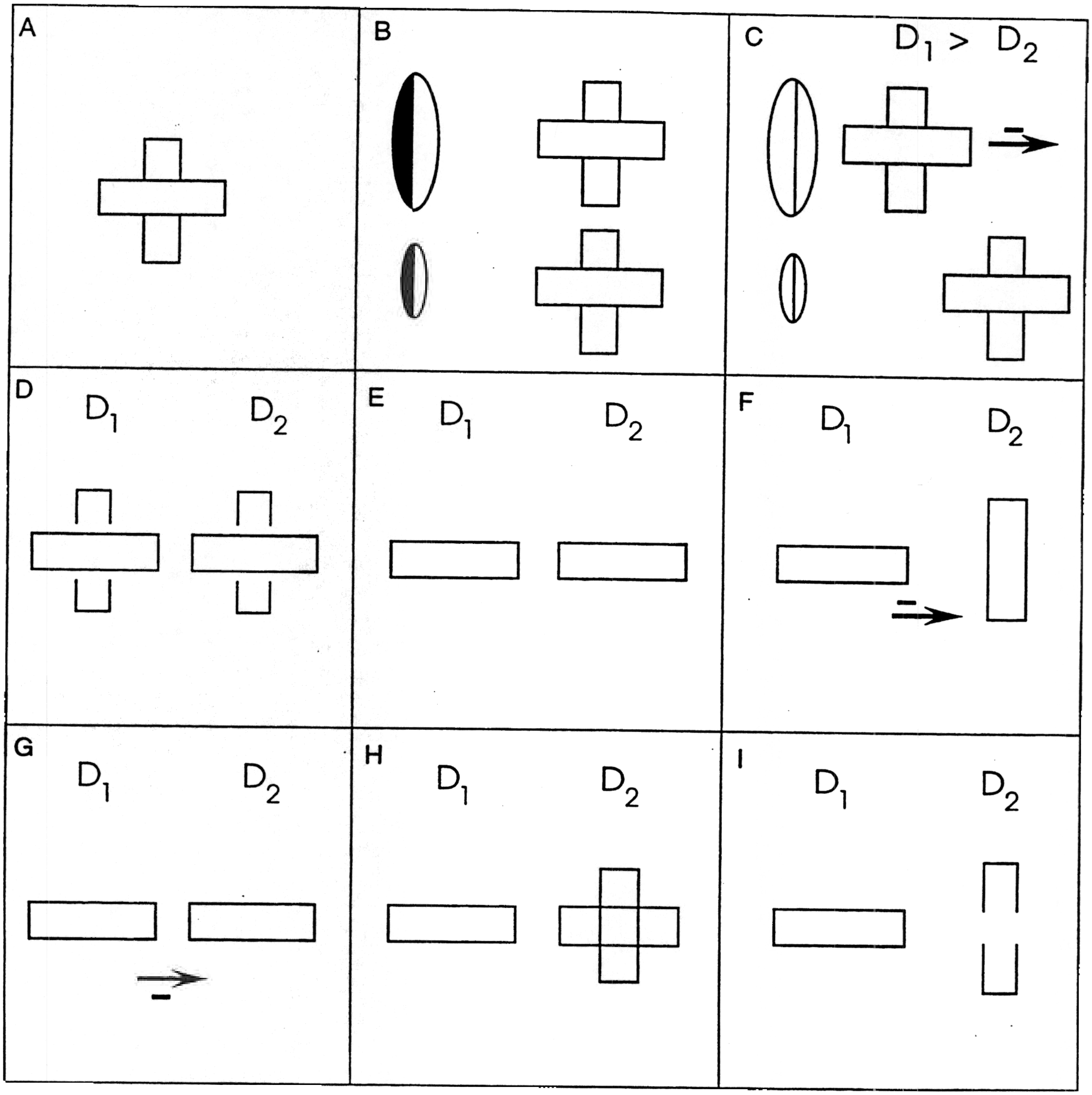

Figure 30. An explanation of how the image in Figure 3A generates a percept of pop-out of the horizontal outline bar and amodal completion of the partially occluded vertical outline bar. See Section 21 for details.

because the image in Figure 31H represents BCS boundaries, whereas the image in Figure 31I represents the FCS surface contrasts that fill in the binocular FIDOs, including the black-to-white contrasts that render the lines visible.

22. Why Do Brighter Kanizsa Squares Look Closer?

As noted in Section 6, brighter regions can look closer, whether in Egusa (1983) or Kanizsa square displays. This section proposes an explanation of these percepts that emphasizes the role of surface-to-boundary feedback in generating figure–ground percepts. The explanation also provides more detailed information about how this feedback is distributed across multiple depth representations.

A convenient point of departure is a proposal by Wilson, Blake, and Halpern (1991) that there is a coarse-to-fine interaction during stereo processing such that larger receptive fields inhibit smaller receptive fields; for example, lower frequency "far" units inhibit higher frequency "near" units. This inhibi-

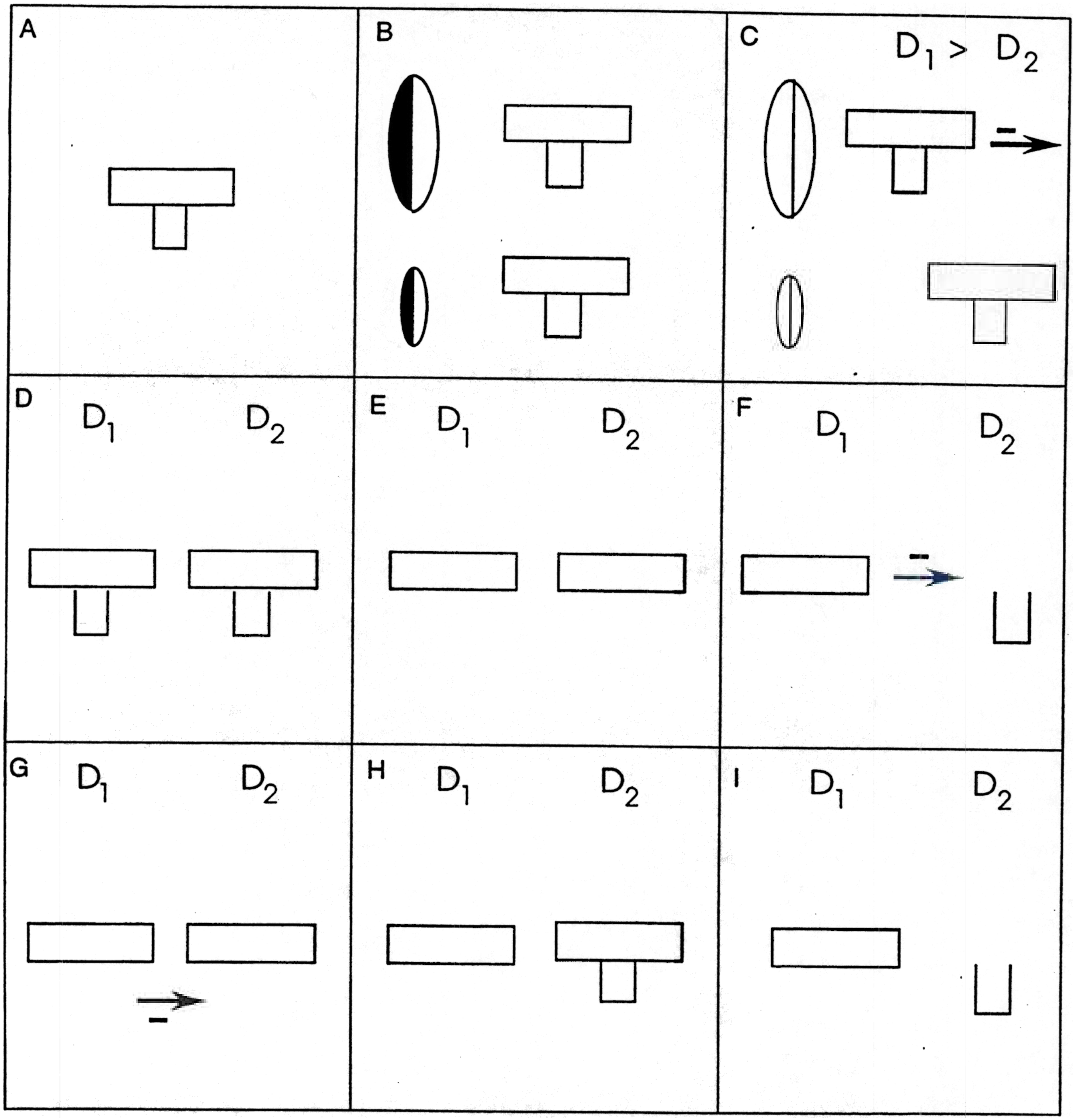

Figure 31. An explanation of how the image in Figure 3B can generate a percept of pop-out of the horizontal outline bar, even though the vertical outline bar cannot be completed amodally behind it. See Section 21 for details.

tion is proposed to decrease as the difference between scales increases in order to explain how depth transparency can be perceived when information defining the transparent planes is separated by approximately four octaves in spatial frequency.

Such a direct inhibitory effect between spatial frequencies is hard to reconcile with data showing that both low spatial-frequency and high spatial-frequency sinusoids can signal either near or far depth percepts, depending on the scenic context in which they are found (Brown & Weisstein, 1988; Grossberg, 1994; Klymenko & Weisstein, 1986) and that larger spatial frequencies can fuse a larger range of disparities, including small disparities, due to the size–disparity correlation (see Figure 19).

Two related types of mechanisms in FACADE theory replace Wilson et al.'s (1991) proposal and escape its problems. One mechanism concerns the manner in which multiple spatial scales interact through bipole cooperation to form BCS copies that represent boundaries at a prescribed depth range (see Figure 17B). As noted in Section 11, this mechanism can be used to explain how positionally accurate boundaries can be formed within each depth range and to thereby explain various data concerning inhibition among multiple spatial scales.

The second mechanism is more relevant to explaining why brighter Kanizsa squares look closer. This is the boundary pruning mechanism that was summarized in Figures 12 and 20. Here, FCS → BCS feedback signals within each depth range enhance those boundaries that define successfully filled-in FCS regions, whereas they inhibit boundaries that correspond to more distant depths. This inhibition across depths is now proposed to decrease with the depth difference.

The decrease in inhibitory strength across depth is used below to explain why brighter surfaces can look closer and how depth transparency can occur when four octaves in spatial frequency separate the defining inputs. Given that transparency is a surface property, rather than a property of early filtering, the present FCS-based explanation provides a way out of the difficulties faced by Wilson et al.'s (1991) proposal while helping to explain additional data about brightness–depth correlations.

The main paradox about the Kanizsa depth percept derives from the fact that the enhanced brightness is not a local property of its Pac-man inducers. Rather, it is an emergent property of how illusory contours are completed and surface representations are filled in. How does this emergent surface property alter the perceived depth of the square? Given the above analysis of figure–ground perception, it is natural to recaste this question as follows: How does the enhanced brightness of the FCS surface representation of the square alter the BCS boundaries so that the Kanizsa square can pop out in front of its Pac-man inducers and the Pac-man inducers can be amodally completed behind the square? FCS → BCS feedback is naturally invoked for this purpose, and the paradoxical brightness–depth correlation is reduced to a consequence of boundary–surface consistency.

The proposed explanation is shown schematically in Figure 32. Figures 32A–D recapitulate the processing stages used to explain the Bregman–Kanizsa percept (Bregman, 1981; Kanizsa, 1979) in Figure 26. The simple-cell processing stage of Figure 26B is omitted in Figure 32, so that Figure 32B represents the complex-cell processing stage. Figure 32C shows illusory square completion. Figure 32D shows the filled-in surface representations with enhanced brightness of the Kanizsa square due to brightness contrast and filling-in (see Gove et al., 1995, for a computer simulation of this property). In Figure 32D, the contrast between the filled-in square and Pac-men is greater than the contrast between the Pac-men and the background. As a result, the FCS → BCS feedback signals are stronger from the corners of the square than from the circular Pac-man contours. Figure 32E shows the effect of this FCS → BCS feedback when it acts in an excitatory way within each depth. The BCS boundaries at the square corners are differentially strengthened and therefore strengthen the entire Kanizsa square boundary by means of bipole-cell cooperative feedback. As this occurs, competitive feedback from the strengthened square boundary breaks the ends of the weaker circular boundaries to form end-gaps at the ends of the Pac-men. These end-gaps allow dissipation of the black color from the Pac-men at the nearer depth of D_1. Thus, only the Kanizsa square can fill in effectively at this depth after FCS → BCS feedback acts. Figure 32F depicts the inhibitory FCS → BCS feedback from the contours of the filled-in Kanizsa square at D_1 to the corresponding positions at larger depths. The square boundaries at the larger depths are hereby eliminated. The Pac-men are then free to amodally complete their boundaries into (almost) circular boundaries. The remainder of the explanation now goes through just as in the Bregman–Kanizsa percept, including how the occluded parts of the Pac-men are amodally completed and how the Kanizsa square and the unoccluded Pac-men surfaces are modally completed at the different depths of D_1 and D_2.

It remains to say how a larger brightness difference between the square and the background yields a larger perceived depth difference. This property is suggested to follow from the balance of excitatory FCS → BCS feedback within each depth and the inhibitory FCS → BCS feedback between nearby depths. When the brightness difference is very small, the excitatory feedback from the square is not substantially greater than that from the curved Pac-man edges. Hence, no end-gaps, or only weak end-gaps, can form, and there is little pop-out or depth difference. As the brightness difference increases, end-gaps do form in the Pac-men, and pop-out between adjacent depth can begin to occur. A larger brightness difference enables FCS → BCS inhibition to eliminate square boundaries over a wider range of depths and thus to complete Pac-men into circles at these depths. The maximum achievable brightness difference leads to the maximum inhibition, which, combined with FCS pruning of redundant boundaries and surfaces, limits the extent to which the Pac-men recede from the surface depth of the square.

23. Are Both Boundaries and Surfaces Amodally Completed?

The explanations of amodal completion have heretofore emphasized amodal completion of BCS boundaries, as in Figures 26F and 30F. These completed boundaries are recognized via direct BCS → ORS pathways, as in Figure 9, which are interpreted neurobiologically in terms of interactions between extrastriate visual cortex and temporal cortex, respectively (Desimone, 1991; Desimone, Schein, Moran, & Ungerleider, 1985; Desimone & Ungerleider, 1989; Gochin, Miller, Gross, & Gerstein, 1991; Harries & Perrett, 1991; Mishkin, 1978, 1982; Mishkin & Appenzeller, 1987; Perrett, Mistlin, & Chitty, 1987; Schiller, 1994, 1995; Schwartz, Desimone, Albright, & Gross, 1983; Zeki, 1983a, 1983b). The amodally completed boundaries are perceptually invisible if only because BCS outputs are derived from a complex-cell pooling process that combines signals from opposite contrast polarities and all colors to define the strongest possible boundaries (Thorell, DeValois, & Albrecht, 1984).

These completed boundaries are, by themselves, often sufficient to recognize an object, as various data and modeling studies have suggested. On the data side, object superiority effects occur using outline stimuli with little surface detail (Davidoff & Donnelly, 1990; Homa, Haver, & Schwartz, 1976). The number of errors in tachistoscopic recognition and the speed of identification are often similar using appropriately and unappropriately colored objects (Mial, Smith, Doherty, & Smith, 1974; Ostergaard & Davidoff, 1985). Recognition occurs with equal speed using black-and-white photographs or line drawings that are carefully derived from them (Biederman & Ju, 1988). On the modeling side, it has been shown that BCS boundaries are often

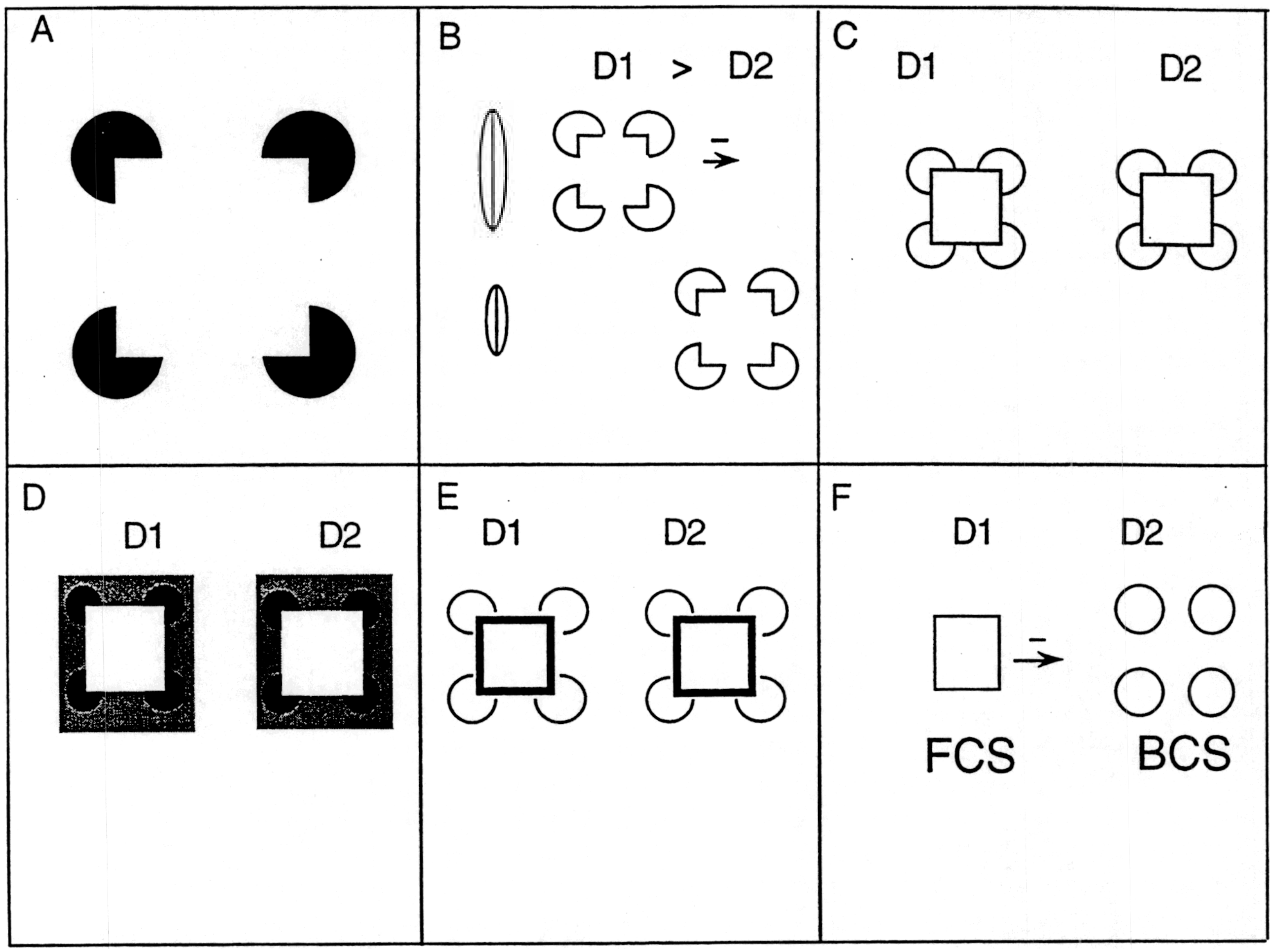

Figure 32. Why brighter Kanizsa squares look closer. A: Image. B: Complex cell responses at disparities D_1 and D_2. C: Completed boundaries before FCS → BCS feedback acts. D: Filled-in activities before FCS → BCS feedback acts. E: Effect of excitatory FCS → BCS feedback on boundary strength within each depth. The Kanizsa square boundaries are strengthened, and end-gaps appear in the Pac-man boundaries at both D_1 and D_2. F: Effect of inhibitory FCS → BCS feedback between depths. The contours of the filled-in square at D_1 generate inhibitory signals that eliminate the square boundary at D_2 and enable the Pac-men to induce completion of circular boundaries at D_2.

sufficient to recognize complex 3-D objects from sequences of their 2-D views (Bradski & Grossberg, 1995).

When viewing images such as Figure 8, one also perceives that the black cross and the white cross that are amodally completed behind the gray disks have an amodal surface quality. At the very least, they seem to span the locations that are occluded by each disk on a definite surface representation. This impression could, in principle, be the result of at least two processes: interpolation by spatial attention or amodal filling-in. In the first process, attending to the four visible corners of a partially occluded cross could focus attention on the FIDO that represents the cross and center it on the region that is occluded by the disk. In the second process, surface filling-in on the monocular FIDOs that represent the checkerboard pattern completes an amodal surface representation behind each occluding disk. The brightness signals from the unoccluded portions of each cross are hereby completed behind the occluding disk. Given that this occurs, it remains to clarify how one "knows" that the occluded region has the same color as the unoccluded parts of the cross, even though one cannot "see" this color.

To understand the proposed spatial attention process better, recall that the BCS → FCS interactions are depth-specific, as in Figure 18. The checkerboard pattern that surrounds the gray disks in Figure 8 generates a filled-in surface representation up to the disk boundaries on a prescribed binocular FIDO (Figure 12). Spatial attention is proposed to be mediated by reciprocal interactions between these binocular FIDOs and a spatial localization network, or multiplexed spatial map (Figure 33). These model interactions are interpreted neurobiologically in terms of the reciprocal pathways that exist between extrastriate visual cortex and parietal cortex. The latter region is well-known for its role in directing attention and action toward the spatial locations of salient targets (R. A. Anderson, Essick, & Siegel, 1985; Fischer, 1986; Fischer & Breitmeyer, 1987; Goodale & Milner,

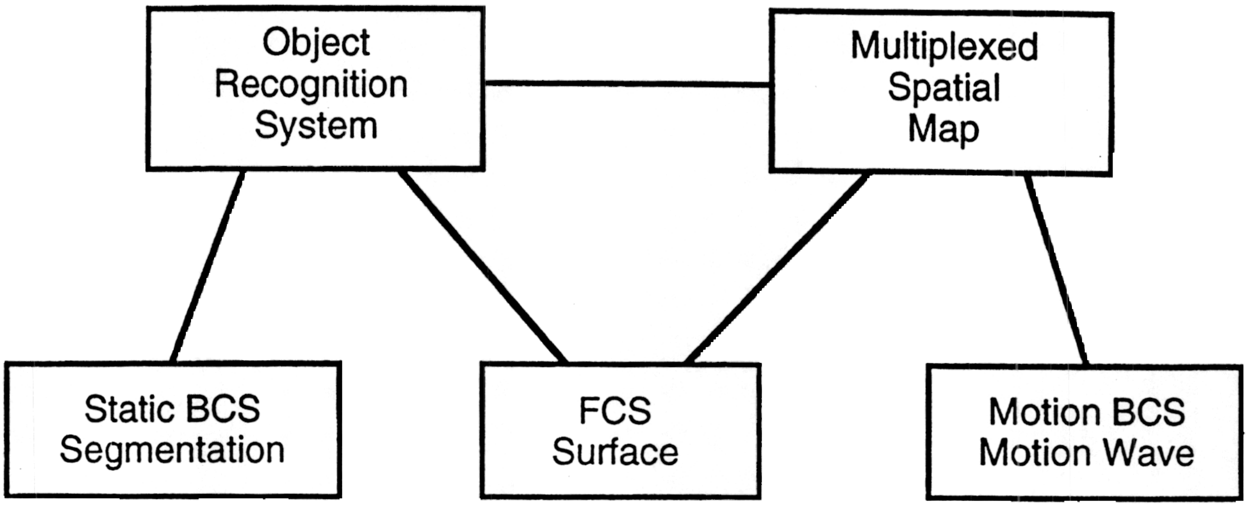

Figure 33. The reciprocal interactions of the object recognition system (ORS) with the boundary contour system (BCS) and the feature contour system (FCS) are supplemented by reciprocal interactions with an attentive spatial map. These object-based and spatial-based interactions are used to coordinate attentive object recognition, spatial orientation, and visual search. Expressed somewhat more technically, the static BCS and FCS (which model aspects of the interblob and blob cortical processing streams) interact reciprocally with the ORS (which models aspects of the temporal cortex) for purposes of attentive visual object recognition. The FCS and a motion BCS (which models aspects of the magnocellular cortical processing stream) interact reciprocally with a multiplexed spatial map (which models aspects of the parietal cortex) for purposes of attentive spatial localization and orientation. Both systems interact together to define spatially invariant ORS recognition categories and to control visual search. From "3-D Vision and Figure-Ground Separation by Visual Cortex," by S. Grossberg, 1994, *Perception & Psychophysics, 55,* p. 58. Copyright 1994 by the Psychonomic Society. Reprinted with permission.

1992; Maylor & Hockey, 1985; Mountcastle, Anderson, & Motter, 1981; Rizzolatti, Riggio, Dascola, & Umità, 1987; Wurtz, Goldberg, & Robinson, 1982). Such interactions have been modeled earlier to simulate data concerning attentive visual search. This model has been called the *spatial object search* (SOS) *model* because of the importance of spatial attention in the simulated search process (Grossberg et al., 1994).

The data analyzed by the SOS model are all consistent with the idea that spatial attention can be focused on 3-D surface representations in a depth- and color-specific way. These include the data of Egeth, Virzi, and Garbart (1984), who found that visual search times for conjunctive targets wherein three items share the same target color are the same regardless of the number of distractors; the data of Wolfe and Friedman-Hill (1992) on color–color conjunctive search that may be accomplished by focusing spatial attention on groupings of surface regions that share the same color; the data of Nakayama and Silverman (1986) on fast search of targets that are defined by conjunctions of color and depth; and the data on search of 3-D surface properties (Aks & Enns, 1992; He & Nakayama, 1992; Kleffner & Ramachandran, 1992).

These explanations are also consistent with the idea that spatial attention may span more than one colored location at a time. In particular, spatial attention could interpolate the four white bars or the four black bars of each cross in Figure 8 within the depth- and color-specific binocular FIDO that carries these representations. Spatial attention could hereby contribute to the sense that the occluded surface region of each cross is not "empty." In summary, the binocular FIDO on which the checkerboard in Figure 8 fills in may draw depth-selective attention to the modally completed regions of each cross. The focus of spatial attention on this FIDO may occur behind the occluding disks and may thereby contribute to the impression that a surface exists with the appropriate color and depth at these locations because that FIDO always represents this color and depth.

The proposed amodal surface completion process exploits the property that the occluded regions behind the gray disks fill in a surface representation in the FACADE model as it stands. In fact, the monocular FIDOs (see Figure 12) can fill in surface representations behind occluders. In the explanation of Bregman–Kanizsa (Bregman, 1981; Kanizsa, 1979) figure–ground pop-out, for example, note that the boundaries in Figure 26F that feed into the monocular FIDOs surround the completed *B* shapes at depth D_2 and the occluder at depth D_1, so both forms may fill in completely at their respective surface depths.

Why are these completed surfaces at the monocular FIDOs not seen as visible surface qualities? FACADE theory proposes that only the surface representations of the binocular FIDOs are consciously seen under normal viewing conditions, including both monocular- and binocular-viewing conditions. (A binocular FIDO may be activated by monocular viewing, as in its explanation of Fechner's paradox.) The theory does not attempt to offer a biochemical reason for this property but rather presents it as a working hypothesis. Given this hypothesis, it follows that the binocular FIDO surfaces generate visible filled-in signals only from unoccluded surface regions, as illustrated in Figures 26G–I.

Is there a functional rationale for why only the filled-in binocular FIDOs are consciously visible? This visible representation is proposed to signal which material surfaces are exposed to the viewer and therefore are accessible as targets for goal-oriented action. In this conception, extrastriate visual cortex attracts spatial attention through interactions with the parietal cortex and uses it to activate eye movements and arm-reaching movements toward visible targets. This proposed role is consistent with the fact that the binocular FIDOs are the first processing stage within the model at which figure–ground separation is fully achieved. Thus, the binocular FIDOs are the first stage in the model at which object surface representations are separated well enough to direct actions toward them. In vivo, figure–ground separation seems to occur in cortical area V4 of the monkey (Schiller, 1994, 1995; Schiller & Lee, 1991), which the binocular FIDO is proposed to model.

Let us, therefore, assume that only binocular FIDOs carry visible signals and are used to direct goal-oriented movements. If this is so, then activities at monocular FIDOs are perceptually invisible. By what means, then, could the monocular FIDOs lead to an awareness of amodal surface completion? In particular, how does an observer determine which amodally completed disk in Figure 8 is white or black? This question can be technically restated as follows: Do monocular FIDOs, as well as binocular FIDOs, influence surface recognition by the ORS? The answer that is proposed herein goes as follows.

As schematized in Figure 33, FCS surface representations within the model interact reciprocally with the ORS as well as with the spatial attention system. These FCS interactions help to direct object attention (Duncan, 1984) as well as spatial attention (Posner, 1980) on FCS surface representations. Object attention and spatial attention may be attributed to the IT and parietal cortical streams, respectively, that are indicated in Figure 10. Object attention plays a key role in categorizing and recognizing objects, whereas spatial attention helps to locate and act on them. Data about the *what* and *where* of cortical processing streams through the temporal and parietal cortices, respectively, have greatly clarified this distinction (Goodale & Milner, 1992; Mishkin, Ungerleider, & Macko, 1983; Ungerleider & Mishkin, 1982). Thus, one may consider the possibility that the surface representations of the monocular FIDOs, as well as those of the binocular FIDOs, send signals to the ORS in the temporal cortex. In a similar way, one can ask if both monocular and binocular FIDOs guide the allocation of spatial attention, albeit possibly in different ways.

The hypothesis that monocular FIDOs signal the ORS with occluded surface properties is supported by the observation that the correctly completed boundaries of occluded objects are represented at the monocular FIDOs, but not at the binocular FIDOs, where boundary enrichment occurs (Figure 18B). For example, the correctly completed *B* boundaries occur in Figure 26F, but not in Figure 26H, where they are summed. That is why the unsummed BCS boundaries (possibly in cortical area V2) are proposed to input directly into the ORS (in the temporal cortex) before they are added on their way to the binocular FIDOs (in cortical area V4). The ORS, in turn, sends reciprocal top-down expectation signals back to the BCS that focus object attention on the active boundaries there.

Both the boundary and the surface representations that are formed at this unsummed level input to the ORS. The surface recognition achieved in this way is assumed to subserve the awareness of amodal surface quality. Because the monocular FIDOs are depth- and color-specific, this recognition event carries with it an awareness of surface depth and color, even if it is not visible.

More needs to be said about how surface qualities can become conscious, even if they are not visible. A central tenet of adaptive resonance theory is that conscious events are resonant events that develop over time as bottom-up signals and top-down expectations interact to select an attentional focus (Carpenter & Grossberg, 1993; Grossberg, 1980, 1995). In the present instance, the bottom-up signals are the boundary and surface outputs to the ORS. The ORS, in turn, sends reciprocal top-down expectation signals back to the BCS and the FCS. These top-down signals focus object attention on the active boundaries and surfaces there. The resonance that develops between boundary or surface representations and the categorical representations of the ORS is proposed to be capable of supporting a conscious event, even if it is not visible.

Various data support the hypothesis that FCS surface representations interact with the ORS, as in Figure 32. These include the following: A failure to attentively bind colored surfaces to the correct boundaries can occur during illusory conjunctions (McLean, Broadbent, & Broadbent, 1983; Stefurak & Boynton, 1986; Treisman & Schmidt, 1982). Color can facilitate object naming if the objects to be named are structurally similar or degraded (Christ, 1975; Price & Humphreys, 1989). Colors are coded categorically prior to the processing stage at which they are named (Davidoff, 1991; Rosch, 1975). Further studies are needed to determine if these color properties are mediated by binocular FIDOs, monocular FIDOs, or as yet undiscovered additional surface representations.

This summary has considered how the monocular and binocular FIDOs of Figure 12 may interact with the object attention system and the spatial attention system. Assuming that the monocular FIDOs are computed within the thin stripes of cortical area V2, the binocular FIDOs within area V4, the object attention system within the temporal cortex, and the spatial attention system within the parietal cortex, then the above hypotheses make testable predictions about how cortical areas V2 and V4 directly or indirectly interact with the temporal and parietal cortices. A full analysis of this issue is beyond the scope of this article. My goal in this section has been to point out that filling-in within the monocular FIDOs and spatial attention to monocular and binocular FIDOs are processes that may subserve the amodal awareness of an occluded surface representation.

24. Concluding Remarks

This article extends the explanatory range of FACADE theory to explain data concerning how 2-D pictures may give rise to 3-D percepts of occluding and occluded objects. The theory considers pictures that are derived from line drawings, color fields, and combinations thereof. The percepts analyzed herein probe how geometrical constraints and contrast-based constraints influence the boundary and surface representations that subserve pictorial percepts. Sometimes these boundary and surface constraints cooperate with one another, and sometimes they compete. The theory's ability to handle the subtle perceptual changes resulting from manipulations that change this balance provides additional evidence that its model principles and mechanisms incorporate a substantial kernel of truth.

References

Aks, D. J., & Enns, J. T. (1992). Visual search for direction of shading is influenced by apparent depth. *Perception & Psychophysics, 52,* 63–74.

Anderson, B. L., & Julesz, B. (1995). A theoretical analysis of illusory contour formation in stereopsis. *Psychological Review, 102,* 705–743.

Anderson, R. A., Essick, G. K., & Siegel, R. M. (1985). Enclosing of spatial location by posterior parietal neurons. *Science, 230,* 456–458.

Arrington, K. F. (1993). Binocular rivalry model using multiple habituating nonlinear reciprocal connections. *Neuroscience Abstracts, 19,* 1803.

Arrington, K. F. (1994). The temporal dynamics of brightness filling-in. *Vision Research, 34,* 3371–3387.

Ashley, M. L. (1898). Concerning the significance of intensity of light in visual estimates of depth. *Psychological Review, 50,* 19–25.

Bergen, J. R., & Landy, M. S. (1991). Computational modeling of visual texture segregation. In M. S. Landy & J. A. Movshon (Eds.), *Computational models of visual processing* (pp. 253–271). Cambridge, MA: MIT Press.

Biederman, I., & Ju, G. (1988). Surface versus edge-based determinants of visual recognition. *Cognitive Psychology, 20,* 38–64.

Blake, R. (1977). Threshold conditions for binocular rivalry. *Journal of Experimental Psychology: Human Perception and Performance, 3,* 251–257.

Blake, R., & Camisa, J. (1979). On the inhibitory nature of binocular rivalry suppression. *Journal of Experimental Psychology: Human Perception and Performance, 5,* 315–323.

Blake, R., & Fox, R. (1974). Binocular rivalry suppression: Insensitive to spatial frequency and orientation change. *Vision Research, 14,* 687–692.

Blake, R., & Lema, S. A. (1978). Inhibitory effect of binocular rivalry suppression is independent of orientation. *Vision Research, 18,* 541–544.

Blasdel, G. G. (1989). Topography of visual function as shown with voltage-sensitive dyes. In J. J. Lund (Ed.), *Sensory processing in the mammalian brain* (pp. 242–268). New York: Oxford University Press.

Bradley, D. R., & Dumais, S. T. (1984). The effects of illumination level and retinal size on the depth stratification of subjective contour figures. *Perception, 13,* 155–164.

Bradski, G., & Grossberg, S. (1995). Fast learning VIEWNET architectures for recognizing 3-D objects from multiple 2-D views. *Neural Networks, 8,* 1053–1080.

Bregman, A. L. (1981). Asking the "what for" question in auditory perception. In M. Kubovy & J. R. Pomerantz (Eds.), *Perceptual organization* (pp. 99–118). Hillsdale, NJ: Erlbaum.

Bressan, P. (1995). A closer look at the dependence of neon colour spreading on wavelength and illuminance. *Vision Research, 35,* 375–379.

Brown, J. M., & Weisstein, N. (1988). A spatial frequency effect on perceived depth. *Perception & Psychophysics, 44,* 157–166.

Carpenter, G. A., & Grossberg, S. (1993). Normal and amnesic learning, recognition, and memory by a neural model of cortico–hippocampal interactions. *Trends in Neurosciences, 16,* 131–137.

Chey, J., Grossberg, S., & Mingolla, E. (1995). *Neural dynamics of motion processing and speed discrimination* (Tech. Rep. No. CAS/CNS-TR-94-030). Boston: Boston University.

Chey, J., Grossberg, S., & Mingolla, E. (in press). Neural dynamics of motion grouping: From aperture ambiguity to plaid coherence. *Journal of the Optical Society of America A.*

Christ, R. E. (1975). Review and analysis of color coding research for visual displays. *Human Factors, 17,* 562–570.

Cohen, M. A., & Grossberg, S. (1984). Neural dynamics of brightness perception: Features, boundaries, diffusion, and resonance. *Perception & Psychophysics, 36,* 428–456.

Davidoff, J. B. (1991). *Cognition through color.* Cambridge, MA: MIT Press.

Davidoff, J. B., & Donnelly, N. (1990). Object superiority: A comparison of complete and part probes. *Acta Psychologica, 73,* 225–243.

Desimone, R. (1991). Face-selective cells in the temporal cortex of monkeys. *Journal of Cognitive Neuroscience, 3,* 1–8.

Desimone, R., Schein, S. J., Moran, J., & Ungerleider, L. G. (1985). Contour, color, and shape analysis beyond the striate cortex. *Vision Research, 25,* 441–452.

Desimone, R., & Ungerleider, L. G. (1989). Neural mechanisms of visual processing in monkeys. In F. Boller & J. Grafman (Eds.), *Handbook of neuropsychology* (Vol. 2, pp. 267–299). Amsterdam: Elsevier.

DeYoe, E. A., & van Essen, D. C. (1988). Concurrent processing streams in monkey visual cortex. *Trends in Neurosciences, 11,* 219–226.

Douglas, R. J., Koch, C., Mahowald, M., Martin, K. A. C., & Suarez, H. H. (1995). Recurrent excitation in neocortical circuits. *Science, 269,* 981–985.

Duncan, J. (1984). Selective attention and the organization of visual information. *Journal of Experimental Psychology: General, 113,* 501–517.

Egeth, H. E., Virzi, R. A., & Garbart, H. (1984). Searching for conjunctively defined targets. *Journal of Experimental Psychology: Human Perception and Performance, 10,* 32–39.

Egusa, H. (1983). Effects of brightness, hue, and saturation on perceived depth between adjacent regions in the visual field. *Perception, 12,* 167–175.

Ejima, Y., Redies, C., Takahashi, S., & Akita, M. (1984). The neon color effect in the Ehrenstein pattern: Dependence on wavelength and illuminance. *Vision Research, 24,* 1719–1726.

Felleman, D. J., & van Essen, D. C. (1991). Distributed hierarchical processing in the primate visual cortex. *Cerebral Cortex, 1,* 1–47.

Ferster, D. (1988). Spatially opponent excitation and inhibition in simple cells of the cat visual cortex. *Journal of Neuroscience, 8,* 1172–1180.

Fischer, B. (1986). The role of attention in the preparation of visually guided eye movements in monkey and man. *Psychological Research, 48,* 251–257.

Fischer, B., & Breitmeyer, B. (1987). Mechanisms of visual attention revealed by saccadic eye movements. *Neuropsychologia, 25,* 73–83.

Fox, R., & Check, R. (1972). Independence between binocular rivalry suppression duration and magnitude of suppression. *Journal of Experimental Psychology, 93,* 283–289.

Francis, G., & Grossberg, S. (1996a). Cortical dynamics of boundary segmentation and reset: Persistence, afterimages, and residual traces. *Perception, 25,* 543–567.

Francis, G., & Grossberg, S. (1996b). Cortical dynamics of form and motion integration: Persistence, apparent motion, and illusory contours. *Vision Research, 36,* 149–173.

Francis, G., Grossberg, S., & Mingolla, E. (1994). Cortical dynamics of feature binding and reset: Control of visual persistence. *Vision Research, 34,* 1089–1104.

Gerrits, H. J. M., & Timmermann, J. G. M. E. N. (1969). The filling-in process in patients with retinal scotomata. *Vision Research, 9,* 439–442.

Gerrits, H. J. M., & Vendrick, A. J. H. (1970). Simultaneous contrast filling-in process and information processing in man's visual system. *Experimental Brain Research, 11,* 411–430.

Gilbert, C. D., & Wiesel, T. N. (1990). The influence of contextual stimuli on the orientation selectivity of cells in primary visual cortex of the cat. *Vision Research, 30,* 1689–1701.

Gochin, P. M., Miller, E. K., Gross, C. G., & Gerstein, G. L. (1991). Functional interactions among neurons in inferior temporal cortex of the awake macaque. *Experimental Brain Research, 84,* 505–516.

Goodale, M. A., & Milner, D. (1992). Separate visual pathways for perception and action. *Trends in Neurosciences, 15,* 20–25.

Gove, A., Grossberg, S., & Mingolla, E. (1995). Brightness perception, illusory contours, and corticogeniculate feedback. *Visual Neuroscience, 12,* 1027–1052.

Gregory, R. L. (1970). *The intelligent eye.* New York: McGraw-Hill.

Griffiths, A. F., & Chubb, C. (1993). Integration of information across spatial frequency channels in detection of contrast boundaries. *Investigative Ophthalmology and Visual Science, 34,* 1289.

Grosof, D. H., Shapley, R. M., & Hawken, M. J. (1993). Macaque V1 neurons can signal "illusory" contours. *Nature, 365,* 550–552.

Grossberg, S. (1980). How does a brain build a cognitive code? *Psychological Review, 87,* 1–51.

Grossberg, S. (1983). The quantized geometry of visual space: The coherent computation of depth, form, and lightness. *Behavioral and Brain Sciences, 6,* 625–657.

Grossberg, S. (1984). Outline of a theory of brightness, color, and form perception. In E. Degreef & J. van Buggenhaut (Eds.), *Trends in mathematical psychology* (pp. 5559–5586). Amsterdam: Elsevier/North-Holland.

Grossberg, S. (1987a). Cortical dynamics of three-dimensional form, color, and brightness perception, I: Monocular theory. *Perception & Psychophysics, 41,* 87–116.

Grossberg, S. (1987b). Cortical dynamics of three-dimensional form, color, and brightness perception, II: Binocular theory. *Perception & Psychophysics, 41,* 117–158.

Grossberg, S. (1991). Why do parallel cortical systems exist for the perception of static form and moving form? *Perception & Psychophysics, 49,* 117–141.

Grossberg, S. (1993). A solution of the figure–ground problem for biological vision. *Neural Networks, 6,* 463–483.

Grossberg, S. (1994). 3-D vision and figure–ground separation by visual cortex. *Perception & Psychophysics, 55,* 48–120.

Grossberg, S. (1995). The attentive brain. *American Scientist, 83,* 438–449.

Grossberg, S., & Marshall, J. (1989). Stereo boundary fusion by cortical complex cells: A system of maps, filters, and feedback networks for multiplexing distributed data. *Neural Networks, 2,* 29–51.

Grossberg, S., & McLoughlin, N. (in press). Cortical dynamics of 3-D surface perception: Binocular and half-occluded scenic images. *Neural Networks.*

Grossberg, S., & Merrill, J. W. L. (1996). The hippocampus and cerebellum in adaptively timed learning, recognition, and movement. *Journal of Cognitive Neuroscience, 8,* 257–277.

Grossberg, S., & Mingolla, E. (1985a). Neural dynamics of form perception: Boundary completion, illusory figures, and neon color spreading. *Psychological Review, 92,* 173–211.

Grossberg, S., & Mingolla, E. (1985b). Neural dynamics of perceptual grouping: Textures, boundaries, and emergent segmentations. *Perception & Psychophysics, 38,* 141–171.

Grossberg, S., & Mingolla, E. (1987). Neural dynamics of surface perception: Boundary webs, illuminants, and shape-from-shading. *Computer Vision, Graphics, and Image Processing, 37,* 116–165.

Grossberg, S., & Mingolla, E. (1993). Neural dynamics of motion perception: Direction fields, apertures, and resonant grouping. *Perception & Psychophysics, 53,* 243–278.

Grossberg, S., & Mingolla, E. (1994). Visual motion perception. In V. S. Ramachandran (Ed.), *Encyclopedia of human behavior* (Vol. 4, pp. 469–486). New York: Academic Press.

Grossberg, S., Mingolla, E., & Ross, W. D. (1994). A neural theory of attentive visual search: Interactions of boundary, surface, spatial, and object recognition. *Psychological Review, 101,* 470–489.

Grossberg, S., Mingolla, E., & Ross, W. D. (1997). Visual brain and visual perception: How does the cortex perceive grouping? *Trends in Neuroscience, 20,* 106–111.

Grossberg, S., Mingolla, E., & Todorović, D. (1989). A neural network architecture for preattentive vision. *IEEE Transactions on Biomedical Engineering, 36,* 65–84.

Grossberg, S., Mingolla, E., & Williamson, J. (1995). Synthetic aperture radar processing by a multiple scale neural system for boundary and surface representation. *Neural Networks, 8,* 1005–1028.

Grossberg, S., & Rudd, M. E. (1989). A neural architecture for visual motion perception: Group and element apparent motion. *Neural Networks, 2,* 421–450.

Grossberg, S., & Rudd, M. E. (1992). Cortical dynamics of visual motion perception: Short-range and long-range apparent motion. *Psychological Review, 99,* 78–121.

Grossberg, S., & Todorović, D. (1988). Neural dynamics of 1-D and 2-D brightness perception: A unified model of classical and recent phenomena. *Perception & Psychophysics, 43,* 241–277.

Grossberg, S., & Wyse, L. (1991). Invariant recognition of cluttered scenes by a self-organizing ART architecture: Figure–ground separation. *Neural Networks, 4,* 723–742.

Harries, M. H., & Perrett, D. I. (1991). Visual processing of faces in temporal cortex: Physiological evidence for a modular organization and possible anatomical correlates. *Journal of Cognitive Neuroscience, 3,* 9–24.

He, Z. J., & Nakayama, K. (1992). Surface features in visual search. *Nature, 359,* 231–233.

Helmholtz, H. von. (1873). *Popular scientific lectures.* New York: Appleton.

Helson, H. (1964). *Adaptation level theory.* New York: Harper & Row.

Hollins, M., & Bailey, G. W. (1981). Rivalry target luminance does not effect suppression depth. *Perception & Psychophysics, 30,* 201–203.

Homa, D., Haver, B., & Schwartz, T. (1976). Perceptibility of schematic face stimuli: Evidence for a perceptual Gestalt. *Memory and Cognition, 4,* 176–185.

Hubel, D. H., & Wiesel, T. N. (1977). Functional architecture of macaque monkey visual cortex. *Proceedings of the Royal Society of London (B), 198,* 1–59.

Hubel, D. H., & Wiesel, T. N. (1979). Brain mechanisms of vision. *Scientific American, 241,* 150–163.

Jameson, D., & Hurvich, L. M. (1955). Some quantitative aspects of an opponent-colors theory: I. Chromatic responses and spectral saturation. *Journal of the Optical Society of America, 45,* 546–552.

Julesz, B., & Schumer, R. A. (1981). Early visual perception. *Annual Review of Psychology, 32,* 575–627.

Kanizsa, G. (1955). Margini quasi-percettivi in campi con stimolazione omogenea. *Revista di Psicologia, 49,* 7–30.

Kanizsa, G. (1974). Contours without gradients or cognitive contours. *Italian Journal of Psychology, 1,* 93–113.

Kanizsa, G. (1979). *Organization in vision: Essays in Gestalt perception.* New York: Praeger.

Kanizsa, G. (1985). Seeing and thinking. *Acta Psycologia, 59,* 23–33.

Kapadia, M. K., Ito, M., Gilbert, C. D., & Westheimer, G. (1995). Improvement in visual sensitivity by changes in local context: Parallel studies in human observers and in V1 of alert monkeys. *Neuron, 15,* 843–856.

Kaufman, L. (1974). *Sight and mind: An introduction to visual perception.* New York: Oxford University Press.

Kisvárday, Z. F., Toth, E., Rausch, M., & Eysel, U. T. (1995). Comparison of lateral excitatory and inhibitory connections in cortical orientation maps of the cat. *Society for Neuroscience Abstracts, 21,* 907.

Kleffner, D. A., & Ramachandran, V. S. (1992). On the perception of shape from shading. *Perception & Psychophysics, 52,* 18–36.

Klein, S., & Stromeyer, C. F., III. (1980). On inhibition between spatial frequency channels: Adaptation to complex gratings. *Vision Research, 20,* 459–466.

Klymenko, V., & Weisstein, N. (1986). Spatial frequency differences can determine figure–ground organization. *Journal of Experimental Psychology: Human Perception and Performance, 12,* 324–330.

Krauskopf, J. (1963). Effect of retinal image stabilization on the appearance of heterochromatic targets. *Journal of the Optical Society of America, 53,* 741–744.

Kulikowski, J. J. (1978). Limit of single vision in stereopsis depends on contour sharpness. *Nature, 275,* 126–127.

Lennie, P. (1984, July). Recent developments in the physiology of color vision. *Trends in Neurosciences,* 243–248.

Liu, Z., Gaska, J. P., Jacobson, L. D., & Pollen, D. A. (1992). Interneuronal interaction between members of quadrature phase and anti-phase pairs in the cat's visual cortex. *Vision Research, 32,* 1193–1198.

Livingstone, M. S., & Hubel, D. H. (1984). Anatomy and physiology of a color system in the primate visual cortex. *Journal of Neuroscience, 4,* 309–356.

Livingstone, M. S., & Hubel, D. H. (1987). Psychophysical evidence for separate channels for the perception of form, color, movement, and depth. *Journal of Neuroscience, 7,* 3416–3468.

Livingstone, M. S., & Hubel, D. H. (1988). Segregation of form, color, movement, and depth: Anatomy, physiology, and perception. *Science, 240,* 740–749.

Malik, J., & Perona, P. (1990). Preattentive texture discrimination with early vision mechanisms. *Journal of the Optical Society of America A, 7,* 923–932.

Maylor, E. A., & Hockey, R. (1985). Inhibitory components of externally controlled covert orienting in visual space. *Journal of Experimental Psychology: Human Perception and Performance, 11,* 777–787.

McLean, J. P., Broadbent, D. E., & Broadbent, M. H. P. (1983). Combining attributes in rapid serial visual presentation tasks. *Quarterly Journal of Experimental Psychology, 35,* 171–186.

Mial, R. P., Smith, P. C., Doherty, M. E., & Smith, D. W. (1974). The effect of memory color on form identification. *Perception & Psychophysics, 16,* 1–3.

Michotte, A., Thines, G., & Crabbe, G. (1964). *Les complements amodaux des structures perceptives.* Louvain, Belgium: Publications Universitaires de Louvain.

Mishkin, M. (1978). Memory in monkeys severely impaired by combined but not separate removal of the amygdala and hippocampus. *Nature, 273,* 297–298.

Mishkin, M. (1982). A memory system in the monkey. *Philosophical Transactions of the Royal Society of London B, 298,* 85–95.

Mishkin, M., & Appenzeller, T. (1987). The anatomy of memory. *Scientific American, 256,* 80–89.

Mishkin, M., Ungerleider, L. G., & Macko, K. A. (1983). Object vision and spatial vision: Two cortical pathways. *Trends in Neurosciences, 6,* 414–417.

Moulden, B., & Kingdom, F. (1989). White's effect: A dual mechanism. *Vision Research, 29,* 1245–1259.

Mountcastle, V. B., Anderson, R. A., & Motter, B. C. (1981). The influence of attentive fixation upon the excitability of the light-sensitive neurons of the posterior parietal cortex. *Journal of Neuroscience, 1,* 1218–1235.

Mueller, T. J., & Blake, R. (1989). A fresh look at the temporal dynamics of binocular rivalry. *Biological Cybernetics, 61,* 223–232.

Nakayama, K., Shimojo, S., & Silverman, G. H. (1989). Stereoscopic depth: Its relation to image segmentation, grouping, and the recognition of occluded objects. *Perception, 18,* 55–68.

Nakayama, K., & Silverman, G. H. (1986). Serial and parallel processing of visual feature conjunctions. *Nature, 320,* 264–265.

Ostergaard, A. L., & Davidoff, J. B. (1985). Some effects of color on naming and recognition of objects. *Journal of Experimental Psychology: Learning, Memory, and Cognition, 11,* 579–587.

Paradiso, M. A., & Nakayama, K. (1991). Brightness perception and filling-in. *Vision Research, 31,* 1221–1236.

Perrett, D. I., Mistlin, A. J., & Chitty, A. J. (1987). Visual cells responsive to faces. *Trends in Neurosciences, 10,* 358–364.

Pessoa, L., Mingolla, E., & Neumann, H. (1995). A contrast- and luminance-driven multiscale network model of brightness perception. *Vision Research, 35,* 2201–2223.

Petter, G. (1956). Nuove ricerche sperimentali sulla totalizzazione percettiva. *Rivista di Psicologia, 50,* 213–227.

Posner, M. I. (1980). Orienting of attention. *Quarterly Journal of Experimental Psychology, 32,* 2–25.

Price, C. J., & Humphreys, G. W. (1989). The effects of surface detail on object categorization and naming. *Quarterly Journal of Experimental Psychology, 41A,* 797–827.

Purghé, F., & Coren, S. (1992). Amodal completion, depth stratification, and illusory figures: A test of Kanizsa's explanation. *Perception, 21,* 325–335.

Quinn, P. C. (1985). Suprathreshold contrast perception as a function of spatial frequency. *Perception & Psychophysics, 38,* 408–414.

Rauschecker, J. P. J., Campbell, F. W., & Atkinson, J. (1973). Colour opponent neurons in the human visual system. *Nature, 245,* 42–45.

Redies, C., & Spillman, L. (1981). The neon color effect in the Ehrenstein illusion. *Perception, 10,* 667–681.

Richards, W., & Kaye, M. G. (1974). Local versus global stereopsis: Two mechanisms. *Vision Research, 14,* 1345–1347.

Rizzolatti, G., Riggio, L., Dascola, I., & Umità, C. (1987). Reorienting attention across the horizontal and vertical meridians. *Neuropsychologia, 25,* 31–40.

Rock, I. (1993). The logic of "the logic of perception." *Italian Journal of Psychology, 20,* 841–867.

Rosch, E. (1975). The nature of mental codes for color categories. *Journal of Experimental Psychology: Human Perception and Performance, 1,* 303–322.

Sagi, D., & Hochstein, S. (1984). The contrast dependence of spatial frequency channel interactions. *Vision Research, 24,* 1357–1365.

Schiller, P. H. (1994). Area V4 of the primate visual cortex. *Current Directions in Psychological Science, 3,* 89–92.

Schiller, P. H. (1995). Effect of lesions in visual cortical area V4 on the recognition of transformed objects. *Nature, 376,* 342–344.

Schiller, P. H., & Lee, K. (1991). The role of the primate extrastriate area V4 in vision. *Science, 251,* 1251–1253.

Schor, C. M., & Tyler, C. W. (1981). Spatio-temporal properties of Panum's fusional area. *Vision Research, 21,* 683–692.

Schor, C. M., & Wood, I. (1983). Disparity range for local stereopsis as a function of luminance spatial frequency. *Vision Research, 23,* 1649–1654.

Schor, C. M., Wood, I., & Ogawa, J. (1984). Binocular sensory fusion is limited by spatial resolution. *Vision Research, 24,* 661–665.

Schwartz, E. L., Desimone, R., Albright, T., & Gross, C. G. (1983). Shape recognition and inferior temporal neurons. *Proceedings of the National Academy of Sciences, 80,* 5776–5778.

Spehar, B., Gilchrist, A., & Arend, L. (1995). The critical role of relative luminance relations in White's effect and grating induction. *Vision Research, 35,* 2603–2614.

Stefurak, D. L., & Boynton, R. M. (1986). Independence of memory for categorically different colors and shapes. *Perception & Psychophysics, 39,* 164–174.

Sutter, A., Beck, J., & Graham, N. (1989). Contrast and spatial variables in texture segregation: Testing a simple spatial-frequency channels model. *Perception & Psychophysics, 46,* 312–332.

Thorell, L. G., DeValois, R., & Albrecht, D. G. (1984). Spatial mapping of monkey V1 cells with pure color and luminance stimuli. *Vision Research, 24,* 751–769.

Todorović, D. (1987). The Craik–O'Brien–Cornsweet effect: New varieties and their theoretical implications. *Perception & Psychophysics, 42,* 545–560.

Treisman, A., & Schmidt, H. (1982). Illusory conjunctions in the perception of objects. *Cognitive Psychology, 14,* 107–141.

Tyler, C. W. (1975). Spatial organization of binocular disparity sensitivity. *Vision Research, 15,* 583–590.

Tyler, C. W. (1983). Sensory processing of binocular disparity. In C. M. Schor & K. J. Cuiffreda (Eds.), *Vergence eye movements* (pp. 199–295). Boston: Butterworths.

Ungerleider, L. G., & Mishkin, M. (1982). Two cortical visual systems: Separation of appearance and location of objects. In D. L. Ingle, M. A. Goodale, & R. J. W. Mansfield (Eds.), *Analysis of visual behavior* (pp. 549–586). Cambridge, MA: MIT Press.

van Tuijl, H. F. J. M. (1975). A new visual illusion: Neonlike color spreading and complementary color induction between subjective contours. *Acta Psychologica, 39,* 441–445.

van Tuijl, H. F. J. M., & de Weert, C. M. M. (1979). Sensory conditions for the occurrence of the neon spreading illusion. *Perception, 8,* 211–215.

von der Heydt, R., Peterhans, E., & Baumgartner, G. (1984). Illusory contours and cortical neuron responses. *Science, 224,* 1260–1262.

Wales, R., & Fox, R. (1970). Incremental detection thresholds during binocular rivalry suppression. *Perception & Psychophysics, 8,* 90–94.

Watanabe, T., & Cavanagh, P. (1993). Transparent surfaces defined by implicit X junctions. *Vision Research, 33,* 2339–2346.

Watanabe, T., & Sato, T. (1989). Effects of luminance contrast on color spreading and illusory contour in the neon color spreading effect. *Perception & Psychophysics, 45,* 427–430.

Watanabe, T., & Takeichi, H. (1990). The relation between color spreading and illusory contours. *Perception & Psychophysics, 47,* 457–467.

White, M. (1979). A new effect of pattern on perceived lightness. *Perception, 8,* 413–416.

White, M. (1981). The effect of the nature of the surround on the perceived lightness of grey bars within square-wave test gratings. *Perception, 10,* 215–230.

Wilson, H. R., Blake, R., & Halpern, D. L. (1991). Coarse spatial scales constrain the range of binocular fusion on file scales. *Journal of the Optical Society of America, 8,* 229–236.

Wilson, H. R., & Richards, W. A. (1989). Mechanisms of contour curvature discrimination. *Journal of the Optical Society of America, 6,* 106–115.

Wolfe, J. M., & Friedman-Hill, S. R. (1992). Part–whole relationships in visual search. *Investigative Ophthalmology and Visual Science, 33,* 1355.

Wurtz, R. H., Goldberg, M. E., & Robinson, D. E. (1982, June). Brain mechanisms of visual attention. *American Scientist,* 124–135.

Yarbus, A. L. (1967). *Eye movements and vision.* New York: Plenum Press.

Zaidi, Q. (1990). Apparent brightness in complex displays: A reply to Moulden and Kingdom. *Vision Research, 30,* 1253–1255.

Zeki, S. (1983a). Colour coding in the cerebral cortex: The reaction of cells in monkey visual cortex to wavelengths and colours. *Neuroscience, 9,* 741–766.

Zeki, S. (1983b). Colour coding in the cerebral cortex: The responses of wavelength-selective and colour coded cells in monkey visual cortex to changes in wavelength composition. *Neuroscience, 9,* 767–791.

Zrenner, E., Abramov, I., Akita, M., Cowey, A., Livingstone, M., & Valberg, A. (1990). Color perception: Retina to cortex. In L. Spillmann & J. S. Werner (Eds.), *Visual perception: The neurophysiological foundations.* San Diego, CA: Academic Press.

Received April 22, 1995
Revision received July 11, 1996
Accepted August 15, 1996 ■